ISSN 2078-7405

МІНІСТЕРСТВО ОСВІТИ ТА НАУКИ УКРАЇНИ

РІЗАННЯ ТА ІНСТРУМЕНТИ

В ТЕХНОЛОГІЧНИХ СИСТЕМАХ

93’2020

МІНІСТЕРСТВО ОСВІТИ ТА НАУКИ УКРАЇНИ

НАЦІОНАЛЬНИЙ ТЕХНІЧНИЙ УНІВЕРСИТЕТ
«ХАРКІВСЬКИЙ ПОЛІТЕХНІЧНИЙ ІНСТИТУТ»

Ministry of Education & Science of Ukraine
National Technical University
«Kharkiv Polytechnic Institute»

РІЗАННЯ ТА ІНСТРУМЕНТИ в технологічних системах

CUTTING & TOOLS IN TECHNOLOGICAL SYSTEM

Міжнародний науково-технічний збірник
International Scientific-Technical Collection

Заснований у 1966 р. М. Ф. Семко
Found by M. F. Semko in 1966

ВИПУСК № 93
Edition № 93

Харків НТУ «ХПІ» – 2020 – Kharkiv NTU «KhPI»

ББК 34.63
УДК 621.91

Державне видання
Свідоцтво Державного комітету телебачення і радіомовлення України
КВ № 7840 від 8 вересня 2003 року
Друкується за рішенням Вченої Ради НТУ "ХПІ",
протокол № 6 від 13 листопада 2020 р.

У збірнику представлені наукові статті, в яких розглядаються актуальні питання в області механічної обробки різних сучасних матеріалів із застосуванням високопродуктивних технологій, нових методик, вимірювальних приладів для контролю якості оброблених поверхонь і високоефективних різальних інструментів. Розглядаються аспекти оптимізації та математичного моделювання на різних етапах технологічного процесу.

Для інженерів і наукових співробітників, що працюють в області технології машинобудування, різання матеріалів, проектування різальних інструментів в технологічних системах.

Науковий збірник «Різання та інструменти в технологічних системах» включений в Перелік фахових видань України категорії «Б», наказ МОН України від 17.03.2020 р., №409

Р34 Резание и инструменты в технологических системах: Междунар. науч.- техн. сб. – Харьков: НТУ «ХПИ», 2020. – Вып. 93. – 150 с.

Адреса редакційної колегії: вул. Кирпичова, 2, Харків, 61002, Національний технічний університет «Харківський політехнічний інститут», кафедра «Інтегровані технології машинобудування» ім. М.Ф. Семка, тел. +38 (057) 706-41-43.

ББК 34.63

UDK 621.923.7 **doi: 10.20998/2078-7405.2020.93.01**

V. Ferencsik, V. Gal, Miscolc, Hungary

FE INVESTIGATION OF SURFACE BURNISHING TECHNOLOGY ABSTRACT

Abstract. *This paper investigates the finite element analysis of cold forming diamond burnishing process on aluminium alloy, where the input parameters are force, feed rate and speed, as an output parameter the changing of surface roughness is analysed. This lifetime increasing process effectively reduces roughness, improves shape correctness, and increases the hardness of the sub-surface area. Machining simulation of the turned surface before burnishing is based on the real model, corresponding to the measured values, by using DEFORM-2D software in order to validate the improvement of surface quality with numerical values too.*
Keywords*: lifetime-increasing surface hardening technologies; burnishing process; surface roughness; polycrystalline diamond; finite element (FEM) model.*

1. INTRODUCTION

During operation, the individual components and their surfaces of a machine are subjected to several forms of damage caused by stress (mechanical, thermal, chemical, etc.), so lifetime-increasing surface hardening technologies have an important role in industrial practice [1-2]. Furthermore, there is a growing demand for material- and energy-saving processes that can be implemented environmentally friendly without special conditions [3-4] even to be applied to non-iron-based material quality such as the subject of the present study.

A preferred and efficient solution is burnishing, which use sliding relative displacement, decreases surface roughness, increases the micro-hardness of the sub-surface area and corrosion resistance by rearranging the dislocations. It also improves shape correctness and does not require large amounts of coolant lubrication [3-6]. Industries apply, for example, to finishing hydraulic cylinders, pistons, bearing bushes and rings, crankshafts [6].

The aim of our study is to model the effects of the different burnishing parameters (burnishing force, speed, feed rate) on the surface quality. In the past many researchers have placed great emphasis on the theoretical study of technology [7-11] and there is still a special need for a reliable finite element (FEM) model that provides a basic understanding of the mechanics of the process.

In this paper 2D FEM model for surface burnishing technique is established and results show that the developed model is useful for predicting the surface roughness. The usage of this method allows to reducing partial or totally the high cost of experimental testing.

2. BURNISHING PROCESS AND THE IMPLEMENTATION OF IT

Burnishing is used as a finishing treatment. If the surface integrity of the previously machined surfaces need to be improved, it is also suitable as a substitute for conventional machining such as grinding and lapping.
The surface quality of the manufactured parts is a constant priority in the development of mechanical engineering technology and machining. It is determined by the condition of the surface layer and the created topography. As it has a decisive influence on the functional properties and lifetime of components, investigations to pre-determine (estimate) surface roughness parameters are important. In these publications, researchers use different approaches, one of the important directions is the analysis by determining the roughness of the theoretical surface created by modelling. This approach has been successfully applied to machined surfaces, so the change of roughness values for rotating tools could be analysed for special tools [12] and different inserts [13, 14].
During burnishing the reduction of surface roughness is caused by the interaction between the tool and the specimen with surface sliding friction between them. The kinematic relations in the burnishing process can be seen in Fig. 1.

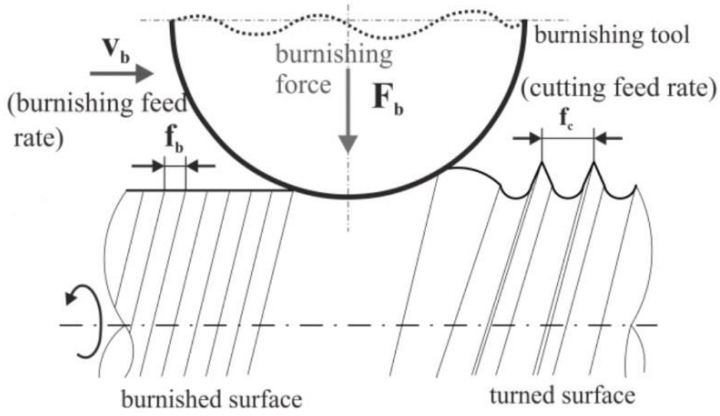

Figure 1 – Schematic illustration of burnishing [15]

Burnishing of outer cylindrical surfaces can be realized on conventional lathes and CNC lathes as well. In this experiment the operation was executed on OPTIMUM (OPTIturn L-Series 440) flatbed CNC lathe using PCD (polycrystalline diamond) tool with 3.5 mm radius with 12 N burnishing force, 0.001 mm/rev burnishing feed and 15 m/min burnishing speed.

3. FINITE ELEMENT ANALYSIS OF BURNISHING PROCESS

The finite element simulation of burnishing process was made by the DEFORM FE code. The simulation was created as a 2D problem to achieve the best comparability between the physical and modelled surface roughness reduction.
For the simulation of the technology, a hemispherical tool with 3.5 mm radius was needed. The burnishing force was 12 N and the relative movement on the surface was constant 0.001 mm/s, while the moving direction was parallel to the axis of the workpiece and perpendicular to the surface. The modelled specimen's surface is based on the physical surface. Before burnishing, the physical workpiece was measured on a 4 mm long distance with Altisurf 520 free dimensional topography measuring device. The surface points - determined with the physical measurement - were imported to the DEFORM FE code to define the surface of the simulated workpiece. To create the accurate axisymmetric problem, the thickness of the 2D workpiece has to be equal to the radius of the specimen used for physical measurement. The results of the preliminary conducted simulations with the above-mentioned parameters show that the process has an effect up to 0.15-0.17 mm in the subsurface area. Accordingly, the thickness of the workpiece was set to 0.2 mm. The tool was rigid, and the workpiece was assumed as an elastoplastic body. In FE modelling, the application of the appropriate mesh is a critical issue in the point of view of results. In the present case, careful attention had to be paid to ensure, the surface roughness is not changing as a result of the meshing. Thus, square elements with a side length of 0.01 mm was used at the surface. After meshing, the surface roughness changed from the physically measured from 1.478 µm to 1.457 µm. With an even smaller side length of the mesh, the surface roughness can be more accurately following, but in this case the calculation time would increase significantly. Fig. 2 shows a section of the tool and the meshed workpiece.

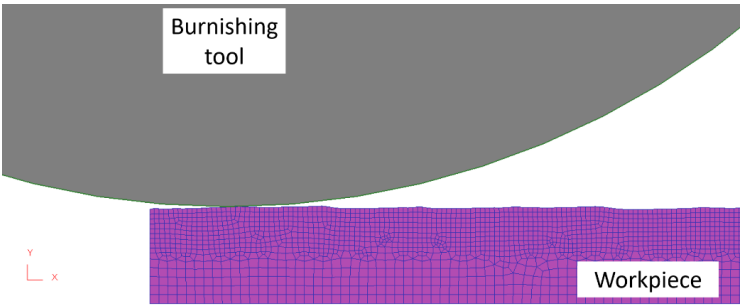

Figure 2 – Section of the 2D burnishing model with the workpiece and tool in DEFORM FE code

For describe the formability of the workpiece made of 6065 high strength aluminium in T0 condition, the mechanical properties of it need to be specified. The elastic behaviour of the material was specified with the Young modulus (68900 MPa) and a Poisson's ration (0.33). At elastoplastic materials beyond the Yield stress, elastic and plastic deformations occur simultaneously. The stress value required for further plastic deformation (so the flow stress) changes with the deformation of the material. The DEFORM FE code provides different methods to defining the flow stress changing along deformation. In this paper we have used the Power law which can be described by the following equation:

$$\bar{\sigma} = c\bar{\varepsilon}^{n}\dot{\bar{\varepsilon}}^{m} + y \qquad (1)$$

where $\bar{\sigma}$ is the flow stress, $\bar{\varepsilon}$ is the effective plastic strain, $\dot{\bar{\varepsilon}}$ is the effective strain rate, c is a material constant, n is a strain exponent, m is a strain rate exponent, and y is an initial value [16].

After determining the geometries and behaviour of the material, the contact between the tool and the workpiece and boundary conditions had to be specified. The simulation was carried out as an isothermal problem, so the change in the temperature was not considered. Since lubrication was used during the physical measurement the friction between the tool and the specimen was considered zero. To achieve an accurate result the separation criteria (which defines how the nodes of the workpiece on the surface of the tool will behave when tensile force appears) was also considered as zero.

4. RESULTS

After running the FE model made from the physical measurement, the comparison was performed based on the change in the surface geometries. Diagram 1 clearly shows the difference between the turned meshed workpiece surface (before burnishing) and the surface profile obtained after running the simulation.

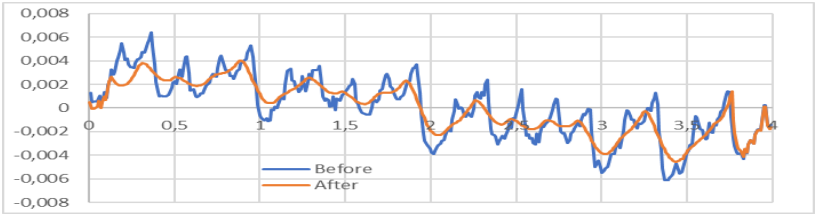

Diagram 1 – Change in the surface profile after the burnishing simulation

The numerical results of the realized experiment and the simulation are summarized in Table 1.

Table 1 – Numerical results of arithmetical mean roughness (R_a)

R_a [μm]		
	Experiment	FE model
Turned	1,478	1,457
Burnished	0,0965	0,0916

5. SUMMARY AND DISCUSSIONS

In this paper 2D finite element model of ball burnishing process was developed with the same parameters as the empirical experiment by DEFORM-2D software. After running the simulation and evaluating the results, the following conclusions can be stated:

- Burnishing can be used effectively with these parameters (F_b = 12 N; f = 0.001 mm/rev; v_b = 15 m/min) according to the experiment and the modelling results as well.
- During simulation, choosing the right mesh size has a great importance for the credibility of the model.
- Numerical roughness Ra presented a good approximation with the experimental result considering that minimal simplifications of the model, the extent of the deviation is 5.35 %, so applying the simulation, the optimum ball burnishing conditions can be obtained to control the surface response.

The undertaken numerical studies will be continued, in the future we would like to examine and simulate the changing of stress conditions and surface micro-hardness caused by burnishing process.

ACKNOWLEDGEMENTS

"The described study was carried out as part of the EFOP-3.6.1-16-00011 "Younger and Renewing University – Innovative Knowledge City – institutional development of the University of Miskolc aiming at intelligent specialisation" project implemented in the framework of the Szechenyi 2020 program. The realization of this project is supported by the European Union, co-financed by the European Social Fund."

"Project no. NKFI-125117 has been implemented with the support provided from the National Research, Development and Innovation Fund of Hungary, financed under the K_17 funding scheme."

References: 1. *L. Balint, L. Gribovszki:* A gépgyártástechnológia alapjai, Miskolci Eyetem, (1975) 418-442. **2.** *G. Bagyinszki, E. Bitay:* Felületkezelés, Erdélyi Múzeum-Egyesület, Műszaki tudományos füzetek 5. (2009) 9-85. **3.** *A.A., El-Nasr:* Thermomechanical fatigue behavior of burnished 7075-T6 aluminium alloy, Proceedings of the 15th Int. AMME Conference (2012) 40-50. **4.** *Z.D., Kadhim, M.A., Abdulrazzaq, W.S., Hussain:* Mechanical properties of burnished steel AISI 1008, Al-Khwarizmi Engineering Journal, 14: 4 (2018) 133-142. **5**. *L., Gribovszki:* Gépipari megmunkálások, Miskolc, Egyetemi Tankönyvkiadó (1977) 421. **6.** *A., Abodena:* Optimization of surface roughness of brass by burnishing, The International Journal of Engineering and

Information Technology, 5: 2 (2019) 90-96. **7.** *A., Bougharriou, K., Sai, W., Bouzid:* Finite element modeling of burnishing process, Materials Technology: Advanced Performance, Materials 25:, (2010) 56-67. **8.** *A., Rodriguez, L. N., Lopez De Lacalle, A., Celaya, A., Lamikiz, J., Albizuru:* Surface improvement of shafts by the deep ball-burnishing technique, Surface and Coatings Technology, 206:1, (2012) 2817-2824. **9.** Y.C., Yen, P., Sartkulvanich, T., Altan: Finite element modeling of roller burnishing process, CIRP Annals-Manufacturing Technology, 54:1, (2005) 237-240. **10.** *F., Klocke, V., Backer, H., Wegner, M., Zimmermann:* Finite element analysis of the roller burnishing process for fatigue resistance increase of engine components, Proceedings of the Institution of Mechanical Engineers, Part B: Journal of Engineering Manufacture 225:1, (2011) 2-11. **11.** *M., Sayahi, S., Sghaier, H., Belhadjsalah:* Finite element analysis of ball burnishing process: comparisons between numerical results and experiments, The International Journal of Advanced Manufacturing Technology 67:5-8, (2013) 1665-1673. **12.** *J., Kundrák, C., Felhő:* 3D Roughness Parameters of Surfaces Face Milled by is Special Tools, MANUFACTURING TECHNOLOGY, 16:3 (2016) 532-538. **13.** *C., Felho, A., Nagy, J., Kundrak:* Effect of Shape of Cutting Edge on Face Milled Surface Topography, LECTURE NOTES IN MECHANICAL ENGINEERING, 46:10, (2020) 525-534. **14.** *J., Kundrak, C., Felho:* Comparison of theoretical and real surface roughness in face milling with octagonal and circular inserts, KEY ENGINEERING MATERIALS 581, (2014) 360-365. **15.** *M., Posdzich, R., Stöckmann, F., Morczinek, M.,Putz:* Investigation of a plain ball burnishing process on differently machined Aluminium EN AW 2007 surfaces, MATEC Web of Conferences 190:11005 (2018) 1-7. **16.** DEFORM v12sp2 System Documentation July 2, 2020; Scientific Forming Technologies Corporation.

Вікторія Ференчик, Віктор Гал, Мішкольц, Угорщина

КІНЦЕВО-ЕЛЕМЕНТНЕ ДОСЛІДЖЕННЯ ТЕХНОЛОГІЇ ВИГЛАДЖУВАННЯ ПОВЕРХОНЬ

Анотація. *Технології поверхневого зміцнення, що збільшують термін служби деталей машин, грають важливу роль в промисловій практиці. Кращим і ефективним рішенням є вигладжування, при якому використовується відносне переміщення з ковзанням, зменшується шорсткість поверхні, збільшується мікротвердість підповерхневої області і корозійна стійкість за рахунок перестановки дислокацій. Метою цього дослідження є моделювання впливу різних параметрів процесу вигладжування (сила притиску, швидкість вигладжування, швидкість подачі) на якість поверхні. Існує особлива потреба в надійній кінцево-елементної моделі (МСЕ), яка дає базове розуміння механіки процесу. У цій статті представлена 2D-модель FEM для методу вигладжування поверхні. Використання цього методу дозволяє значно знизити вартість експериментальних випробувань. Під час вигладжування зменшення шорсткості поверхні викликано взаємодією інструменту і зразка з поверхневим тертям ковзання між ними. В цьому експерименті операція була виконана на токарному верстаті з ЧПУ OPTIMUM (OPTIturn L-Series 440) з використанням інструменту PCD (полікристалічний алмаз) з радіусом 3,5 мм із зусиллям притиску 12 Н, подачею 0,001 мм / об і швидкістю вигладжування 15 м / хв. У даній роботі 2D звичайно-елементна модель процесу вигладжування кулькою була розроблена з тими ж параметрами, що і емпіричний експеримент за допомогою програми DEFORM-2D. Після моделювання і оцінки результатів можна зробити наступні висновки: вигладжування може бути ефективно використано з параметрами (F_b = 12 Н; f = 0,001 мм / об; V_b = 15 м / хв) відповідно до експериментом і результатами моделювання. Під час моделювання вибір правильного розміру сітки має велике значення для достовірності моделі. Величина шорсткості R_a являє собою добре наближення до експериментального результату, враховуючи, що при мінімальних спрощення моделі ступінь відхилення становить 5,35%, тому, застосовуючи моделювання, можна отримати оптимальні умови вигладжування.*

Ключові слова*: поверхневе зміцнення; вигладжування; шорсткість поверхні; полікристалічний алмаз; кінцево-елементна модель.*

UDC 004.94 (045) **doi: 10.20998/2078-7405.2020.93.02**

L. Fükő, B. Illés, P. Tamás, R. Skapinyecz,
Á. Cservenák, Miskolc, Hungary

METHODS FOR DETERMINING MATURITY EVALUATION SYSTEM IN INDUSTRY 4.0

Abstract. *Nowadays, developments are being started to implement in the companies' production and logistics systems based on the so-called Industry 4.0 concept as an increasing role. On the one hand, market competition generates this need, but in many cases the use of Industry 4.0 solutions is the main driving force, in order of the truly higher level of automation with significant cost savings. On the other hand, the different levels of development individual companies are an achievement, which is further complicated by different industry characteristics. Therefore, a great benefit can be from developing a methodology that can help across the industry to determine the level of development required to make a particular Industry 4.0 development feasible. Partially laying down the theoretical foundations is the goal of this publication for the creation of such a maturity evaluation system in the field of Industry 4.0.*
Keywords: *Industry 4.0; lean; digitalization;, autonomy; maturity.*

1. INTRODUCTION

Today, the application of the Industry 4.0 concept can be observed in almost all areas of the economy. One of the primary reasons for this is that, from an economic point of view, the application of Industry 4.0 makes it possible to meet individual customer needs at the production costs typical of mass production. [1] The fact that this is possible is, of course, due to the combined use of the new technologies behind the concept, including the creation of so-called cyber-physical systems and the exploitation of the potential of big data. [2] Automation and the use of state-of-the-art artificial intelligence applications play a huge role, especially in the creation of the former systems, while large-scale data analysis allows for the innovative use of data collected from the resulting systems to shed light on previously unknown relationships. Exploring the latter can play a particularly important role in increasing efficiency, for example by predicting equipment failures and product failures with unprecedented accuracy [3], but also by predicting changes in customer demand with previously unattainable accuracy. The role of Industry 4.0 can be increased also in the academic scetor, such as in a laboratory [4].

It is no coincidence, then, that the application of the Industry 4.0 concept has already had a huge impact on both logistics and production. [5] As a result, there has been a need for some time to develop models that can help define the so-called 'Industry 4.0 maturity' for a given organization. Here, it is important to specify that the maturity models measure the maturity of the organization or process actually

achieved during development in relation to a certain target state.

We are also talking about so-called preparedness models, the purpose of which is to record the initial state, which makes it possible to start the development process. Some typical maturity and readiness models from [6] are summarized in the following Table 1. Further maturity models can be found in the literature, for instance a fuzzy rule-based [7], for machine tool companies [8], for SMEs (Small and medium-sized enterprises) [9] or for the defence sector [10]. There is solution for metananalysis of Industry 4.0 maturity models [11].

Table 1 – Overview of Existing Industry 4.0 Readiness and Maturity Models (Evaluation Models) [6]

Model name	Institution / source	Evaluation approach
IMPULS - Industry 4.0 Preparedness (2015)	VDMA, RWTH Aachen, IW consult	Assessment in 6 dimensions, which includes 18 units, showing readiness at 5 levels.
Empowerment and Implementation Strategy for Industry 4.0 (2016)	Lanza	Assessing the maturity of industry 4.0 as a quick check and as part of the implementation process model
Industry 4.0 / Digital Operations Self-Assessment (2016)	Pricewaterhouse Coopers	Online self-assessment in 6 dimensions; focus on digital maturity at 4 levels
Graduation model of the affiliated company (2014)	Rockwell Automaton	The graduation model is part of a five-step approach to implementing Industry 4.0; technology-centric evaluation in 4 dimensions
Schumacher (2016)	TU Wien, Fraunhofer Austria	Evaluation in 9 dimensions. Further details in 62 graduation units
ACATECH Schuh (2017)	acatech – National Academy of Science and Engineering	Assessment in 6 dimensions which is further detailed in 18 areas and shows the level of maturity at 6 levels
SIMMI 4.0 (2016)	TU Dresden	Evaluation in 4 dimensions. Shows the graduation level in 5 levels

2. DEFINING THE BASIC ASPECTS OF THE METHOD TO BE DEVELOPED

It was clear from the above that the existence of prerequisites is important for the assessment of Industry 4.0 maturity. In this chapter, therefore, our goal is to define the basic characteristics of a method that can be used well to determine both Industry 4.0 readiness and maturity for a process or organization. This also means that the method must be applicable both to the so-called readiness assessment before the start of the preparation process and to capture the state during the preparation process (the latter is the maturity assessment). The following general objectives and findings should also be taken into account when designing the method:

- In terms of evaluation, the emphasis should be on production processes. Although digital data collection and processing from non-production areas is not strictly an Industry 4.0 application, the solutions and experiences used there can be a good starting point for its implementation.
- The first step is to create the preconditions for a functioning corporate governance system. This requires the existence of a functioning corporate governance or management system. This ensures basic integrity and controlled operation. Processes must be controlled and repeatable.
- Processes need to be simplified and made transparent. To do this, we need to know and use the principles of lean, which are necessary to be able to identify the losses that occur and to work systematically to reduce them.
- Defined and repeatable processes need to be stabilized and continuously improved. This requires the use of various statistical methods that can be used to perform capability tests and process control. We can evaluate results and identify trends.
- The digital form of data collection facilitates subsequent data processing. It creates the possibility of fast and efficient data processing.
- The computer network within the company speeds up and helps the collection, flow, storage and processing of data. The storage and processing of data and access to them must be managed at the system administrator level. This requires adequate storage capacity and IT infrastructure. In addition, proper user rights management must be provided.
- The use of enterprise management software is both important for the management of the company and can greatly increase the efficiency of processes. The more processes it covers, the higher the level of integration it implements.
- A higher level of capabilities means having software development capabilities, expertise within the company. This can ensure that the data that can be collected and to be collected is stored in an organized form and processed

efficiently. It creates the possibility of customized software data processing from the use of user software.

- Industrial data collection is required for automatic data collection and efficient management of production assets. This creates the opportunity for a wide extension of networked production facilities within the company, which paves the way for the efficient use of various production management software.

The system moves to industry level 4.0 as a result of which a digitally mapped twin pair of the production process is created. It is a system that collects and processes specified data in real time. The processing is done by different algorithms automatically and the decisions made as a result of the physical system are actually actually executed automatically. By this time we were already talking about an autonomous system and we had reached the level of industry 4.0.

horizontal and Important to establish the level of vertical integration, which gives an idea of the scope and depth of the industry 4.0 application within the company.

Industry 4.0 readiness can be assessed according to the following criteria. The more conditions of the system of conditions are met, the higher the level of maturity of the company's Industry 4.0. In addition to each aspect, metrics and weightings can be defined to aid evaluation. The structure of the proposed criteria, taking into account the objectives and findings described above, is therefore as follows:

- Corporate Governance System - Management System
- Introduced and functioning system e.g. According to ISO 9000
- Applying lean principles
- Continuous improvement
- Application of statistical methods (eg statistical process control)
- Systematic digital data collection and processing
- In-house computer network
    - System administrator
    - User authorization management
    - Storage capacity (server)
    - Other IT infrastructure
- Use of enterprise management software (eg SAP)
    - Process coverage
- High level of IT expertise
    - Software development capability
- High level of mechatronic proficiency
    - PLC programming and industrial control technology
    - Industrial automation
- Networked production equipment

- Automatic collection of production data
- Use of production management software (eg MES)
- Digital twin
  - Real-time data collection
  - Algorithms for automatic processing of collected data
  - Decisions made as a result of data processing are automatically implemented in reality
  - Level of horizontal and vertical integration

Thus, the system of criteria laid down above, with an appropriate weighting procedure associated with it, may already be suitable to provide a starting point for the development of the general methodology to be implemented.

3. SUMMARY

The publication presents the significance of the Industry 4.0 concept in the fields of production and logistics. It has also become clear that the definition of Industry 4.0 readiness and maturity is crucial for an organization or process today. In line with this, some typical models for determining the former are also listed, along with their defining characteristics.

In the second part of the publication, we have summarized the objectives and findings that need to be taken into account in order to define an independent set of criteria that can be the starting point for the development of an evaluation method that does not yet exist. By creating the new method, our goal would be to provide a general-purpose tool for organizations that can be used to determine both Industry 4.0 readiness and maturity in any environment, including logistics applications.

On the one hand, possible future research directions should therefore focus on defining the basic steps of the method, which will allow for the development of more detailed procedures. On the other hand, it may be an important research goal to precisely define the possible user groups, which may be of further help in the precise specification of the processes to be developed. We plan to present these research directions in the framework of further publications.

ACKNOWLEDGEMENT

The described study was carried out as part of the EFOP-3.6.1-16-00011 “Younger and Renewing University – Innovative Knowledge City – institutional development of the University of Miskolc aiming at intelligent specialisation” project implemented in the framework of the Széchenyi 2020 program. The realization of this project is supported by the European Union, co-financed by the European Social Fund.

References: 1. *Tamás, P.:* Application of value stream mapping at flexible manufacturing systems Key Engineering Materials 686 pp 168-173, 2016; https://doi.org/10.4028/www.scientific.net/KEM.686.168 **2.** *Mayer, V., Kenneth Cukier, S.:* Big Data, A revolution that will transform how we live, work, and think, ISBN 978-0-544-00269-2, 2013; **3.** *Illés, B., Tamás, P., Dobos, P., Skapinyecz, R.:* New challenges for quality

assurance of manufacturing processes in industry 4.0, Solid State Phenomena. Vol. 261. Trans Tech Publications Ltd, 2017; https://doi.org/10.4028/www.scientific.net/SSP.261.481 **4.** *Tamás, P., Bányai, T., Illés, B., Tollár, S., Veres, P., Cservenák, A., Hardai, I., Skapinyecz, R.:* Development Possibilities of the High-tech Logistics Laboratory Established at the Institute of Logistics of the University of Miskolc, Journal of Engineering Research and Reports 13(3), pp. 60-68, 2020; https://doi.org/10.9734/jerr/2020/v13i317127 **5.** *Bányai T, Petrillo, A, De Felice, F.:* Industry 4.0 – impact on intelligent logistics and manufacturing, 1st ed. London: Intech Open, 2020; https://doi.org/10.5772/intechopen.76554 **6.** *Colli, M., Madsen, O., Berger, U., Møller, C., Wæhrens, BV.:* Contextualizing the outcome of a maturity assessment for Industry 4.0., Ifac-papersonline vol. 51(11), pp. 1347-1352., 2018; https://doi.org/10.1016/j.ifacol.2018.08.343 **7.** *Caiado, R. G. G., Scavarda, L. F., Gavião, L. O., Ivson, P., Nascimento, D. L. D. M., Garza-Reyes, J. A.:* A fuzzy rule-based industry 4.0 maturity model for operations and supply chain management, International Journal of Production Economics, vol. 231, 2021; https://doi.org/10.1016/j.ijpe.2020.107883 **8.** *Rafael, L. D., Jaione, G. E., Cristina, L., Ibon, S. L.:* An Industry 4.0 maturity model for machine tool companies, Technological Forecasting and Social Change, vol. 159, 2020; https://doi.org/10.1016/j.techfore.2020.120203 **9.** *Ganzarain, J., Errasti, N.:* Three stage maturity model in SME's towards industry 4.0, Journal of Industrial Engineering and Management, 9 (5), pp. 1119-1128, 2016; https://doi.org/10.3926/jiem.2073 **10.** *Bibby, L., Dehe, B.:* Defining and assessing industry 4.0 maturity levels–case of the defence sector, Production Planning and Control, 29 (12), pp. 1030-1043, 2018; https://doi.org/10.1080/09537287.2018.1503355 **11.** *de Souza, S.S., Santiago, S.B., de Amorim Francisco Soares Filho, A., de Mendonça, M.B., Oliveira, F.L.:* Metanalysis of industry 4.0 maturity models, Interciencia, vol. 45 (8), pp. 397-401, 2020.

Ласло Фюко, Бела Іллеш, Петер Тамаш, Роберт Скапінець,
Акош Червеняк, Мішкольц, Угорщина

МЕТОДИ ВИЗНАЧЕННЯ СТУПЕНЯ ЗРІЛОСТІ СИСТЕМ У ПРОГРАМІ "ІНДУСТРІЯ 4.0"

Анотація. *В даний час в виробничих і логістичних системах компаній починають впроваджуватися розробки на основі так званої концепції «Індустрії 4.0», роль якої зростає. З одного боку, ринкова конкуренція породжує цю потребу, але в багатьох випадках використання рішень «Індустрії 4.0» є основною рушійною силою, щоб забезпечити дійсно більш високий рівень автоматизації зі значною економією коштів. Отже, велику користь може принести розробка методології, яка може допомогти у всій галузі визначити рівень розвитку, необхідний для реалізації конкретної розробки «Індустрії 4.0». Часткове створення теоретичних основ є метою даної публікації по створенню такої системи оцінки зрілості в області «Індустрії 4.0». У публікації представлена важливість концепції «Індустрії 4.0» в області виробництва і логістики. Також стало ясно, що визначення готовності і зрілості «Індустрії 4.0» має вирішальне значення для організації процесу сьогодні. Відповідно до цього також перераховані деякі типові моделі для визначення готовності, а також їх визначальні характеристики. У другій частині публікації підсумовані мети і висновки, які необхідно прийняти до уваги, щоб визначити незалежний набір критеріїв, які можуть стати відправною точкою для розробки методу оцінки, якого ще не існує. Створюючи новий метод, метою авторів було надати організаціям універсальний інструмент, який можна було б використовувати для визначення готовності і зрілості «Індустрії 4.0» в будь-якому середовищі, включаючи логістичні додатки. З одного боку, можливі напрямки майбутніх досліджень повинні бути зосереджені на визначенні основних етапів методу, що дозволить розробити більш детальні процедури. З іншого боку, важливою дослідницькою метою може бути точне визначення можливих груп користувачів, які можуть в подальшому допомогти в уточнюванні специфікації розроблюваних процесів.*
Ключові слова: *«Індустрія 4.0»; ощадливість; цифровізація; автономія; зрілість.*

UDC 621.923.6 **doi: 10.20998/2078-7405.2020.93.03**

A. Grabchenko, V. Fedorovich, I. Pyzhov,
Y. Ostroverkh, N. Kozakova, Kharkiv, Ukraine

3D METHODOLOGY OF RESEARCH OF DIAMOND-ABRASIVE MACHINING PROCESS

Abstract. *Subsystem of computer-generated determination of conditions of manufacturing of defect-free diamond wheels and grinding of superhard materials on the base of 3D simulation of deflected mode of elements of the "SHM crystal grain – metal phase – grain – bond" system at process of diamond wheel sintering and grinding is developed.*
Keywords: *simulation; system "Wheel working surface (WWS)-SHM"; grinding; destruction; system "polycrystal - grain - bond".*

1. INTRODUCTION

Superhard polycrystal materials (SHM) and superhard composites on the diamond base (DC) becomes more and more widely used both as a tool material (especially in precision machining processes) and as constructional materials. Laboriousness of their processing is comparable with natural diamonds processing laboriousness.

Now diamond grinding is the most manufacturable process of SHM machining. However, available processes of diamond grinding by means of wheels on organic and metal bonds do not solve in full measure a problem of low productivity (which in 10000 times below, than when processing, for example, alumina ceramics), significant specific consumption of diamond grains (which sometimes is 30 carats of grains on 1 carat of removed allowance) and essential percent of a spoilage because of occurrence of microcracks grid on machined SHM surface. Development of expert system of manufacturing process of diamond-abrasive tool and grinding process of SHM is made on the following algorithm:

- Three-dimensional (3D) simulation of sintering process of diamond-bearing layer for determination of conditions at which integrity of diamond grains is kept;
- Determination of parameters of 3D topography of SHM surface to be machined;
- Determination of parameters of 3D topography of wheel working surface;
- Determination of the actual area of contact in the system "Wheel working surface (WWS)-SHM";

- Simulation of thermo-force deflected mode (DM) of cutting region when processings by means of single-point tools made of SHM;
- 3D simulation of thermo-force deflected mode (DM) of the system "SHM-grain-bond" (determination of the conditions excluding a spoilage owing to SHM cracking);
- Calculation of process intensity of thermoactivated lapping of SHM surface to be machined.

2. THREE-DIMENSIONAL SIMULATION OF DIAMOND-BEARING LAYER SINTERING PROCESS

The task, solved in the process of 3D simulation of DM of sintering zone of diamond-bearing layer of wheel on metal bond is the determination of optimal combination of strength properties of diamond grains and bond, at which integrity retention of diamond grains is provided during diamond wheel sintering process.

Contrary to available ideas, proposed to consider the model of diamond-bearing layer of wheel as perfect one, we have stated, that the structure of diamond layer of the wheels contains initial defectiveness in the form of damaged diamond grains, which can be quantitatively defined by dimensionless value of a damage rate of diamond grains [1].

It is established in N.V.Novikov's work [1], that the particle-size analysis of synthetic diamond grains AC50 400/315, extracted by recuperation from tvesal sample, has shown that during sintering only about 10-20 % of grains remain undamaged. So it is shown, that diamond grain concentration influences deeply on damaging rate of diamond grains when sintering DC. The increase of concentration from 50 up to 150 % raises damageability of diamond grains during sintering process in 2.8 times.

Since the technology of sintering of diamond-bearing layer of the wheel, for example, on hard-alloy bond such as BK, is practically identical one with the technology of sintering of DC, it is objectively to expect, that some part of grains at sintering of diamond wheels are damaged too.

Authors [2] have shown that during of diamond wheel sintering the percentage of the basic fraction (coarse grains) is diminished by 20-30 %.

Moreover diamond grains of various strength, obviously, will be destroyed during sintering in different ways. There is no doubt that structure of metal bond and therefore technological parameters of sintering of wheels will essentially affect a degree of damageability of diamond grains.

Our experimental investigation of diamond grains carried out by means of electrochemical opening of new diamond wheel is shown, that part of diamond grains destroys as early as diamond wheel sintering (fig. 1).

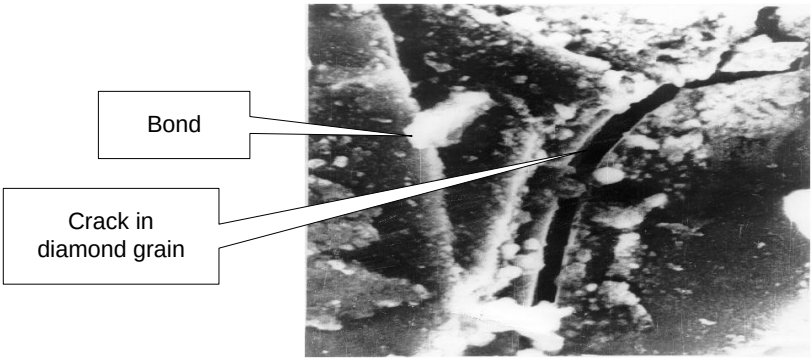

Figure 1 – Diamond grain on the surface of the wheel out of operation

Process of sintering of the diamond grinding wheels was simulated by means of finite element method (FEM) in software package Cosmos-M. At 3D simulation of sintering process the fragment of diamond-bearing layer of wheel was presented as a cube dimensioned 300x300x300 μm, in midpoint of which a diamond grain as an octahedron dimensioned 100x100 μm was placed, that corresponds to 100 % concentration of diamond wheel. At simulation of 50 % diamond grain concentration wheel the size of the cube was redoubled and so on. Metallic phase in diamond grain was simulated as an interlayer of 5-10 μm in thickness and of various form and length. The model was loaded with stress and temperature appropriate to the real process of diamond wheel sintering. It is accepted, that if the reduced stress in diamond grain exceeds ultimate strength it will be considered as destroyed (defective) diamond grain. Sintering process of diamond-bearing layer was simulated for various metal bonds from aluminium up to hard-alloy ones, using diamond grains with various strength from AC2 up to AC160T.

Results of 3D simulation of DM of sintering zone of diamond wheels are presented on fig.2.

Varying combination of diamond grain strength and grain concentration in the wheel for various metal bonds one can determine such their combinations, at which retention of diamond grain integrity was provided i.e. the grains should not be fractured during sintering. It is established, that not all of commercial wheels with usable combination of brand of diamond grains and brand of metal bond can be manufactured with standard concentration of diamond grains without failure of their integrity. So, for example, at sintering of wheel on bond M6-14 with diamond grains of brand AC6 the grain concentration in the wheel should not exceed 7 %, otherwise grains will be fracture as early as wheel sintering. It is shown, that for guaranteed retention of diamond grain integrity practically in all commercial

wheels, their concentration should be much less than applied one. Such tendency coordinates well with possibility and necessity of lowering of diamond grain concentration for wheel up to level of 10-15 % at grinding of superhard materials [3, 4, 5].

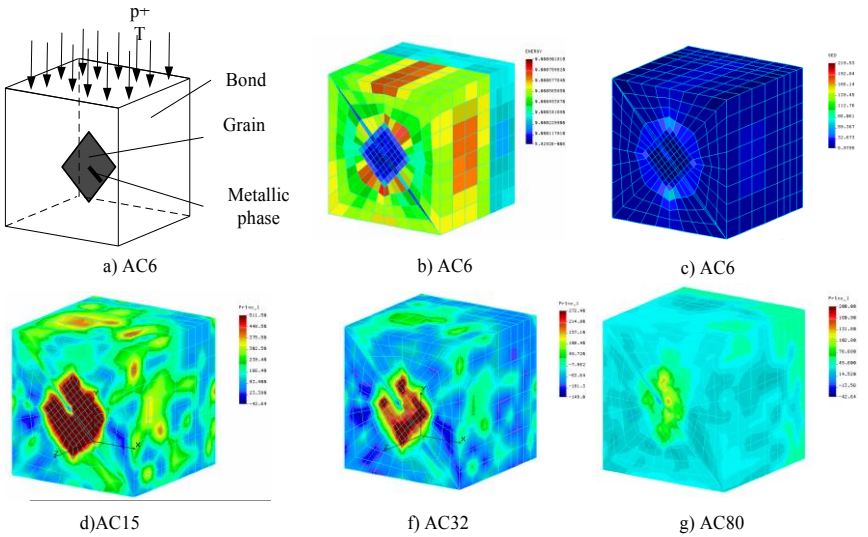

Figure 2 – Influence of grain brand on 3D DM of the system "diamond grain – bond": sintering composition – bond M2-09, graininess 200/160;
a – 3D model of the system "bond – grain – metal phase"; b – energy of deformation; c,d,f – reduced stress, g – strain energy density

It is established, that for retention of diamond grain integrity during sintering of the wheels one must observe combinations of brand of diamond grains and brand of metal bond. Analysis of theoretical computation allows to determine diamond-metal compositions, which ensure integrity of grains in the wheel during the process of its manufacturing (table 1).

Suggested values of concentration in such wheels are less than ones used in commercial wheels, that is important factor of reducing of cost both the diamond wheels and grinding processes.

Thus, at the first stage of the investigations the optimal combinations of strengths of metal bond and diamond grains with their maximum concentration limit in the wheel providing retention of diamond grain integrity during diamond wheel production are established. Optimal relation of strengths of bond, diamond grains and grain concentration, obtained at this stage, are only limiting parameters

and should be determined more precisely for diamond grinding process depending on strength properties of material to be machined.

Table 1 – Diamond-metal compositions suggested for sintering

Grain brand	Coefficient of elasticity of bond, GPa	Graininess, μm	Concentration, %
AC2	40-52	50/40-63/50	5-7
AC4	44-70	50/40-80/63	5-10
AC6	77-95	50/40-100/80	10-16
AC15	86-100	80/63-100/80	15-21
AC32	98-110	80/63-125/100	18-25
AC50	102-119	100/80-160/125	25-28
AC80	143-173	125/100-250/200	25-34
AC100	165-210	125/100-315/250	30-37
AC125	190-260	200/160-315/250	30-40
AC160	210-320	250/200-500/400	35-45

After obtaining of the prescribed limits one should determine optimal combination of strengths of material to be machined, bond, diamond grains and grain concentration in the wheel, which provides maximal efficiency of grinding process. During exploitation optimal combination of strengths of bond, diamond grains and grain concentration is determined depending on strength properties of material to be machined. For this purpose the methodology of 3D simulation of DM, only for grinding zone, will be used too.

3. DETERMINATION OF PARAMETERS OF 3D TOPOGRAPHY OF SHM SURFACE TO BE MACHINED AND WWS

The parameters of 3D topography of WWS were studied by means of laser scanning device "Perthometer S8P" with laser sensor of FOCODYN model, range of vertical resolution of which is ±250 μm, that it is quite enough for measurement of height parameters of WWS for the wheels of graininess up to 630/500. The device allows simultaneously to fix 9 parameters, selected from 86 possible parameters of WWS topography. To estimate topography of diamond grains submicrorelief the scanning pitch of WWS was accepted to be equal 1 μm, i.e. the ray passes some dozens times on each diamond grain [6].

Determination of parameters of 3D topography of SHM surface to be machined was carried out with using the profilograph of "Hammelwerke" corporation, "Turbo Roughness V3.32" model, needle radius is 2 μm.

The examples of 3D topography of SHM and WWS surfaces are shown on fig. 3. The outcomes of study of the parameter of the relative reference area of the

profile t_{ps} are used at experimental determination of the actual area of contact in the system "SHM-WWS" [7]. Since at diamond grinding of SHM the hardness of material to be machined is practically equal (without taking into consideration anisotropy of diamond crystallite properties) to hardness of diamond grains and their intrusion in material to be machined infinitesimally small, the measurement of parameter t_{ps} was realized only at level 0.1-1 μm from a line of peaks.

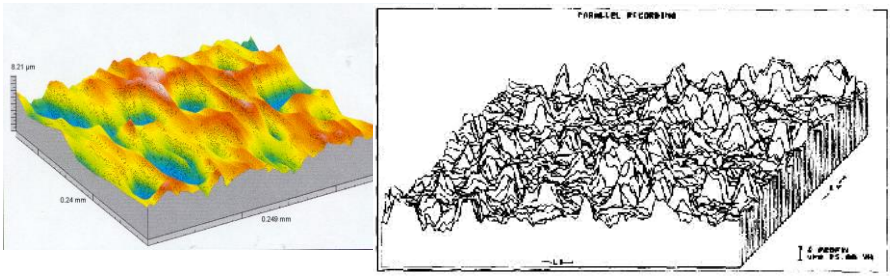

Figure 3 – 3D topography of the surface
a) WWS; b) SHM

Mean value of parameters t_{ps} for WWS and SHM are accepted as actual area of contact (Ar).

$$Ar = \frac{t_{ps}^{Ðï Ê} + t_{ps}^{ÑÒï ì}}{2}$$

Theoretical computation of actual area of contact in the system "SHM-WWS" is carried out using dependences of N.B.Demkin and I.V.Kragelskiy [5].

4. THREE-DIMENSIONAL SIMULATION OF DEFLECTED MODE OF GRINDING AREA

Having determined actual area of contact, let's go on to simulation of deflected mode (DM) in the system "SHM-grain-bond". As there is an opinion [1], that the cause of SHM destruction can be the essential difference in coefficients of thermal expansion (CTE) of diamond and metal phase of SHM, DM of studied system was investigated. Theoretical analysis of thermo-force DM of system "Crystallites-metal phase-grain-bond" by means of finite element method (FEM) was carried out in software package of bundled software such as "Cosmos" with application of eight nodal elements SOLID (1847 nods, 1640 elements). The package allows to decide the problem in three-dimensional measurement (3D-simulation), that favourably distinguishes the given technique from used one

earlier by other authors [8,9]. SHM was simulated as set of crystallites of cubic form of dimensions 0.2x0.2x0.2 mm with the metal phase interlayers of dimensions 20x200x200 μm, arbitrary located in it. Calculation scheme of interaction of the system components simulates the most unfavorable grinding variant with mass formation of wear platforms on diamond grains. Calculation scheme of model and 3D stress in the system "SHM-grain" are shown on fig. 4.

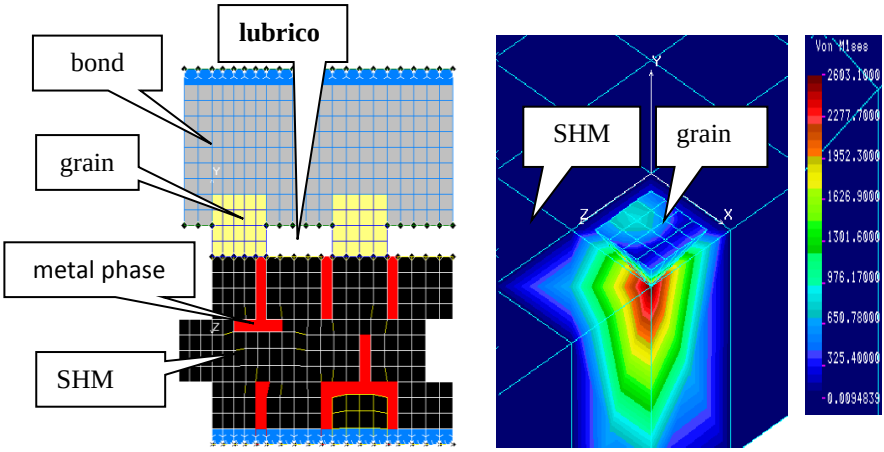

Figure 4 – Finite element calculation scheme of interaction of system "Crystallites-metal phase-grain-bond" (a) and reduced 3D stress in grain and SHM

Advantage of the proposed technique is the possibility in three-dimensional variant (3D-model) to evaluate separately the influence of cross-feed ($S_{c\text{-}f}$), value of normal pressure in contact "WWS-SHM" (P_n), physical-mechanical properties of SHM, diamond grains and bond, temperature in grinding area (in contact "Grain-SHM"), temperature of lubricoolant (or its absence) on temperature fields, value of main and reduced stresses caused by both separately force and thermal factors, and their general effect (thermo-force stress). The package allows also to evaluate strain energy, according to which it is possible, using the Griffith's theory, to determine possibility of formation and development of microcracks both on SHM surface and diamond grains (if they are polycrystallic ones), and development of internal microcracks.

Advantage of the proposed calculation technique is three-dimensional (3D) solution of the problem, obtaining of three-dimensional temperature fields, three-dimensional fields of reduced and main temperature and thermo-force stress in a grain, bond, metal phase and polycrystal.

Possibility of determination of main and reduced thermo-force stress, and also energy of deformation in any point of system " Crystallites SHM-metal phase-grain-bond " allows to use both energy criterion, and force criterion of brittle failure of materials. Using, for example, technique of computer-aided finite element method for prediction of defective layer development at simulation of DM of surface to be machined [9], but, taking into account thus also the thermal factor, is possible to analyze influence of physical-mechanical properties of system components, conditions of grinding and performances of wheels on probability of defect-free machinig of various brands of SHM, including newly created ones.

From the carried out calculations we determine grinding conditions ($S_{c\text{-}f}$, P_n, number of grains in contact, performances of wheel, availability of lubricoolant), at which the probability of formation of defective layer, i.e. reject is eliminated at sharpening the tool made of SHM.

The developed subsystem "Defekt" allows to analyze not only condition of defect-free machining of SHM, but also as the subsystem of the common theoretical expert system allows to optimize process of allowance removal taking account of thermal factor, as it is made, for example, in the work [10], with reference to grinding of glassceramics.

5. CONCLUSIONS

Developed subsystem of theoretical expert system of diamond grinding allows to determine the conditions of defect-free manufacturing of diamond wheels and defect-free machining of SHM at sharpening of tools made of superhard materials.

References: **1.** *Novikov N.V., Maystrenko A.L., Kulakovskiy V.N.* Soprotivlenie razrusheniyu sverhtverdyih kompozitsionnyih materialov. - Kyiv: Nauk. dumka, 1993. - 220 p. **2.** *Kizikov E.D., Vernik E.B., Koshevoy N.S.* Almazno-metallicheskie kompozitsii. - Kyiv.: Tehnika, 1988. - 136 p. **3.** *Fedorovich V.A.* Razrabotka nauchnyih osnov i sposobov prakticheskoy realizatsii upravleniy aprisposablivaemostyu pri almaznom shlifovanii sverhtverdyih materialov: Dis... dokt. tehn. nauk: 05.03.01. - Kharkiv., 2002. - 469 p. **4.** *Grabchenko, A., Fedorovich, V., Pyzhov, I., Babenko, E., Klimenko, V.* Simulation of Grinding Process of Polycrystalline Superhard Materials / Key Engineering Materials Vol. 581 (2014) pp. 217-223. **5.** *János Kundrák, Vladimir Fedorovich, Ivan Pyzhov, Angelos P. Markopoulos* Improving the effectiveness of combined grinding processes for processing superhard materials/ Journal of Manufacturing Processes, Volume 43, Part A, July 2019, pp. 270-275. **6.** *Fedorovich V.A., Rusanov V.V., Kavalets. M., Yankovyak M* Novyie vozmozhnosti izucheniya parametrov rezhuschego relefa almaznyih krugov // Vyisokie tehnologii, razvitie i kadrovoe obespechenie, Kharkiv, NTU "HPI", 2001. pp.214-222. **7.** *Fedorovich V.A., Grinko S.A.* Opredelenie fakticheskoy ploschadi kontakta RPK s obrabatyivaemyim STM //VisokI tehnologIYi v mashinobuduvannI, ZbIrnik naukovih prats HDPU, Kharkiv, 2000, pp 266-272. **8.** *Novikov N.V., Voronin G.A.* Raschet napryazhenno-deformirovannogo sostoyaniya kristallov sinteticheskih almazov metodom konechnyih elementov. - Sverhtverdyie materialyi, 1983, # 1, pp 13-16. **9.** *Kalafatova L.P.* Tehnologicheskie osnovyi povyisheniya effektivnosti obrabotki i obespecheniya kachestva izdeliy iz tehnicheskih stekol i sitallov. Diss.dokt. tehn. nauk: 05.02.08. – Donetsk:DGTU, 2001. – 442 pp.

10. *Burmistrov V.V* Nauchnyie osnovyi nadezhnosti tehnologicheskih sistem almazno-abrazivnoy obrabotki tehnicheskoy keramiki i sitallov. Samara, izd. Diamant-Feniks. 2001. 122 p.

Анатолій Грабченко, Володимир Федорович, Іван Пижов,
Євгеній Островерх, Наталія Козакова, Харків, Україна

3D МЕТОДОЛОГІЯ ДОСЛІДЖЕННЯ ПРОЦЕСУ АЛМАЗНО-АБРАЗИВНОЇ ОБРОБКИ

Анотація. *Запропонована 3D методологія комп'ютерного визначення умов виготовлення бездефектних алмазних кругів та шліфування надтвердих матеріалів (НТМ) яка грунтується на основі тривимірного моделювання напружено -деформованого стану елементів системи «оброблений матеріал - металева фаза - зерно - зв'язка». На першому етапі досліджень встановлюються оптимальні поєднання міцності металевої зв'язки і алмазних зерен з межею їх максимальної концентрації в крузі, що забезпечує збереження цілісності алмазних зерен при виготовленні алмазного круга. Оптимальне співвідношення міцності зв'язки, алмазних зерен і концентрації зерен, отримане на цьому етапі, є лише обмежуючими параметрами і повинні бути визначені більш точно для процесу алмазного шліфування залежно від міцності оброблюваного матеріалу. На другому етапі слід визначити оптимальне поєднання міцності оброблюваного матеріалу, зв'язки, алмазних зерен і концентрації зерна в крузі, що забезпечує максимальну ефективність процесу шліфування. В процесі експлуатації визначається оптимальне поєднання міцності зв'язки, алмазних зерен і концентрації зерен в залежності від міцності оброблюваного матеріалу. Параметри тривимірної топографії робочої поверхні круга (РПК) досліджувалися за допомогою лазерного скануючого пристрою «Perthometer S8P» з лазерним датчиком моделі FOCODYN, діапазон розділення по вертикалі якого, становить ± 250 мкм, що цілком достатньо для вимірювання висотних параметрів РПК. Визначення параметрів тривимірної топографії оброблюваної поверхні НТМ виконувалося на профілографі фірми «Hammelwerke» моделі «Turbo Roughness V3.32», з радіусом голки 2 мкм. Розроблена підсистема «Дефект» дозволяє аналізувати не тільки стан бездефектної обробки НТМ, але і бути як підсистема єдиної теоретичної експертної системи, що дозволяє оптимізувати процес зняття припуску з урахуванням теплового фактора. Розроблена підсистема теоретичної експертної системи алмазного шліфування дозволяє визначати умови бездефектного виготовлення алмазних кругів та бездефектної обробки надтвердих матеріалів при заточуванні інструменту з них.*

Ключові слова: *моделювання; система "робоча поверхня круга - НТМ"; шліфування; руйнування; система "полікристал - зерно - зв'язка".*

UDC 621.923.6 **doi: 10.20998/2078-7405.2020.93.04**

A. Grabchenko, V. Fedorovich, I. Pyzhov,
Y. Ostroverkh, Kharkiv, Ukraine

INCREASE OF EFFICIENCY OF DIAMOND GRINDING SUPERHARD OF MATERIALS

Abstract. *The analysis of algorithm of expert system of process of diamond grinding superhard of materials (SHPM) is given. For realization of the offered expert system the ways of grinding with the combined control of parameters of a working surface of diamond circles are developed.The designed ways of superhard polycrystallic material diamond grinding basing on control of a grinding wheel surface with usage of simulation of destruction processes of the system "polycrysta-grain–wheel bond" considered.*
Keywords: *superhard polycrystallic materials; destruction processes; diamond grinding; wheel working surface; combined direction; system "polycrystal - grain - bond".*

1. THE EXPERT SYSTEM OF THE SHPM GRINDING

A wide spectrum of different brands of superhard polycrystallic materials (SHPM) and nomenclature of diamond wheels hamper experimental definition of optimal conditions of SHPM grinding. It is connected with a great number of experiments and their high cost price. For definition of a range of such conditions the theoretical expert system, permitting to simplify this task, is created. The SHPM diamond grinding is process of mutual controlled destruction of system components "SHPM-grain-bond", and "grain-SHPM" can destroy mainly by friable microdestruction (productive process) or by the thermal-activated processes (ultra precision grinding).

The theoretical description of destruction processes of system units "SHPM-grain-bond" is extremely difficult, and practically it is impossible at raising on new output parameters of grinding. However estimated expert system permitting to narrow down a range of experimental researches for definition of optimal conditions of machining different SHPM by different wheels, can be created. The scheme of such expert system is represented on fig.1.

That the grinding process was steady, it is necessary, that the intensity of grain protrusion height was equal to speed of forced bond deleting ($V_в$). Thus working grain protrusion height from bond (h_p) should eliminate fallout of non-working grains, i.e. the capacity coefficient of grains should be more than 1 ($K_C \geq 1$). Thus h_p should be not less maxheight of bond microroughness ($h_в$) for exception of contact it with processed SHPM. At such working grain protrusion height it is easy to define number of grains in contact with processed SHPM.

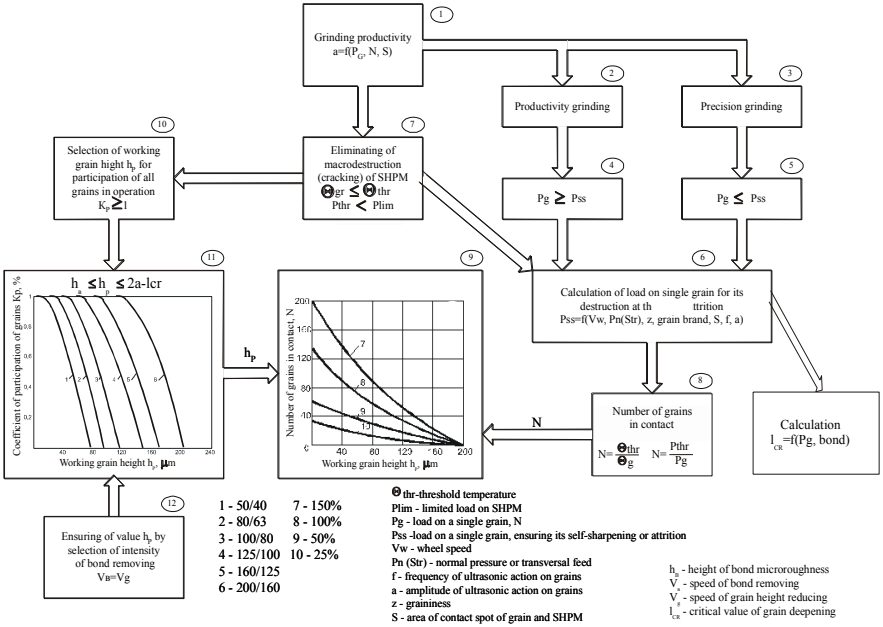

Figure 1 – Scheme of calculation algorithm of optimal SHPM grinding conditions

$$n = \frac{2a \cdot S \cdot K}{\pi \cdot d_{cp}^2} \qquad (1)$$

where $a=h_P/l_G$; l_P - maximal value of a grain; S - single square; K - coefficient of diamond concentration in a wheel; d_{cp} - average grain size.

If the number of grains in contact for serially manufactured wheels is too great (that will not allow to put on each grain load, sufficient for friable self-sharpening of grains and for reason of cracking of a SHPM processed surface), it is necessary to decrease the concentration (for example, till 1-10%).

When we selected the number of grains in contact and received the load on a single grain, we solve the task of definition of diamond grain destruction intensity V_B in case of friable microdestruction in contact (productive grinding) or attrition of grains on wear platforms (ultra precision grinding). Thus the intensity of linear destruction of grains is caused both by contact with processed SHPM (V_{G1}) and ultrasonic effect in a direction zone (V_{B2}). Besides, according to physical-mechanical characteristics of bond, we define intensity "deepening" of grains to bond due to ultrasonic effect in a direction zone (V_{G3}). Then for stability of the

grinding process the speed of bond deleting in a direction zone (V_B) should be equal:

$$V_B=V_{G1}+V_{G2}-V_{G3} \quad (2)$$

The algorithm of such expert system represented on a fig.2.

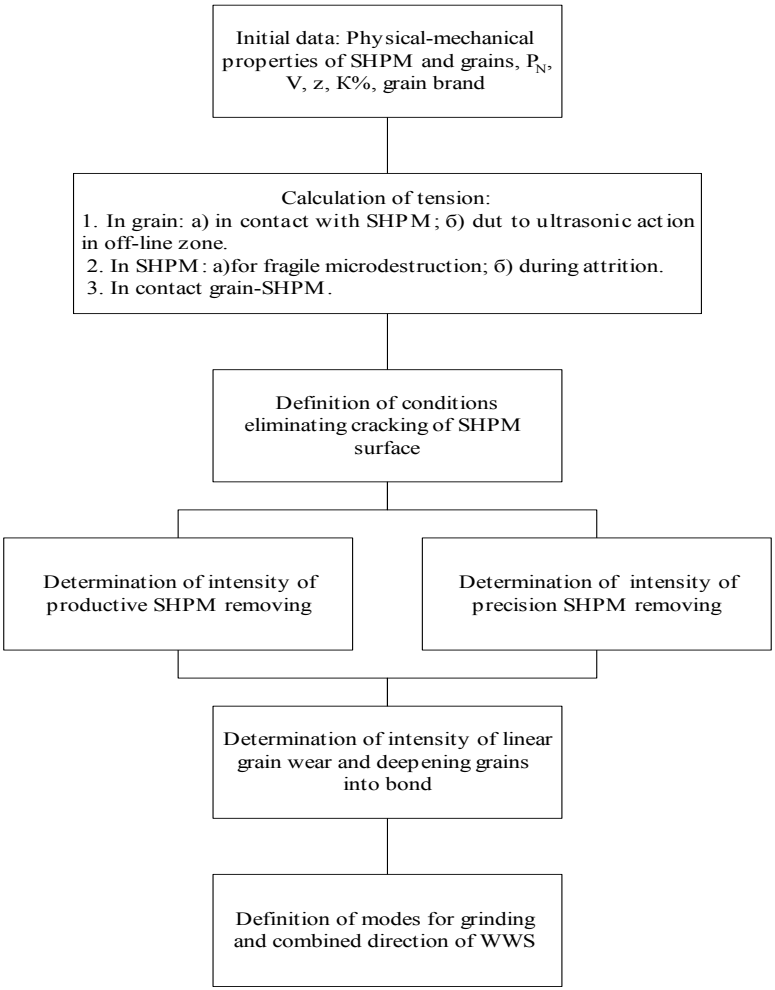

Figure 2 – The block-scheme of expert system

The algorithm of definition of optimal conditions of SHPM diamond grinding (expert system) can be as: analytically we consider the contacting task of a single grain and SHPM surface and define, what conditions for the given SHPM brand will be optimal from the point of view of intensity tolerance removing. It is a grain brand (i.e. its physical-mechanical characteristic, size, orientation of grain to SHPM surface by a "hard" or "soft" plane), speed, contact pressure. Having received load for a single grain, we are set in working grain height $h_B<h_P<2a-l_{CR}$, and having calculated a common maximum safe load, not causing cracking of polycrystal surface, we define maximum safe number of grains in contact. In accordance to assigned h_P and number of grains in contact, we assign optimal concentration in a wheel.

The special ways of diamond grinding are necessary for realization of the developed expert system.

2. WAYS OF SHPM GRINDING WITH COMBINED CONTROL OF A WHEEL CUTTING RELIEF

At the Kharkov State Polytechnic University the ways of diamond grinding with combined direction of a metal-bonded wheel cutting relief have been worked out [1,2,3,4,5].

These ways allow to realize controlled bond removing in an off-line zone (for example, by electroerosional or electrochemical ways) and to realize ultrasonic effect on tops of diamond grains, thus to control character and intensity of their microdestruction. These ways provide double effect on a working surface in an off-line zone. To guarantee constant fragile microdestruction of a diamond grain working surface and to avoid forming of grain wear platforms, the grains are treated by the means of continuous vibrational-shock dressing [6] with required intensity. For continuous and successive introduction of new diamond grains instead of worn out, in an off-line zone the electroerosional or electrochemical removing of bond with intensity, which equals intensity of decrease of grain height, is carried out. Besides, vibrational-shock influence on diamond grains is characterized by effect of deepening of the grains in the bond with intensity V_D, that helps more long-lived holding of grains on a WWS surface. On the basis of such combined direction of wheel cutting relief, we propose three ways of grinding. For all of them the ultrasonic control of developmentness of submicrorelief of diamond grains (fig.3) is proper.

The vibrational influence on the grains is carried out by the means of a plane tool – shocking tool (4) with dimensions 25x25x15, which working surface is equipped by the "tablets" (5) of a superhard material, for example by SKM-R.

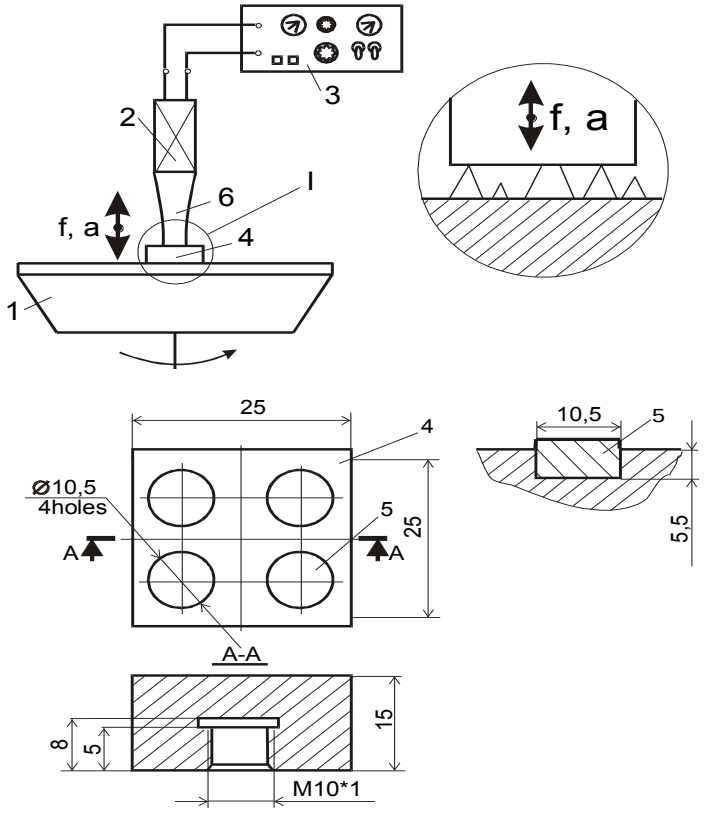

Figure 3 – The scheme of vibrational-shock influence on a wheel working surface in an off-line zone: 1 – diamond wheel, 2 – magnetostrictive vibrator, 3 – ultrasonic oscillator, 4 – working tool, 5 – "tablet" from SHPM, 6 – concentrator

This tool (4) is attached to the concentrator of oscillation (6) of magnetostrictive vibrator (2). The operation of the vibrator is actuated by means of the ultrasonic oscillation generator (3). The calculation of the form and dimensions of the concentrator (6) and the way of the mounting of the shocking tool is realized according to the known method [7]. An oscillation frequency f and amplitude a are defined experimentally depending on required intensity of grain microdestruction.

For SHPM processing based on nitride of boron, when the intensity of a linear wear of diamond grains is rather insignificant, and consequently the intensity of bond removing should also be corresponding, the most simple way of grinding with vibrational-erosive control of WWS by means of the source of a direct current

(fig.4b) can be applied. Electroerosive spark (bond removing) between a metal surface of the shocking tool and the bond takes place owing to the varying gap at vibrations from h_{max} up to h_{min}.

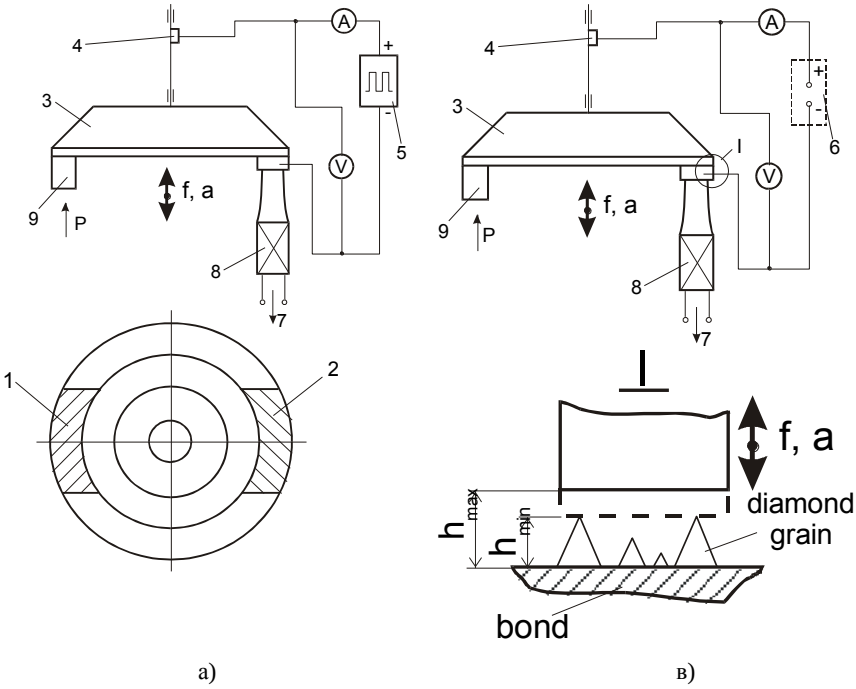

Figure 4 – The ways of grinding with vibrational-erosive control of WWS:
1 – grinding area; 2 – zone of vibrational - erosive control of WWS; 3 – diamond wheel;
4 – current-collector; 5 – pulsing oscillator ШГИ-40-440; 6 – source of a direct current;
7 – to the generator of ultrasonic oscillations; 8 – device of ultrasonic dressing;
9 – machined sample; 10 – shocking tool-electrode

During SHPM processing based on the diamond, when the intensity of a wear of diamond grains is extremely high, and consequently the same intensive directed action on the wheel bond is required, use a source of direct current is not enough. In this case pulsing oscillator ШГИ-40-440 (fig.4a) is applied to erosive control of parameters of WWS. The modes of operations of this generator are defined experimentally, depending on required intensity of directed influence on the wheel bond.

This way has more wide opportunities in comparison with the first one, but it is more expensive.

The way of electrochemical bond dissolution in a control zone has the greatest intensity of bond removing from wheel working surface [8]. Therefore, the way of grinding with vibrational-electrochemical direction of a wheel cutting surface (fig.5) will be the most effective in case of sharpening cutters from SHPM together with steel holder, when besides removing bond, it is also required to remove waste of grinding (metal chip).

In this case there are three zones on the wheel working surface:

- grinding area;
- zone of vibrational control of diamond grain maturity;
- zone of electrochemical control of WWS maturity.

The worked out ways of grinding with combined direction of wheel cutting relief allow to stabilize the process of grinding at any level in a range from productive one up to ultra precision. These ways provide:

- directed microdestruction of tops (wear platforms) of diamond grains due to vibrative-shock influence by means of the shocking tool in an off-line zone;
- deepening of grains into the bond in an off-line zone by means of the ultrasonic shocking tool, that prolongs action period of grains on WWS;
- directed bond removing to ensure entrance of new diamond grains in exchange of worn ones and ones, dropped out from the bond, in operation.

In this case stability of grinding process, that is extremely important in automatized productions, is achieved under condition of:

$$V_B=V_1+V_2+V_3 \qquad (3)$$

where V_B - linear speed of bond removing; V_1 – linear grain wear intensity in a grinding area; V_2 - intensity of destruction of grains in a zone of control; V_3 - intensity of bond "ramming" in the bond in zones of direction and grinding.

Such combined ways of control of a state of wheel working surface allow to use wider potential cutting properties of diamond grains and to increase efficiency of SHPM grinding. In case of disconnect of controlling influences on wheel working surface, on diamond grains in the mass order the wear platforms will be derivated and the process is transformed practically to the process of friction "diamond - diamond" with the removal value on a nanolevel. When using precision equipment under these conditions it is possible to realize ultraprecision grinding of superhard materials.

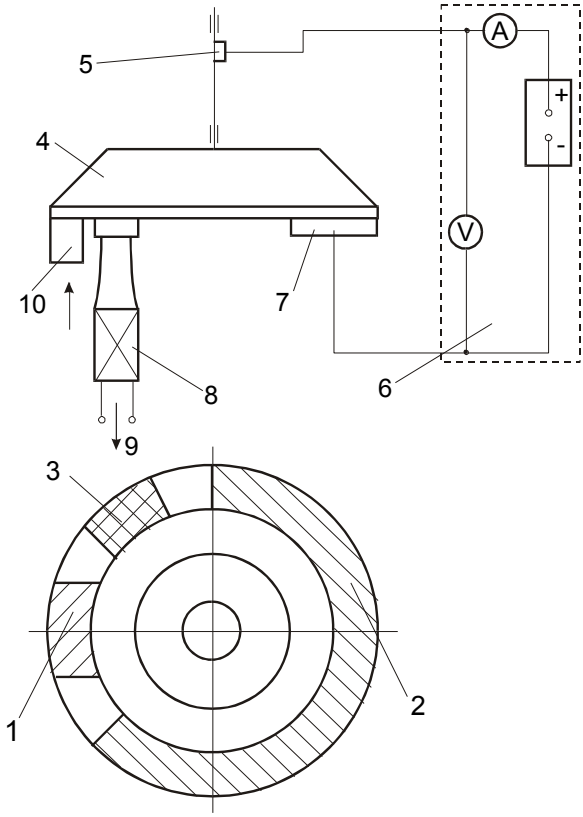

Figure 5 – The way of grinding with vibrational – electrochemical direction of WWS: 1 – grinding area; 2 – zone of electrochemical direction of WWS; 3 – zone of ultrasonic direction of WWS; 4 – diamond wheel; 5 – current-collector; 6 – source of a direct current; 7 – cathode device; 8 – device of ultrasonic dressing; 9 – to the generator of ultrasonic oscillations; 10 – machined sample

References: 1. *Kundrák, J., Fedorenko, D.O. Fedorovich, V., Fedorenko, E.Y., Ostroverkh, E.V.* Porous diamond grinding wheels on ceramic binders: Design and manufacturing/ Manufacturing Technology 2019, Vol. 19, No. 3, pp 446-454. **2.** *A.I. Grabchenko, V.A. Fedorovich, I. Pyzhov, J. Kundrak.* 3D simulation of Vibrating Diamond Grinding / Manufacturing Technology June 2014, Vol. 14, № 2. pp. 153 – 160. MK CR E 20470 ISSN 1213–2489; **3.** *Grabchenko, A., Fedorovich, V., Pyzhov, I., Babenko, E., Klimenko, V.* Simulation of Grinding Process of Polycrystalline Superhard Materials / Key Engineering Materials Vol. 581 (2014) pp 217–223. Trans Tech Publications, Switzerland. **4**. *Mamalis, A.G., Grabchenko, A.I., Fedorovich, V.A., Paulmier, D., Horvath, M.* Development of an expert system of diamond grinding of superhard polycrystalline materials considering grinding

wheel/International Journal of Advanced Manufacturing Technology. 2001, pp .498-507; **5.** *V.A.Fedorovich.* The ways of grinding with combined control of cutting wheel relief. Kharkov, MicroCAD`99, 1999; **6.** *Wilks E.M. and Wilks I.* Experiments on the grinding and polishing of diamond. I.D.R., 1966. V.26. №304. **7.** *V.A.Fedorovich, S.A.Grinko.* Algorithm of interaction model of system elements "SHPM-grain" during grinding. Kharkov, Cutting and Tools, 1999, Vol.53. **8.** *V.A.Fedorovich.* Specific consumption and specific wear of diamond grains during SHPM grinding. Kharkov, Cutting and Tools, 1999, Vol.54.

Анатолій Грабченко, Володимир Федорович, Іван Пижов,
Євгеній Островерх, Харків, Україна

ПІДВИЩЕННЯ ЕФЕКТИВНОСТІ АЛМАЗНОГО ШЛІФУВАННЯ НАДТВЕРДИХ МАТЕРІАЛІВ

Анотація. *Для реалізації запропонованої експертної системи розроблені способи шліфування з комбінованим управлінням параметрами робочої поверхні алмазних кругів. Розроблено способи алмазного шліфування надтвердих полікристалічних матеріалів з управлінням робочою поверхнею шліфувального круга на основі моделювання процесів руйнування в зоні обробки. Розроблені раніше способи шліфування з автономним управлінням ріжучим рельєфом кругів (РРК) істотно розширюють технологічні можливості алмазного шліфування. Однак недоліком цих методів, особливо при шліфуванні надтвердих полікристалічних матеріалів, є те, що при масовому виникненні на РПК площадок зносу, які стають обмежуючим фактором процесу шліфування, такі зерна примусово видаляються зі зв'язки. Такий процес істотно знижує коефіцієнт використання потенційно високих ріжучих властивостей алмазних зерен і збільшує їх питомі витрати. Отже, постає завдання управління процесом утворення площадок на зернах, тобто забезпечити їх крихке мікроруйнування з утворенням субмікрокромок. Запропоновані авторами способи передбачають подвійний вплив на робочу поверхню в автономній зоні. Для забезпечення постійного крихкого мікроруйнування робочої поверхні алмазних зерен і виключення утворення на них площадок зносу вони піддаються безперервній вібраційній правці з необхідною інтенсивністю. А для безперервного послідовного введення в роботу все нових алмазних зерен замість зношених, в автономній зоні здійснюється електроерозійне або електрохімічне видалення зв'язки з інтенсивністю, рівною інтенсивності зносу зерен. Такі комбіновані методи управління станом робочої поверхні кругів дозволяють більш повно використовувати потенційні ріжучі властивості алмазних зерен і підвищити ефективність шліфування надтвердих матеріалів. При відключенні управляючих впливів на робочу поверхню круга, на алмазних зернах в масовому порядку утворюються площадки зносу і процес трансформується практично в процес тертя «алмаз-алмаз» з величиною знімання на нанорівні. При використанні прецизійного (надточного) обладнання в цих умовах можна реалізувати ультрапрецізійне шліфування надтвердих матеріалів.*

Ключові слова: *надтверді полікристалічні матеріали; процеси руйнування; алмазне шліфування; робоча поверхня круга; комбінована схема; система "полікристал - зерно - зв'язка"***.**

UDC 621.825.7 **doi: 10.20998/2078-7405.2020.93.05**

V. Kurgan, I. Sydorenko, V. Litvinov, V. Vaysman,
K. Kirkopulo, V. Kulik, Odessa, Ukraine

MATHEMATICAL MODELING OF TRANSMISSION START WITH AN ASYNCHRONOUS ELECTRIC MOTOR

Abstract. *The most difficult moment in the work with an asynchronous motor is the launch. And the more powerful drive is the more difficult launch. This is due to certain features of the asynchronous motors: a limited starting torque and starting throws of the current of the stator motor chain.*
The mathematical modeling of oscillating process of actuation of the actuator with an asynchronous motor, which includes an elastic coupling with nonlinear mechanical feedback, is carried out. The influence of the type of elastic characteristics of the coupling on the magnitude of the amplitude and frequency of the oscillation process and its time was studied. A single-mass rotational system model was used for the studies. According to the Runge-Kutta method, the oscillation processes of starting the transmission of a machine unit with an induction motor were investigated. To determine the coefficient of vibration isolation, a system with an elastic coupling having a linear elastic characteristic was calculated. A study was also conducted in the case where the coupling determines the elastic characteristics of the Duffing type "soft" and "hard" type.
Keywords: *elastic coupling; mechanical feedback; elastic characteristic; oscillation process; rotational mass; starting torque.*

1. INTRODUCTION

In modern machine-building, elastic couplings with metal elastic elements have become widespread. This is facilitated by the ability of these devices not only to transmit torque, but also to prevent negative oscillations in the technical system. This is achieved by introducing into the design an elastic coupling of mechanical feedback, which provides a wide range of elastic characteristics, including also nonlinear. Studies in this direction have shown that the nonlinearity of the elastic characteristics of one of the components of the machine aggregate can significantly change the nature of the oscillating processes, which occur.

2. PROBLEM STATEMENT

Studies using mathematical model proved that elastic couplings with a nonlinear elastic characteristic show the most positive results [1]. However, already existing elastic couplings do not fully meet the stated requirements due to their narrow working range [2-4]. Up to now created potential designs of elastic couplings that implement a nonlinear elastic characteristic are not widely used due to the small number of their actual mechanical constructions.

3. ANALYSIS OF RECENT RESEARCH AND PUBLICATIONS

At this stage, most of drives use asynchronous motors. The features of their operation, specifically the startup of the engine, cause the considerable oscillatory load on the drive, this is due to the large and short-term starting torque. Because of this, there is a significant number of works devoted to oscillating starting torque. Because of this, there is a significant number of works devoted to oscillating processes in technical systems [5-8]. A mathematical modeling of the start of an asynchronous electric motor was carried out by using software packages [9,10]. Developed the promising designs of nonlinear elastic couplings, which reduce the load on the drive and prevent negative oscillations [11]. The following studies show the feasibility of using elastic couplings with nonlinear mechanical feedback.

4. OBJECTIVES AND PROBLEMS OF RESEARCH

Mathematical modeling of oscillatory process of transmission starting of a machine assembly with an asynchronous electric motor, which consist of an elastic coupling with nonlinear mechanical feedback and studying the effect of elastic characteristics on the magnitude of the amplitude, frequency of the oscillatory process and its time.

5. RESULTS OF THE STUDY

The chosen aim of the research is based on the fact that the results of the researches carried out in the field of nonlinear oscillation mechanics indicate that the nonlinearity of the elastic characteristics of one of the components of the machine assembly can significantly change the nature of oscillatory processes.

In the given research area it is believed that the starting torque M_{start} of the asynchronous motor shaft is a torque that advances on the shaft of an asynchronous electric motor under the following conditions: the speed of rotation is equal to 0, the current has a constant value, the electric motor windings are connected to rated supply frequency and voltage, the winding connection corresponds to the rated operating mode of the electric motor.

In mathematical modeling of the oscillatory processes of the machine assembly, the starting torque $M_s(t)$ is modeled by a function of time characterized by two time intervals: the build-up time t_1 to the maximum value and the time of decrease to the rated value t_2. In order to calculate the maximum starting torque the following expression is used

$$M_{\max} = M_r \cdot k_{tr}, \qquad (1)$$

where M_r – rating moment on the electric motor shaft; k_{tr} – starting torque ratio. The value of this parameter varies within 1,5…6 for different types of engines and loads.

Duration of the starting torque is determined experimentally, depending on the type of engine and the type of its load. Usually the value of this parameter varies within 0,5...1,6 s.

In order to achieve this goal a two-mass rotatory mechanical system (J_1 – main rotating mass, subject to protection against the negative demonstration of the starting torque), which includes the proposed passive elastic coupling with a nonlinear mechanical linkage (J_2 – the second rotating mass, which is the mass of the coupling) should be subject to mathematical modeling. In this case the system of differential equations has the following form

$$\begin{cases} J_1\ddot{\varphi}_1 + b_1\dot{\varphi}_1 - b_2(\dot{\varphi}_2 - \dot{\varphi}_1) + c_1\varphi_1 - c_2(\varphi_2 - \varphi_1) = 0 \\ J_2\ddot{\varphi}_2 + b_2(\dot{\varphi}_2 - \dot{\varphi}_1) + c_2(\varphi_2 - \varphi_1) = M_s(t) \end{cases}. \quad (2)$$

However, the rotating mass of the J_2coupling in several cases is less than the rotating mass of J_1 transmission objects ($J_2 >> J_1$) and the stiffness of the shaft sections, which determines the torsion angle φ_1, is several times greater than the stiffness of the elastic coupling, which determines the torsion angle $\varphi_1(\varphi_2 >> \varphi_1)$.

Taking this into account it is advisable to carry out mathematical studies of the process of transmission starting of a machine assembly with an asynchronous electric motor, which includes the proposed elastic coupling, using a mathematical model of a single-mass rotatory system. In this case, the model treats the rotating mass J_1 as an object to be protected from the negative demonstration of the starting torque, and the elastic coupling is considered as an elastic linkage between it and the engine. Then the corresponding differential equation will have the following form

$$J\ddot{\varphi} + M_{el}(\varphi) + M(\dot{\varphi}) = M_s(t), \quad (3)$$

where J – moment of inertia of the rotating mass; $M_{el}(\varphi)$ – elastic characteristic, which depends on the stiffness of elastic elements applied in the coupling; $M(\dot{\varphi})$ – moment of dissipation, which determines the irreversible energy dissipation; $\dot{\varphi}$ and $\ddot{\varphi}$ – corresponding derivatives of the angular displacement in time t.

Initial conditions are as follows

$$\varphi(0) = 0,\ \dot{\varphi}(0) = 0,\ M_s(0) = 0. \quad (4)$$

On the basis of the equation (3) mathematical modeling of the oscillatory processes of transmission starting of a machine assembly with an asynchronous

electric motor AIR112MV6 with the following characteristics was carried out: P = 4 kW, n = 1000 rpm; rating moment M_{rat} = 34,5 N□m; starting torque ratio k_{tr} = 1,8; time of the starting torque t_s = 0,8 s.

$$\begin{aligned} &t_{s1} = 0...0{,}26\text{s}, && M_{mot} = M_{s1}(t) = 162299t^2 + 6312{,}1t + 3{,}4857; \\ &t_{s2} = 0{,}26...0{,}8\text{s}, && M_{mot} = M_{s2}(t) = 16229t^2 - 4512{,}1t - 2{,}5734; \\ &t_s > 0{,}8\text{s} && M_{mot} = M_r = 34{,}5\text{N}\cdot\text{m} \end{aligned} \quad (5)$$

In calculations the starting torque is presented in the form of two non-linear sections associated with time and has a maximum M_{smax}(0,026)=61 N□m (fig. 1, a).

For the possibility of conducting a comparative analysis in order to determine the appropriate efficiency ratios the calculation of the accepted conditions of the system, which containsan elastic coupling with a linear elastic characteristic, was carried out (fig. 1, b). Using the Maple 18 mathematical package, where the corresponding function implements the Runge-Kutta method, the solution of equation (3) was carried out in numerical form taking into account the initial conditions (4) and external load (5), which made it possible to state the following. Emerging at the process of starting a transmission of a machine assembly with an asynchronous electric motor, the oscillatory process is fading and low frequency with a constant frequency T = 2 Hz (fig. 1, c). Oscillatory processes with the frequency of the first frequency octave, that is T = 2, 4, 8, 16, 31,5 and 63 Hz, refer to the low-frequency oscillatory process. The response of the system to external disturbance in the form of M_{J1} = 59,3 N□m occurs with the delayafter the appearance of the maximum external load equal to t^* = 0,18 s, which is due to the presence of an elastic linkage. Oscillation decay time under condition of $M_{J1} = M_r$ equals t = 6,7s.

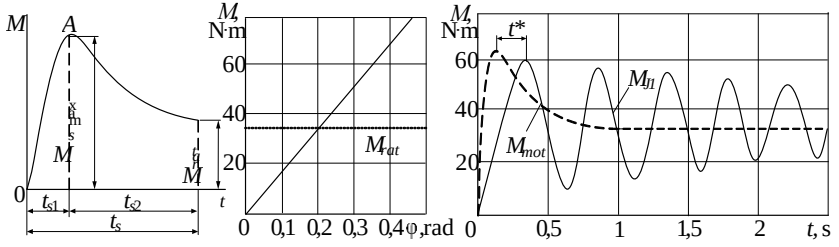

a) b) c)

Figure 1 – Modelling of oscillatory processes of transmission starting of a machine assembly: starting torque (a); linear elastic characteristic (b); oscillatory process of transmission starting of a machine assembly with a couplingthat possesses linear elastic characteristic

The coefficient that determines the efficiency of using an elastic coupling with a linear elastic characteristic is the coefficient of vibration isolation

$$k_R = \frac{M_0}{A_0}, \tag{6}$$

where M_0 – amplitude of the moment behind the coupling; A_0 – amplitude of the moment of disturbance.

In this case the coefficient of vibration isolation is

$$k_R = \frac{M_0}{A_0} = \frac{59{,}3}{61} = 0{,}97. \tag{7}$$

Numerical solution of the equation (3), taking into account the general parameters of the system, the initial conditions (4) and the external load (5), is carried out in cases where the elastic characteristic of the coupling is nonlinear.

In the first case the coupling determined an elastic characteristic of a "soft" Duffing type. The value of the elastic torque at a certain nominal torsion angle of half-couplings φ = 0,2 rad was equal to the value of the elastic torque of the previously considered linear characteristic M = 34,5 N□m (fig. 2, a).

Emerging at the start of the transmission of the machine assembly with an asynchronous electric motor, the oscillatory process is fading and low frequency with frequency T, which increases over time (fig. 2, b).

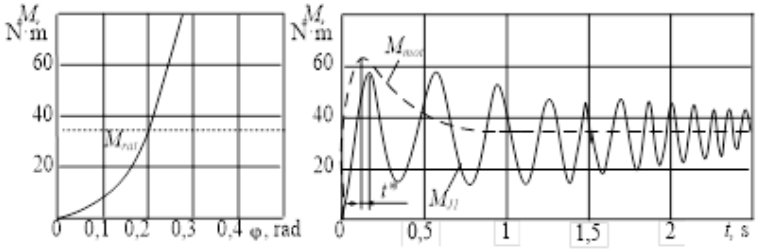

a) b)

Figure 2 – Oscillatory process of asynchronous motor starting: elastic characteristic of a “soft” Duffing type coupling (a); oscillatory process (b)

The response of the system to external disturbance in the form of M_{J1} = 57,23 N□m occurs with the delay after the appearance of the maximum external load equal to t^* = 0,38 s, which is defined by the value of the elastic torque, that is less

than the similar one in the linear system, and lays in the range of the torsion angle of the half-couplings equal to φ = 0,2…0,6 rad. Oscillation decay time, which is determined by $M_{J1} = M_r$, equals t^* = 3,8 s. The coefficient of vibration isolation k_R in this case is

$$k_R = \frac{M_0}{A_0} = \frac{57{,}34}{61} = 0{,}94\,. \qquad (8)$$

In the second case the coupling determined an elastic characteristic of a "hard" Duffing type. The value of the elastic torqueat a certain nominal torsion angle of half-couplings φ = 0,2 rad was equal to the value of the elastic torque of the previously considered linear characteristic M = 34,5 N□m (fig. 3,a).

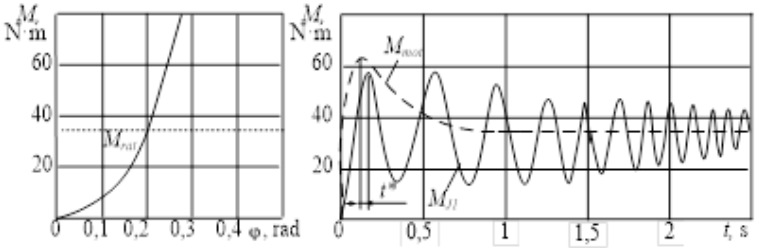

a) b)

Figure 3 – Oscillatory process of asynchronous motor starting: elastic characteristic of a "hard" Duffing type coupling (a); oscillatory process (b)

Emerging at the start of the transmission of a machine assembly with an asynchronous electric motor, the oscillatory process is fading and low frequency with a frequency T decreasing over time (fig. 3, b). The response of the system to external disturbance in the form of M_{J1} = 59,16 N□m occurs with the delay after the appearance of the maximum external load equal to t^* = 0,16 s, which is defined by the value of the elastic torque, that is higher than the similar one in the linear system, and lays in the range of the torsion angle of the half-couplings equal to φ = 0,2…0,6 rad. The decay time of the oscillatory process is determined by $M_{J1} = M_r$ and equals t = 3,4 s. The coefficient of vibration isolation k_r in this case is

$$k_R = \frac{M_0}{A_0} = \frac{59{,}13}{61} = 0{,}96\,. \qquad (9)$$

Results of mechanical studies conducted to optimize the oscillatory process during the starting of transmissions with an asynchronous motor show that the use

of nonlinear couplings with elastic characteristics of a "hard" Duffing type can reduce the time of the oscillatory process, however itdetermines the transmission load close to the starting torque. Application of nonlinear couplings with elastic characteristics of a "soft" Duffing type allows slight reduction of the transmission load, at the same time it lengthens the time of the oscillatory process. Taking this into account it is proposed to use nonlinear couplings with a combined characteristic in order to solve such a problem. The basis for such a proposal is the results of research done by professor G.V. Arkhangelskiy [12]. It has been established that optimization of the oscillatory process occurring at the start of transmission with an asynchronous motor can be obtained by applying a nonlinear elastic coupling in the transmission, which implements a combined characteristic with two sections, determined by the value of the rating rotary moment. The first section ($M = 0 \ldots M_r$) must correspond the elastic characteristic of the "soft" Duffing type and the second section ($M = M_r \ldots 1{,}3M_s$) must relate with the elastic characteristic of the "hard" Duffing type. The researcher has proposed a specialized design of an elastic coupling that implements a similar characteristic, but because of structural constraints its elastic characteristic corresponds to the target characteristic with a compliance coefficient equal to $k_c = 0{,}89$ and is fragmentarily linear (line 1, see fig. 4, a).

From this perspective the calculations of the oscillatory process during the start of the transmission with the asynchronous motor, while applying the proposed coupling both with mentioned above elastic characteristic (combined, type 1) and with the synthesized target characteristic with the coefficient of compliance k_c = 0,99 (hereafter combined, type 2) have been carried out. The synthesized elastic characteristic consists of the corresponding nonlinear sections that share borders at a certain value of the elastic torque and determine the rating rotary moment of half-couplings φ = 0,2 rad. (curve 2, fig. 4, a). Emerging at the start of the transmission of a machine assembly with an asynchronous motor in two calculation cases the oscillatory process is fading and low frequency with the frequency *T*, which varies over time (fig. 4, b).

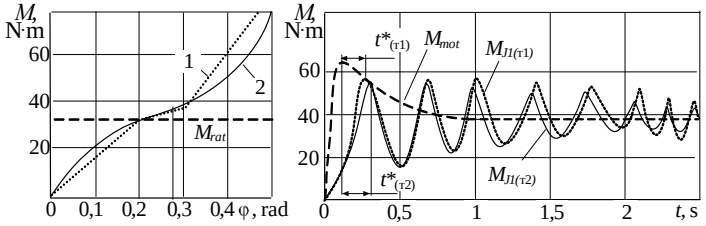

a) b)

Figure 4 – Oscillatory process of asynchronous motor starting: combined elastic characterictics (a); oscillatory process (b)

The response of the system to external disturbance in the form of $M_{J1(t1)}$ = 56,26 N□m occurs with the delay after the appearance of the maximum external load in the first case equal to $t^*_{(t1)}$ = 0,18 s and in the second $M_{J1(t2)}$ = 56,26 N□m with the delay equal to $t^*_{(t1)}$ = 0,21 s.

Thus it is established that the average value of the elastic torque lays in the range of the torsion angle of the half-coupling φ = 0,2…0,6 rad, which is higher than in the linear system and less than in a system with a "hard" Duffing type characteristic. The decay time of the oscillatory process is determined by $M_{J1} = M_r$ and in the first case $t_{(t1)}$ = 3,18 s, while in the second case $t_{(t2)}$ = 2,8 s, being the smallest indicators in the performed calculations. This is due to the fact that at high amplitudes of oscillations elastic characteristics cause an increase in their frequency. This, in turn, indicates the presence of high velocities and the greater effect of dissipative forces than in the previously considered variants. In this case the coefficient of vibration isolation k_R for the first calculation is as follows and for the second calculation

$$k_R = \frac{M_0}{A_0} = \frac{56{,}79}{61} = 0{,}931, \tag{10}$$

$$k_R = \frac{M_0}{A_0} = \frac{56{,}13}{61} = 0{,}92. \tag{11}$$

Table 1 – Coefficients of vibration isolation k_R and oscillation decay time at the start of the transmission with asynchronous motor with an elastic coupling

Type of elastic characteristic of coupling	Coefficient of vibration isolation k_R	Oscillation decay time t, (s)
Linear	0,98	6,7
"Soft" Duffing type	0,94	8,3
"Hard" Duffing type	0,96	3,4
Combined, type 1	0,93	3,2
Combined, type 2	0,92	2,8

The results of the conducted analytical studies are presented in the table 1.

6. CONCLUSIONS

Implementation of elastic characteristics of the "soft" Duffing type of the

coupling in comparison with the case of implementation of a linear elastic characteristic of the coupling enables reduction of negative demonstrations of oscillations by 3...4%, however it leads to an increase in duration of oscillatory process 1,5...2 times. Implementation of elastic characteristics of the "hard" Duffing type of the coupling in comparison with the case of implementation of a linear elastic characteristic of the couplingallows to reduce the negative demonstrations of oscillations by 2...3% and leads to a decrease in duration of oscillatory process 1,5...2 times.

Results of research of prof. G.V. Arkhangelskiy conserning optimization of oscillatory process in case of start of transmission of a machine assembly with an asynchronous motor using elastic coupling with a combined nonlinear elastic characteristic have been confirmed. Mathematical modeling of the system starting with the proposed coupling structure, which implements the target characteristic in the form of a fragmentarily linear characteristic with a compliance coefficient k_c = 0,89, resulted in a decrease of negative demonstration of oscillations by 5...6% and reduction of the time of oscillatory process 1,5...2,5 times, comparing with the case of realization of a linear elastic characteristic by a coupling.

Mathematical modeling of the system starting using an elastic coupling with a mechanical feedback that implements a nonlinear target combined characteristic with a compliance coefficient k_c=0,98 caused a decrease of negative demonstration of oscillations by 7...10 %, and reduction of the time of oscillatory process 2,8...3 times, compared with the case of realization of a linear elastic characteristic by a coupling.

References: 1. *I. Sydorenko, V. Kurgan* Synthesis of target elastic characteristics on the basis of elastic move with nonlinear mechanical refractory connection. Bulletin of the Khmelnytsky National University, 2017, no. 5(2), pp. 26-31. **2.** *Szolc T., Konowrocki R.* Influence of Various Control Strategies on Transient Torsional Vibrations of Rotor-Machines Driven by Asynchronous Motors. In: Cavalca K., Weber H. (eds) Proceedings of the 10th International Conference on Rotor Dynamics – IFToMM. IFToMM 2018. Mechanisms and Machine Science, 2019, vol 63. Springer, Cham. **3.** *Wang L., Jia Z.* Analysis of the Soft Starting of Adjustable Speed Asynchronous Magnetic Coupling Used in Belt Conveyor. Communications in Computer and Information Science, 2018, vol 923. Springer, Singapore. **4.** *Zhang Q., Lu Q.* Analysis on Rigid-Elastic Coupling Characteristics of Planar 3-RRR Flexible Parallel Mechanisms. Lecture Notes in Computer Science, 2017, vol 10463. Springer, Cham. **5.** *V. Olshanskiy, V. Burlaka* Free oscillations of an oscillator with nonlinear positional friction. Ukrainian Journal of Mechanical Engineering and Materials Science, 2018, no. 4(2), pp. 50-57. **6.** *Hmida A., Hammami A.* Modal Analysis of Spur Gearbox with an Elastic Coupling. Applied Condition Monitoring, 2017, vol 5. Springer, Cham. **7.** *X. Chen, J. Hu* Bifurcation and chaos analysis of torsional vibration in a PMSM-based driven system considering electromechanically coupled effect, Nonlinear Dynamics, 2017, no. 88, pp. 277–292. **8.** *A. Andrukhiv, B. Sokil* Asymptotic method in

investigation of complex nonlinear oscillations of elastic bodies, Ukrainian Journal of Mechanical Engineering and Materials Science, 2018, no. 4(2), pp. 58-67. **9.** *A. Andrukhiv, B. Sokil* Resonant phenomena of elastic bodies that perform bending and torsion vibrations, Ukrainian Journal of Mechanical Engineering and Materials Science, 2018, no. 4(1), pp. 65-73. **10.** *Wang C., Sun Q.* Analysis on Asynchronous Start Permanent Magnet Synchronous Motor Cogging Torque Optimization Based on Equivalent Magnetic Motive Force, Lecture Notes in Electrical Engineering, 2018, vol 423. Springer, Singapore. **11.** *Nitzan S., Zega V.* Self-induced parametric amplification arising from nonlinear elastic coupling in a micromechanical resonating disk gyroscope. 2015, Sci Rep 5**,** 9036, doi:10.1038/srep09036. **12.** *G. Arkhangelsk* Efficiency of using an elastic coupling with an extended section of quasi-zero stiffness. Machine parts, 2015, no. 51, pp. 17-22.

Віктор Курган, Ігор Сидоренко, Володимир Літвінов, Владислав Вайсман, Катерина Кіркопуло, Володимир Кулік, Одеса, Україна

МАТЕМАТИЧНЕ МОДЕЛЮВАННЯ ПУСКУ ТРАНСМІСІЇ З АСИНХРОННИМ ДВИГУНОМ

Анотація. *Найскладнішим моментом в роботі приводу з асинхронним електродвигуном є запуск. І чим потужніший привід - тим цей запуск складніший. Це пов'язано з певними особливостями асинхронних двигунів: обмеженого пускового моменту і пускових кидків струму ланцюга статора двигуна. В роботі проведено математичне моделювання коливного процесу пуску приводу з асинхронним електродвигуном, до складу якої входить пружна муфта з нелінійним механічним зворотним зв'язком. Досліджувався вплив виду пружних характеристик муфти на величини амплітуди та частоти коливного процесу та його час. Для досліджень використана модель одномасової обертальної системи. За методом Рунге-Кутта проведено дослідження коливних процесів пуску трансмісії машинного агрегату з асинхронним електродвигуном. Для визначення коефіцієнту ефективності віброізоляції виконано розрахунок системи, що має у своєму складі пружну муфту з лінійною пружною характеристикою. Також проведено дослідження у випадку, коли муфта обумовлює пружні характеристики Дуфінговського типу "м'якого" і "жорсткого" виду. Результати розрахунків показують, що доцільним є використання нелінійної муфти з комбінованою характеристикою. На підставі цього проведено синтез цільової пружної характеристики і дослідження коливного процесу при застосуванні запропонованої пружної муфти. Результати дослідження показують, що використання муфт з пружними характеристиками "жорсткого" типу дозволяє скоротити час коливальних процесів, однак викликати навантажувальні передачі, близькі до пускового моменту, і з пружними характеристиками "м'якого" типу, дозволяють трохи зменшити навантаження на передачу, проте подовжують час коливального процесу.*

Ключові слова: *пружна муфта, механічний зворотний зв'язок, пружна характеристика, процес коливань, обертальна маса, пусковий момент.*

UDC 621.9.048 **doi: 10.20998/2078-7405.2020.93.06**

A. Mitsyk, V. Fedorovich, A. Grabchenko, Kharkiv, Ukraine

THE EFFECT OF A SHOCK WAVE IN AN OSCILLATING WORKING MEDIUM DURING VIBRATION FINISHING-GRINDING PROCESSING

Abstract. *The propagation of a force pulse in a working medium is considered as in a pseudo-gas, that is, the speed of sound. The movement of parts in the working medium is determined. The mechanism of the appearance of a weak shock wave, that is, a jump of the compaction in a pseudo-gas from abrasive granules is considered. The nature of the interaction of the surfaces of vibrating processed parts with granules of the working medium has been established. The characteristic of the Hugoniot adiabatic curve for pseudo-gas from granules of the working medium is given. The influence of the occurrence of a shock wave on the vibration treatment process is determined. The adequacy of theoretical and experimental studies has been established.*

Keywords: *vibration treatment; working medium; processed parts; force impulse; shock wave; kinetic energy; thermodynamic parameters.*

The application of the kinetic theory of gases and the equations of gas dynamics to describe the process of vibration finishing-grinding processing of parts made it possible to explain the movement of the working medium granules circulating in the reservoir of the vibrating machine. The speed of sound as the speed of propagation of disturbances in gas is one of the main characteristics of a gas [1].

With multi-energy technology of vibration treatment, the working medium made of abrasive granules is influenced not only by the walls of the vibrating machine reservoir, but also by the surface of the processed parts [2, 3]. Such a combined effect not only increases the mobility of abrasive granules, but can also lead to interference propagating from the walls of the vibrating machine reservoir, pseudo-waves and pseudo-gas disturbances from the moving surfaces of parts.

When a body moves in gas at a speed to close or exceeding the speed of sound, a phenomenon occurs that is associated with the impossibility of transmitting a force impulse caused by the movement of the body at a speed greater than the speed of sound. This phenomenon is called a weak shock wave or shock wave [4].

To describe the processes accompanying the supersonic motion of processed parts in reservoir, we introduce the Mach number for pseudo-gas from abrasive granules – M_A:

$$M_A = A_d \ \omega_d / C = A_d \, \omega_d / C_V \, 0.745 A\omega \,. \qquad (1)$$

Here A_d, ω_d, ω are the amplitude and frequencies of vibrations of parts and walls of the vibrating machine reservoir.

Continuity equations – $\frac{\partial \rho}{\partial t} + \mathrm{div}\left(\rho \bar{V}\right) = 0$ when a jump occurs in the one-dimensional case can be written as follows:

$$\rho_1 v_1 = \rho_2 v_2 . \quad (2)$$

Here ρ_1, ρ_2, v_1, v_2 are the densities and velocities before and after the shock wave. This means that on the shock wave surface the values of density and gas velocity undergo a discontinuity. However, their production is continuous. At the same time, in the regions before and after the jump, the values of pressure and speed of movement are also continuous.

Neglecting viscosity and mass forces (gravity), we can write the Navier – Stokes equation in the one-dimensional case before and after the shock wave in the following form:

$$P_1 + \rho_1 v_1^2 = P_2 + \rho_2 v_2^2 . \quad (3)$$

The total energy of a small volume of pseudo-gas for abrasive granules of the working medium is equal to $\rho\left(V^2/2 + \varepsilon\right) dU$. Here ε is the internal energy of the gas.

The change in the total energy of the gas is equal to the heat flux passing through the surface of the selected volume due to thermal conductivity, as well as to the work of surface forces acting on the volume, and due to the work of mass forces. Based on this, we can write the equation for the change in the total gas energy in the form:

$$\frac{d}{dt}\int_U \rho\left(V^2/2 + \varepsilon\right) dU = -\int_S Q_n dS + \int_U \rho F V \, dU + \int_S P_n V \, dS . \quad (4)$$

Here Q_n is the heat flux perpendicular to the surface of the small volume. For an ideal gas, the internal energy is equal to $\varepsilon = \rho C_P T$.

Neglecting heat fluxes and mass forces, it is possible, using equation (3), to write expressions for the total pseudo-gas energies of the medium granules before and after the shock wave in the following form:

$$\frac{1}{\mu} C_P T_1 + \frac{v_1^2}{2} = \frac{1}{\mu} C_P T_2 + \frac{v_2^2}{2} . \quad (5)$$

Here μ is the molar mass of the gas. Equation (5) can be converted to:

$$\frac{\gamma}{\gamma-1}\cdot\frac{P_1}{\rho_1}+\frac{v_1^2}{2}=\frac{\gamma}{\gamma-1}\cdot\frac{P_2}{\rho_2}+\frac{v_2^2}{2}. \quad (6)$$

Here $\rho_1,\rho_2,v_1,v_2,P_1,P_2,T_1,T_2$ – pressures and temperatures before and after the shock wave, μ, C_p, γ – molar mass of gas, isobaric heat capacity, Poisson adiabatic exponent. For pseudo-gas from abrasive granules (monoatomic gas) $\gamma=5/3$.

Combining expressions (3) – (6), we obtain a dependence connecting the pressure and density of the pseudo-gas in the volume of the oscillating working medium being in undisturbed and disturbed by the movement of parts. In the theory of shock waves in gas, this dependence is called the Hugoniot adiabatic curve [5]:

$$\frac{P_2}{P_1}=\frac{(\gamma+1)\rho_2-(\gamma-1)\rho_1}{(\gamma+1)\rho_1-(\gamma-1)\rho_2}. \quad (7)$$

The densities of the pseudo-gas after the shock wave and before it are related to the Mach number by the following relationship:

$$\frac{\rho_2}{\rho_1}=\frac{(\gamma+1)M^2}{(\gamma+1)M^2+2}. \quad (8)$$

The relationships between the temperature and pressure before and after the shock wave with the Mach number are:

$$\frac{P_2}{P_1}=\frac{2\gamma M^2-(\gamma-1)}{(\gamma+1)}; \quad (9)$$

$$\frac{T_2}{T_1}=\frac{\left[2\gamma M^2-(\gamma-1)\right]\cdot\left[(\gamma-1)M^2+2\right]}{(\gamma+1)^2M^2}. \quad (10)$$

Unlike gas molecules, the impact of an abrasive granule on the surface of parts is not absolutely elastic. Part of the energy of the abrasive movement is spent on surface deformation and metal removal. The amount of kinetic energy loss can be estimated by the recovery factor. With this in mind, expression (5) can be written as follows:

$$\frac{1}{\mu}C_P T_{g1}+\frac{v_1^2}{2}=\frac{\alpha}{\mu}C_P T_{g2}+\frac{v_2^2}{2}. \quad (11)$$

Taking into account the correction for energy loss due to friction, the basic equations (7) – (10) take the following form:

Hugoniot adiabatic curve or shock adiabat:

$$\frac{P_{g2}}{P_{g1}} = \frac{(\gamma+1)\rho_{g2} - (\gamma-1)\rho_{g1}}{\left(\gamma\left(2\alpha^2-1\right)+1\right)\rho_{g1} - (\gamma-1)\rho_{g2}}. \tag{12}$$

Pressure ratio before shock and after shock wave:

$$\frac{P_{g2}}{P_{g1}} = 1 - \frac{\gamma\left\{\alpha^2 - M^2\left[\gamma\left(\alpha^2-1\right)+1\right]\right\}}{\left[\gamma\left(2\alpha^2-1\right)+1\right]} + \\ + \sqrt{\frac{\gamma^2 M^2\left(\alpha^2-1\right)}{\left[\gamma\left(2\alpha^2-1\right)+1\right]} + \frac{\gamma^2\left\{\alpha^2 - M^2\left[\gamma\left(\alpha^2-1\right)+1\right]\right\}^2}{\left[\gamma\left(2\alpha^2-1\right)+1\right]^2}}. \tag{13}$$

The ratio of the densities of the pseudo-gas before and after shock wave:

$$\frac{\rho_{g1}}{\rho_{g2}} = 1 + \frac{\left\{\alpha^2 - M^2\left[\gamma\left(\alpha^2-1\right)+1\right]\right\}}{M^2\left[\gamma\left(2\alpha^2-1\right)+1\right]} - \\ - \sqrt{\frac{\left\{\alpha^2 - M^2\left[\gamma\left(\alpha^2-1\right)+1\right]\right\}^2}{M^4\left[\gamma\left(2\alpha^2-1\right)+1\right]^2} + \frac{2\gamma\left(\alpha^2-1\right)}{M^2\left[\gamma\left(2\alpha^2-1\right)+1\right]}} \tag{14}$$

Temperature ratio:

$$\frac{T_{g1}}{T_{g2}} = \frac{P_{g2}\ \rho_{g1}}{P_{g1}\ \rho_{g2}}, \tag{15}$$

where T_{g1}, T_{g2} – the temperatures before and after the shock wave in pseudo-gas from abrasive granules, α – the reciprocal of the recovery factor – $\beta = \sqrt{\frac{1-f}{1+f}}$, where f – the dry friction coefficient (all variables with index 1 correspond to the values before the shock, with index 2 after the shock wave).

Figures 1 and 2 show the graphs of the above ratios (12) – (15) compared to the ratios for ideal gas (7) – (10).

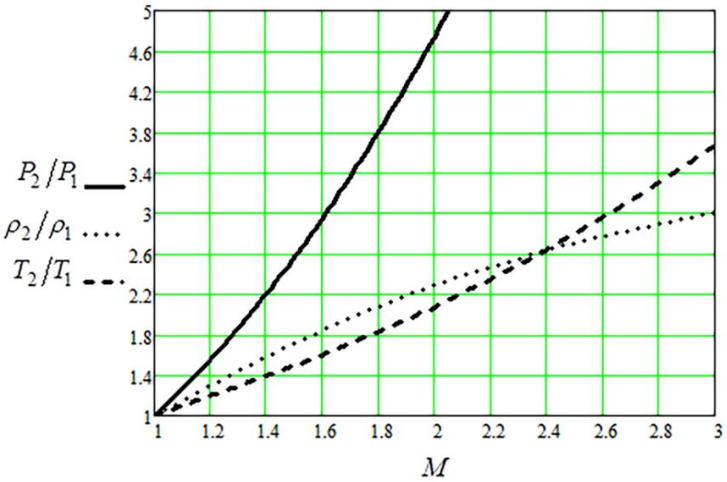

Figure 1 – Dependences of ratios of the pressure, density, and temperature of the gas after and before the shock wave as a function of the Mach number

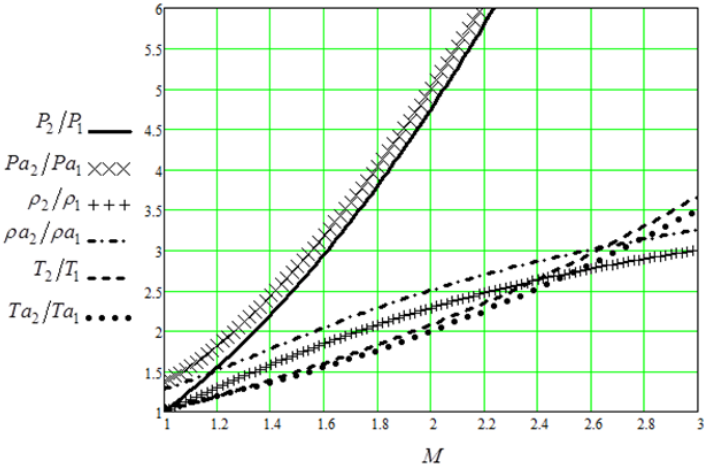

a)

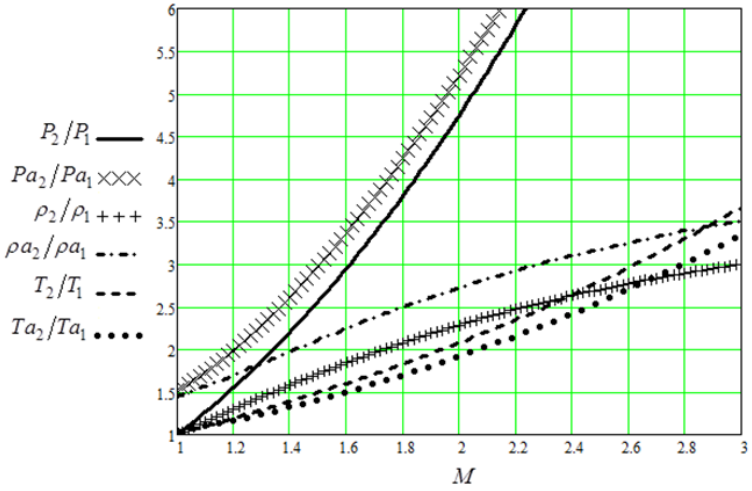

b)

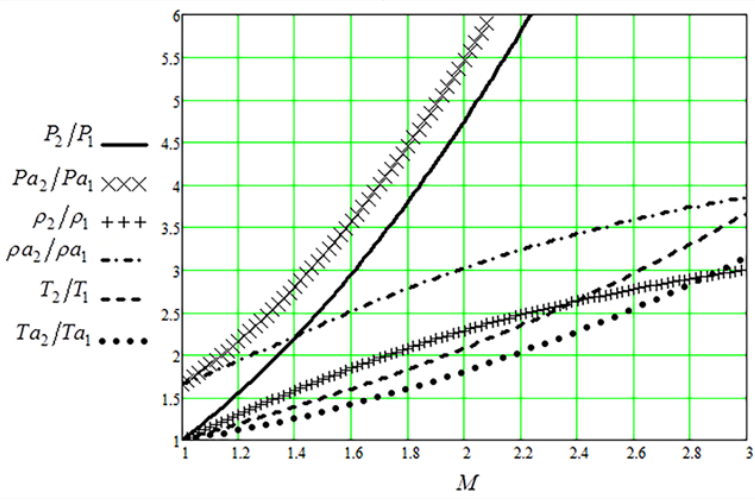

c)

Figure 2 – Dependences of the ratios of pressures, densities and temperatures of pseudo-gas and ideal gas before and after the shock wave in inelastic collision on the Mach number: (a) – $\alpha = 1.03$; (b) – $\alpha = 1.066$; (c) – $\alpha = 1.1$

In all the graphs in Figure 3, the pressure and density ratios at the beginning of the coordinates (with the Mach number equal to one) exceed a value equal to one, as should be in the case for an ideal gas. This is due to the fact that inelastic

collisions of granules with the surface of the part lead to a loss of the kinetic energy of the granules after the collision. Pseudo-gas "cools" near the surface of the parts. This leads to a decrease in the speed of sound in this volume and, therefore, a shock wave occurs on the surface of the parts at a speed lower than the speed of sound in the pseudo-gas of abrasive granules $\left(C \approx 0.745 A\omega\right)$. It can be seen from the figure that the ratio T_{g1}/T_{g2} is less than unity at the speeds of parts less than the speed of sound.

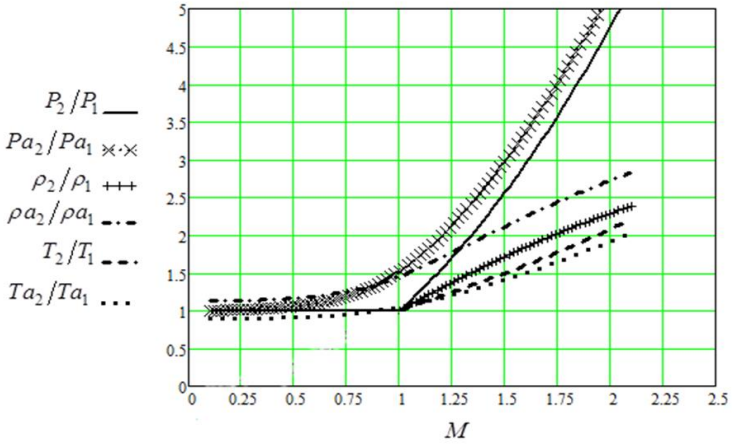

Figure 3 – Ratios P_{g2}/P_{g1}, ρ_{g2}/ρ_{g1}, T_{g2}/T_{g1} at Mach numbers in pseudo-gas from abrasive granules at a considerable distance from the surface of the part, $\alpha = 1.06$

When the processed parts exceed the speed of sound in the pseudo-gas, it is necessary to enter into the formula for calculating metal removal during vibration processing a correction directly proportional to the ratio $\rho a_2/\rho a_1\sqrt{Ta_2/Ta_1}$. The obtained dependences of the values of the correction factor $K = \rho a_2/\rho a_1\sqrt{Ta_2/Ta_1}$ on the Mach number, which is equal to the ratio of the speed of movement of the processed parts to the speed of sound in the abrasive granules pseudo-gas, for various coefficients α are presented graphically in Fig. 4.

The obtained dependences of the values of the correction factor $K = \rho a_2/\rho a_1\sqrt{Ta_2/Ta_1}$ on the Mach number, equal to the ratio of the speed of movement of the processed part to the speed of sound in the abrasive granules pseudo-gas, for various factors α are presented graphically (Fig. 4).

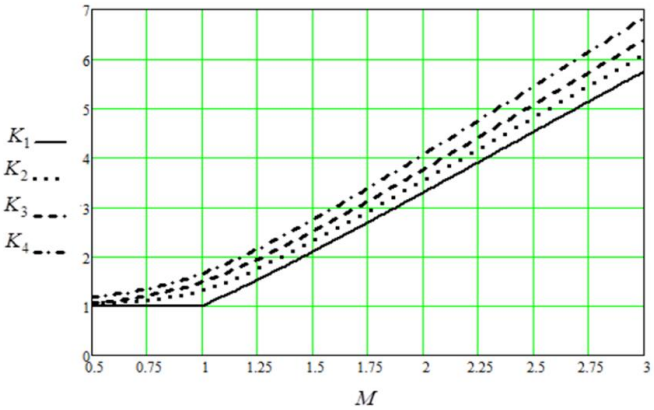

Figure 4 – Dependences of the correction factor K on the Mach number:
K1 – α =1; K2 – α =1,03; K3 – α =1,06; K4 – α =1,1

Then, the curves of metal removal during vibration processing of parts, calculated using the above formulas, were obtained, depending on the amplitude of the reservoir oscillations (Fig. 5). The curve marked with letter Q is constructed without taking into account the occurrence of a shock wave in the pseudo-gas of abrasive granules. Curves Q_1, Q_2, Q_3, Q_4 are constructed taking into account the appearance of a compressed layer on the surface of parts for different coefficients α : $\alpha_1 = 1; \alpha_2 = 1.03; \alpha_3 = 1.06; \alpha_4 = 1.1$.

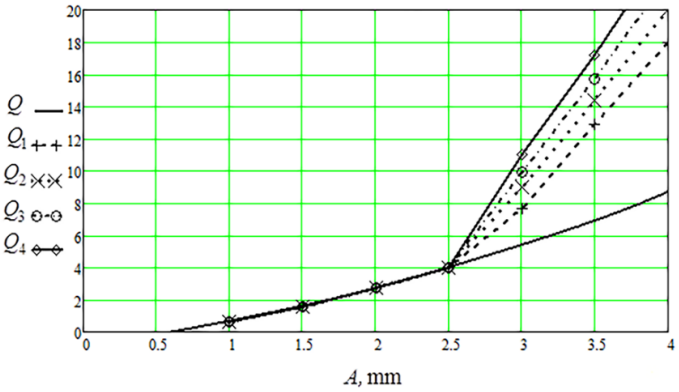

Figure 5 – Dependences of metal removal on the amplitude of reservoir oscillations at an oscillation frequency of 30 Hz without and taking into account the occurrence of a shock wave in the pseudo-gas of abrasive granules (Q_1, Q_2, Q_3, Q_4)

The above formulas were used to calculate metal removal curves during vibration treatment of parts depending on the oscillation frequency of the reservoir (Fig. 6). The curve denoted by letter Q is constructed without taking into account the occurrence of a shock wave in the pseudo-gas of abrasive granules. Curves Q_1, Q_2, Q_3, Q_4 are constructed taking into account the appearance of a compressed layer on the surface of parts for different coefficients α : $\alpha_1 = 1; \alpha_2 = 1.03; \alpha_3 = 1.06; \alpha_4 = 1.1$.

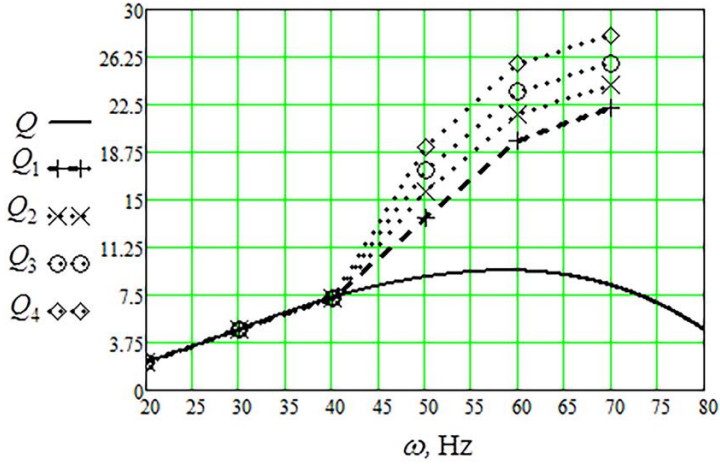

Figure 6 – Dependences of metal removal on the oscillation frequency of the reservoir at an oscillation amplitude of 2.5 mm without and taking into account the occurrence of a shock wave in the pseudo-gas of abrasive granules (Q_1, Q_2, Q_3, Q_4)

In the course of experiments according to multi-energy technologies for the vibrational processing of body brass parts of hydraulic-pneumatic systems the parts were processed "with fixation" in an appliance performing autonomous movement independent of the reservoir [6, 7]. In this case, the following pattern was discovered. In the case of exceeding the amplitude of oscillations of the processed parts, which are oscillating, like a reservoir with an amplitude of 2.5 mm and a frequency of 34 Hz, a noticeable increase in metal removal is fixed. That is, the curve of the dependence of metal removal undergoes a break (Fig. 7). The graph shows that the curve has a break, which cannot be explained by the experimental error. The experimental error is shown with crosses.

An experimental dependence of metal removal on the vibration frequency of brass parts in the appliance, which performs an autonomous movement

independent of the reservoir, has been also obtained. In this case, the oscillation frequency of the reservoir is 43 Hz, the amplitude of the reservoir oscillations is 2.5 mm (Fig. 8).

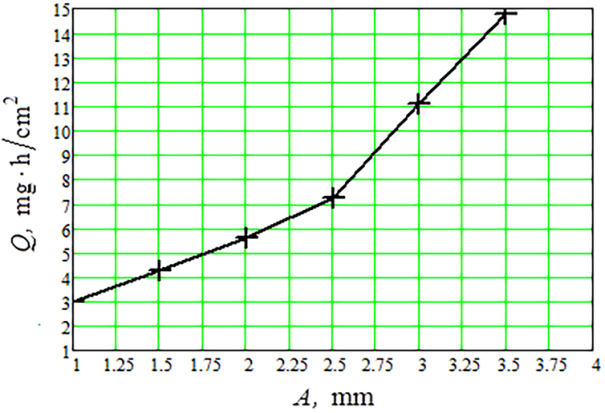

Figure 7 – Dependence of metal removal during vibration treatment of brass parts on the amplitude of their autonomous movement: "+" – the value of the experimental error

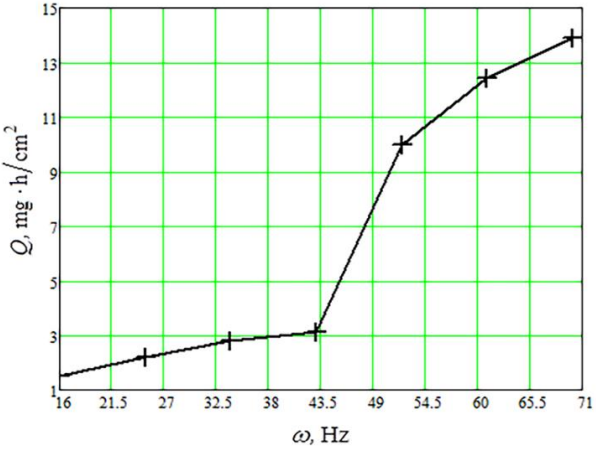

Figure 8 – Dependence of metal removal during vibration treatment of brass parts on the frequency of their autonomous movement: "+" – the value of the experimental error

Obviously, at a vibration frequency of parts exceeding 43 Hz, the curve of

metal removal dependence on frequency, as in the previous case, undergoes a break. This behavior of both curves corresponds to a significant change in the metal removal mechanism with varying parameters of the autonomous movement of parts independent of the reservoir. It is possible to explain this phenomenon by the fact that the abrasive granules are concentrated near the treated surfaces of oscillating parts. This is due to the impossibility of transmitting the force pulse to the working medium layers remote from the parts, since the speed of the parts exceeds the speed of propagation of the power pulse in the abrasive granules pseudo-gas. Under these conditions, the speed of the chaotic movement of the working medium and their concentration near the surfaces of the processed parts increases sharply. As a result, it leads to the intensification of their processing.

Comparison of the calculated dependences (Fig. 5, 6) with the experimental (Fig. 7, 8) indicates the validity of the hypothesis about the possibility of shock waves of an oscillating working medium in the pseudo-gas from abrasive granules, despite the fact that the behavior of the curves (Fig. 5, 6) and (Fig. 7, 8) is rather qualitative than quantitative.

Conclusions

1. During vibration treatment using multi-energy technology, parts move autonomously under the influence of additional energy action. However, an effect similar to a shock wave can occur in an oscillating working medium. For such a physical situation, an analogy is carried out between the ratios of the thermodynamic parameters of the pseudo-gas before and after the shock wave, which are described by the Hugoniot adiabat.

2. One of the main differences in the behavior of pseudo-gas from abrasive granules is that the collisions between the abrasive granules and the surface of the parts are inelastic. When the abrasive granules collide, the power impulse is lost. These losses are forced and have a negative effect on the vibration treatment process, since the collisions of granules with the surface of the processed parts cause metal removal, and they are a practical result of vibration treatment.

3. Modeling of the compressed layer of the oscillating working medium near the surfaces of the processed parts installed in the device and moving autonomously from the reservoir was carried out taking into account the losses of the power impulse of the granules when they collide with the parts. The introduction of the recovery factor into the equation of conservation of the total energy of the gas in combination with the Navier-Stokes equations and the continuity equation refines the expression for the Hugoniot adiabat as applied to an abrasive granules pseudo-gas. This makes it possible to obtain expressions relating the pressure in the pseudo-gas, its density and temperature before and after the shock wave. The obtained ratios make it possible to explain the experimentally established regularity of an increase in metal removal when the frequency and (or)

the amplitude of autonomous vibrations of parts during vibration processing are exceeded.

4. Analysis and experimental studies of the appearance of an effect similar to a shock wave in an abrasive granules pseudo-gas allow:

– To intensify the process of vibration treatment of parts by using multi-energy technologies.

– To optimize the amplitude-frequency characteristics of oscillations of the vibrating machine reservoir and autonomously moving parts in relation to the achievement of the required technological result.

– To optimize the amplitude-frequency characteristics of the autonomous movements of the processed parts and the vibrating machine reservoir, depending on the spatial arrangement of the parts in the volume of the reservoir.

– To optimize the amplitude-frequency characteristics of the autonomous movements of the processed parts and the reservoir of the vibrating machine, depending on the shape and number of simultaneously processed parts.

References: **1.** *Mamalis A.G., Grabchenko A.I., Mitsyk A.V., Fedorovich V.A., Kundrák J.* Mathematical simulation of motion of working medium at finishing – grinding treatment in the oscillating reservoir. The International Journal of Advanced Manufacturing Technology 70, p. 263 – 276 (2014). DOI: https://doi.org/10.1007/s00170-013-5257-6 **2.** *Mitsyk A.V.* Opredelenie vlijanija parametrov vibroobrabotki na velichinu davlenija granul i detalej // Vibracii v tehnike i tehnologijah. 2010. 3(59). s. 75 – 79. **3.** *Mitsyk A.V., Fedorovich V.A.* Puti intensifikacii vibracionnoj otdelochno-zachistnoj obrabotki kombinirovaniem shem jenergeticheskih vozdejstvij na rabochuju sredu i detali // Aviacionno-kosmicheskaja tehnika i tehnologija. 2011. № 6. s. 26 – 34. **4.** *Kundrák J., Morgan M., Mitsyk A.V., Fedorovich V.A.* The effect of the shock wave of the oscillating working medium in a vibrating machine's reservoir during a multi-energi finishing-grinding vibration processing. The International Journal of Advanced Manufacturing Technology 106, p. 4339 – 4353 (2020). DOI: https://doi.org/10.1007/s00170-019-04844-2 **5.** *Matveev A.N.* Molecular Physics. Mir Publishers: Moscow, Russia, 1985. p. 450. **6.** Pat. na korisnu model' № 133705 Ukraina, MPK V24V 31/06. Sposib vibroobrobki detalej / *Mitsyk A.V*; zajavnik ta patentoobladach SNU im. V. Dalja. № u201808772; zajavl. 16.08.2018; opubl. 25.04.2019, Bjul. № 8. **7.** Pat. na korisnu model' № 133708 Ukraina, MPK V24V 31/06. Sposib ozdobljuval'no-zachishhuval'noї obrobki vil'nim abrazivnim seredovishhem / *Mitsyk A.V*; zajavnik ta patentoobladach SNU im. V. Dalja. № u201808775; zajavl. 16.08.2018; opubl. 25.04.2019, Bjul. № 8.

Андрій Міцик, Володимир Федорович, Анатолій Грабченко, Харків, Україна

ЕФЕКТ УДАРНОЇ ХВИЛІ В КОЛИВНОМУ РОБОЧОМУ СЕРЕДОВИЩІ ПРИ ВІБРАЦІЙНІЙ ОЗДОБЛЮВАЛЬНО-ЗАЧИЩУВАЛЬНІЙ ОБРОБЦІ

Анотація. *Розглянуто поширення силового імпульсу в робочому середовищі як у псевдогазі, тобто подібно поширенню акустичного збурення. Встановлено відповідність між кінетичною енергією гранул, їх імпульсом і термодинамічними параметрами температури й тиску. Проаналізовано ефекти руху оброблюваних деталей зі швидкостями близькими до швидкостей переміщення гранул абразиву. Розглянуто рух деталей в робочому середовищі. Визначено ефект*

слабкої ударної хвилі – стрибок ущільнення в псевдогазі з абразивних гранул. Визначено вплив виникнення стрибка ущільнення на процес віброобробки. Розглянуто механізм виникнення слабкої ударної хвилі в середовищі, що коливається. Записано рівняння Нав'є-Стокса в одновимірному випадку до і після стрибка ущільнення. Визначено рух деталей в робочому середовищі. Розглянуто механізм виникнення слабкої ударної хвилі, тобто стрибок ущільнення у псевдогазі з абразивних гранул. Встановлено характер взаємодії поверхонь резервуару з оброблюваними деталями та гранулами робочого середовища. Встановлено зменшення кінетичної енергії псевдогазу з гранул абразиву в результаті зіткнення з поверхнею оброблюваних деталей, що веде до зміни тиску і щільності відповідно до рівняння Менделєєва-Клапейрона. Приведено відношення температур після стрибка ущільнення і до нього через відношення тисків і щільності. Дана характеристика адіабати Гюгоньо для псевдогаза з гранул робочого середовища. Отримано знімання металу при віброобробці деталей в залежності від амплітуди та частоти коливань резервуару. Виявлено зміну механізму знімання металу при варіюванні параметрів автономного руху резервуару та оброблюваних деталей. Розраховано, що швидкість хаотичного руху середовища поблизу оброблюваних поверхонь різко зростає і призводить до інтенсифікації обробки деталей. Встановлено адекватність теоретичних і експериментальних досліджень.

Ключові слова: *віброобробка; робоче середовище; оброблювані деталі; силовий імпульс; ударна хвиля; стрибок ущільнення; кінетична енергія; термодинамічні параметри.*

UDC 621.9 **doi: 10.20998/2078-7405.2020.93.07**

V. Molnár, Miskolc, Hungary

DESIGNATION OF EVALUATION AREA IN MEASURING 3D SURFACE ROUGHNESS

Abstract. *In the automotive industry surface topography is an important issue. The working surfaces of the components require high precision machining. In this paper the minimum 3D roughness evaluation areas were determined to decrease the time and cost of measuring the components.*
Keywords: *surface roughness; S_a, S_{sk};, hard turning; grinding.*

1. INTRODUCTION

With the appearance of super hard materials and single-point tools (turning tools) produced from these materials, it became possible to machine hardened materials (HRC>50). To apply these machining procedures for finishing, numerous research projects were necessary, e.g. analyzing tool-wear [1], describing tool-life as a function of the cutting data [2], designing machine tools with greater rigidity, etc. These preliminary conditions facilitated the analysis methods, whose aim was comparing the surfaces machined by the new technologies with those machined by grinding or substituting the grinding by the new technologies. The foci of these analysis methods were the accuracy and surface quality of the machined components [3].

Table 1 – Examples for 3D evaluation areas

Applied technology	Evaluation area [mm × mm]
Grinding	1.5×1 [4], 2.5×2.5 [5], 0.5×0.5 [11], 1.2×0.9 [13]
Turning	0.705×0.528 [6]
Hard turning	0.8×0.8 [7], 0.5×0.5 [11], 2.5×2.5 [12]
Milling	5×5 [8], 2.5×2.5 [9], 1.2×0.9 [13]
Rolling	0.7×0.525 [110]
Burnishing	2.5×2.5 [12]
Direct Laser Deposition	1.2×0.9 [13]

In this paper the reliability of 3D surface roughness testing is analyzed. Parameters for height (Sa) and area (Ssk) are measured and analyzed in different evaluation areas, and minimum areas were determined by applying descriptive statistical parameters. The reason for such a study was that there are many 3D topography research studies available but there is no exact advice for the evaluation area of the surface. Some studies are cited in Table 1 as examples; it can

be stated that the evaluation area varies in quite a random manner and there is no significant relationship between the area and the applied technology or the technological data compared to the 2D roughness test, where the evaluation length is offered by a standard.

There is another problem in 3D roughness analysis: in several studies important data are neglected, therefore the repeatability of the experiment or analysis cannot be realized. Some examples of poorly reported studies:

- Missing evaluation area [14],
- Missing cut-off and filtering method [15],
- Missing cutting data, evaluation area and cut-off [16, 17].

2. EXPERIMENTAL SETUP AND THE MEASURED ROUGHNESS DATA

In the experiment the bores of two gear wheels were machined and the surfaces of the bores were analyzed. The main data of the hardened component are:

- Material: 16MnCr5
- Hardness: 62 HRC
- Diameter (d): 38 mm
- Bore length (l): 29.85 mm
- Accuracy: IT5
- Allowance (Z): 0.15 mm

Table 2 – Cutting data of the experiment and data of the roughness test

		Hard turning		Grinding	
Machine tool		EMAG VSC 400 DS		SI-4/A	
Applied tools		CNGA 120408S-LO CBN (R) CNGA 120408 7020 (S)		40×20×16-9A80-K7V22	
Cutting	Roughing	$v_{c,R}$ f_R $a_{p,R}$	180 m/min 0.24 mm/rev 0.1 mm	$v_{c,R}$ $v_{w,R}$ $v_{f,L,R}$	30 m/s 18 m/s 2.2 m/min
	Smoothing	$v_{c,S}$ f_S $a_{p,S}$	180 m/min 0.12 mm/rev 0.05 mm	$v_{c,S}$ $v_{w,S}$ $v_{f,L,S}$	30 m/s 18 m/s 2 m/min
Measuring machine				Altisurf 520	
Standard applied for the evaluation				ISO 25178-2:2012	
				Axe X	Axe Y
Evaluation area	Length			1.5 mm	1.5 mm
	Size			1501 points	1501 points
	Spacing			1 μm	1 μm

The internal cylindrical surface of one component was machined by hard turning in roughing and smoothing passes. The bore of the other was hard turned in

the roughing pass and ground in the smoothing. The machine tool, other cutting tools applied, and cutting data are summarized in Table 2. After machining roughness tests were carried out by a 3D roughness measuring machine.

The main data of the setup are summarized in Table 2. As measured surfaces 2.3×2.3 mm^2 squares were designated on the components. Gauss filter was applied for filtering the surface waviness. The cut-off (basis of evaluation) was determined according to the standard ISO 25178-2:2012. Its value was 0.8 in case of both surfaces. This resulted in 1.5×1.5 mm^2 evaluation areas.

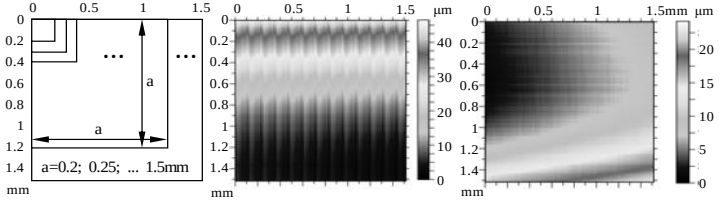

Figure 1 – Designation of the evaluation areas (left), 3D views of the surface topographies (hard turned (middle); ground (right))

Table 3 – Data of the roughness test

Hard turning									
a	**1.5**	**1.45**	**1.4**	**1.35**	**1.3**	**1.25**	**1.2**	**1.15**	**1.1**
Sa	0.7221	0.7204	0.7277	0.7182	0.7241	0.7191	0.7272	0.7158	0.7244
Ssk	0.0114	0.0069	0.0112	-0.0034	0.0171	0.0055	0.0128	0.0146	-0.018
a	**1.05**	**1**	**0.95**	**0.9**	**0.85**	**0.8**	**0.75**	**0.7**	**0.65**
Sa	0.7128	0.7164	0.7229	0.7055	0.7303	0.7107	0.7217	0.716	0.7131
Ssk	0.0282	0.0119	0.0306	0.0387	-0.0014	0.0408	-0.007	0.0364	0.0254
a	**0.6**	**0.55**	**0.5**	**0.45**	**0.4**	**0.35**	**0.3**	**0.25**	**0.2**
Sa	0.7337	0.7125	0.7327	0.6996	0.7101	0.7322	0.6739	0.7405	0.674
Ssk	-0.0029	0.0125	-0.0428	0.0534	-0.0039	0.0534	0.0659	-0.0845	-0.0243
Grinding									
a	**1.5**	**1.45**	**1.4**	**1.35**	**1.3**	**1.25**	**1.2**	**1.15**	**1.1**
Sa	0.2005	0.2024	0.1997	0.2018	0.2008	0.2009	0.2056	0.1981	0.1982
Ssk	-0.0334	-0.0627	-0.0497	-0.0432	-0.0615	-0.0421	-0.08	-0.0828	-0.0583
a	**1.05**	**1**	**0.95**	**0.9**	**0.85**	**0.8**	**0.75**	**0.7**	**0.65**
Sa	0.1994	0.1999	0.2013	0.1962	0.1964	0.1945	0.1938	0.1919	0.192
Ssk	-0.058	-0.056	-0.0417	-0.0066	0.004	-0.0167	-0.0215	-0.0119	0.0036
a	**0.6**	**0.55**	**0.5**	**0.45**	**0.4**	**0.35**	**0.3**	**0.25**	**0.2**
Sa	0.1906	0.1873	0.1884	0.1837	0.1865	0.1812	0.1799	0.1719	0.1596
Ssk	-0.0287	-0.0682	-0.0916	-0.0867	-0.0749	-0.0734	-0.0978	-0.1569	-0.0475

The main goal of the study is to determine the minimum evaluation area in the case of the two chosen roughness parameters. Based on the data obtained by scanning the original area, further smaller areas were designated and evaluated (side lengths of the areas are from 1.5 mm to 0.2 mm). A total of 27 areas of different sizes were evaluated. The scheme of this is demonstrated in Fig. 1. In Fig. 2 the 3D-views of the hard turned and the ground surfaces are demonstrated. In Table 3 the Sa and Ssk 3D surface roughness parameter values are summarized.

3. RESULTS AND DISCUSSION

In Fig. 2 values of the Sa parameters of the hard turned and ground surfaces are demonstrated. A reference value was designated for the analysis: the arithmetic average of the first 5 roughness values. The standard deviations of these data points for the two surfaces are close to zero: 0.0036 μm and 0.0011 μm, respectively. As the evaluation area decreases, the difference between the actual roughness values and the reference values increases. However, the increase in the Sa data of the ground surface is less than in case of the hard turned surface. In addition to that, the values show a slight decrease.

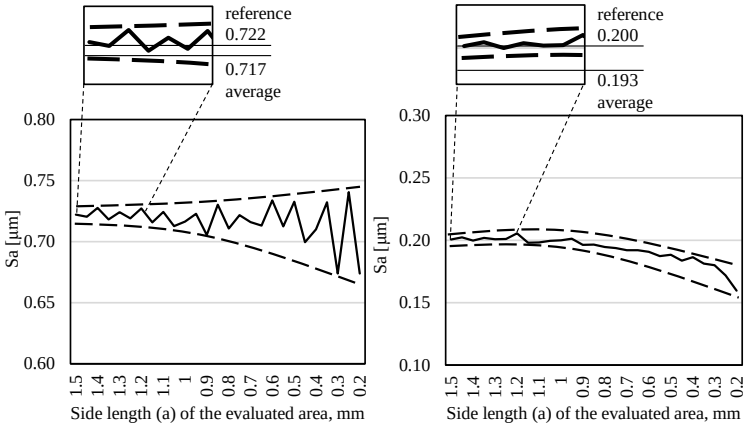

Figure 2 – The Sa parameter values of the hard turned (left) and the ground (right) surfaces

In Fig. 3 the Ssk roughness values of the hard turned and ground surfaces are demonstrated. Here, the standard deviations of the first 5 data points for the two surfaces are 0.0076 and 0.0124, respectively. As the evaluation area decreases the difference between the actual roughness values and the reference values increases.

The bias, which is the difference between the reference value and the average of the 27 parameter values, was also calculated. The biases of the Sa parameters of the hard turned and ground surfaces are -0.005 μm and -0.007 μm, respectively. In the case of the Ssk parameter they are 0.002 and -0.004, respectively. These relatively low values provide the information that the roughness values deviate in a quite symmetrical manner around the reference values, which are considered as reliable roughness values due to the area being large enough for the evaluation.

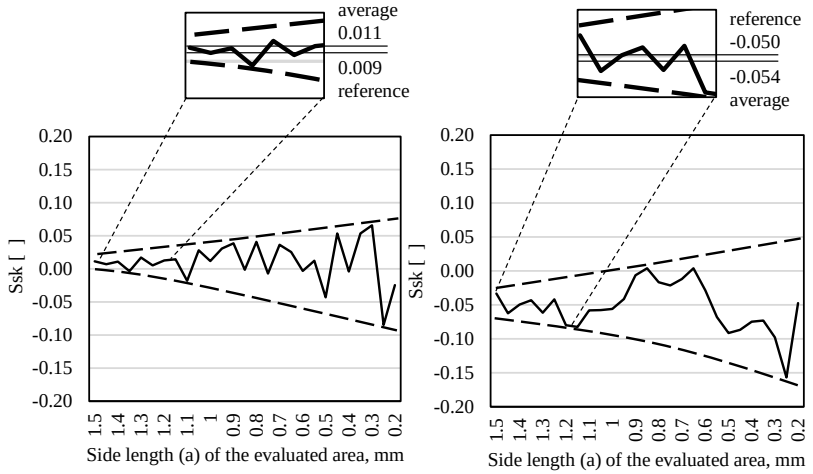

Figure 3 – The Ssk parameter values of the hard turned (left) and the ground (right) surfaces

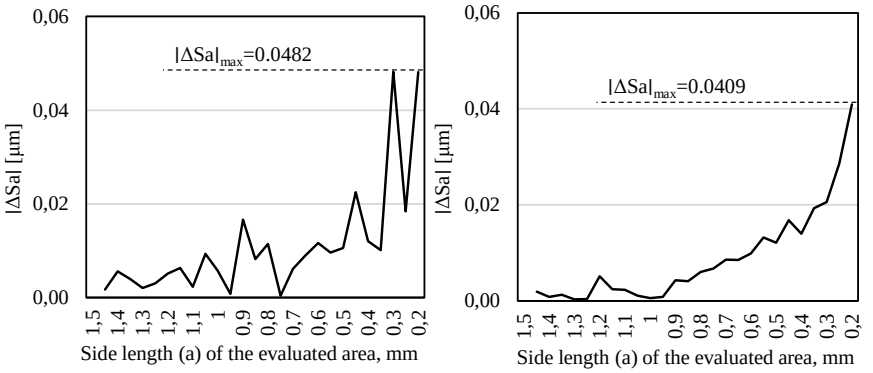

Figure 4 – Absolute differences in the Sa values of the hard turned (left) and the ground (right) surface – basis: Sa values of the 1.5×1.5 mm areas

The roughness values of the decreasing areas were compared to those of the 1.5×1.5 mm area. The absolute values of these differences are plotted in Figs. 4 and 5. Compared to the 1.5×1.5 area in the case of hard turning, the Sa parameter values show less than 1% difference from the areas 1.45×1.45 to 1.1×1.1. The actual Ssk values are closer to 0 than the Sa values, and therefore the percentage differences are greater.

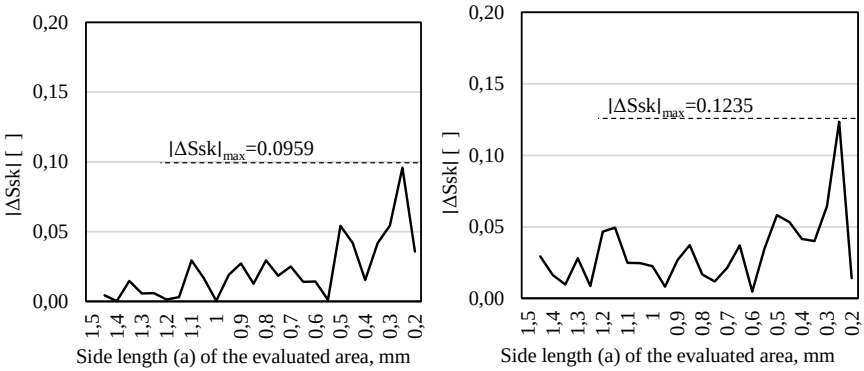

Figure 5 – Absolute differences in the Ssk values of the hard turned (left) and the ground (right) surface – basis: Ssk values of the 1.5×1.5 mm areas

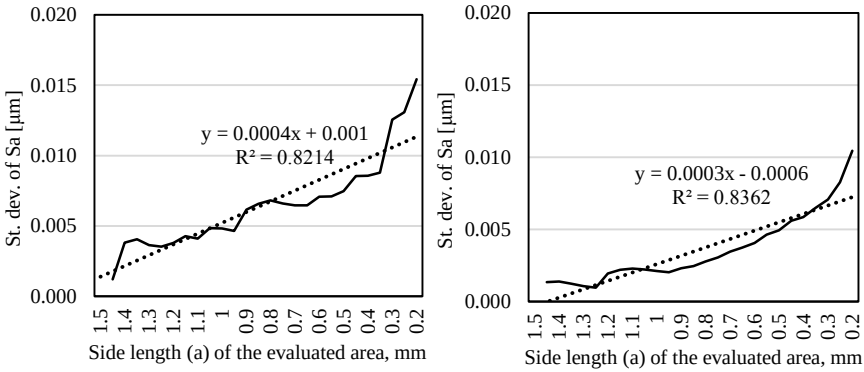

Figure 6 – Standard deviations of the Sa values of the hard turned (left) and the ground (right) surfaces

The parameter values show a less than 100% difference from the area 1.45×1.45 to 1.4×1.4. The 100% difference can be considered as normal. In the case of grinding,

the differences of the Sa parameter values are less than 1% from the area 1.5×1.5 to the area 1.2×1.2. The differences of the Ssk parameters are less than 100% from the area 1.5×1.5 to 1.25×1.25. It is seen that the smaller the evaluation area, the greater this difference is. The relatively low levels of percentage differences help in designating a limit area that can be considered as a reliable minimum for the evaluation of the roughness areas.

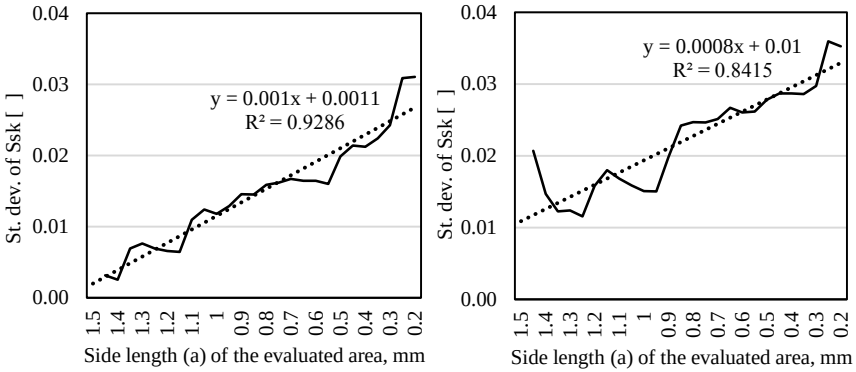

Figure 7 – Standard deviations of the Ssk values of the hard turned (left) and the ground (right) surfaces

Similarly to the analysis of the absolute differences, the change in standard deviations were calculated. The decreasing evaluation area leads to the distortion of the roughness values. This phenomenon is followed by the increased deviation of the data. If the standard deviations of roughness data of more areas are calculated, these values show an increasing tendency (Figs. 6 and 7). The deviation data correspond to the percentage differences data in the designation of minimum evaluation areas, because the first few deviation values can be considered as low enough. This finding is summarized in Table 4. In the case of grinding, the standard deviation limit is significantly greater than that of hard turning but it is still acceptable.

Table 4 – Data of the roughness test

		Sa	Ssk
Hard turning	%Δ, Area	1%, 1.5×1.5-1.1×1.1	100%, 1.5×1.5-1.4×1.4
	St. dev., Area	0.005, 1.5×1.5-0.95×0.95	0.005, 1.5×1.5-1.4×1.4
Grinding	%Δ, Area	1%, 1.5×1.5-1.2×1.2	100%, 1.5×1.5-1.25×1.25
	St. dev., Area	0.005, 1.5×1.5-0.5×0.5	0.02, 1.5×1.5-0.9×0.9

4. SUMMARY

Hard surfaces were machined by hard turning and grinding and evaluated after 3D surface measurement in order to determine a minimum roughness evaluation area which is still acceptable based on a designated reference value. This reference can be the first or the first few measurement on surfaces which are considered large enough for technical evaluation. The reliability of the measurements was demonstrated by calculation of the standard deviation of the values of various (smaller and smaller) evaluation areas When precision components are machined in the automotive industry, surface topography and within that surface roughness are determining parameters whose measurement requires a considerable amount of time by the measuring organizational unit, particularly if 3D parameters are required for the qualification of the surface. The size of the measured area is in a nearly linear function with the measuring time. Therefore, finding the minimum evaluation area is crucial. It was found that in the case of the surface finished by hard turning, the minimum 'a' side length of the evaluation area is 1.1 mm and 1.4 mm based on the Sa and the Ssk roughness parameters, respectively. The minimum length in case of the surface finished by grinding is 1.2 mm and 1.25 mm, respectively. An important limitation of the study is that only two parameters were analyzed. In further studies the remaining 20 or so parameters have to be analyzed. Furthermore, other typical surfaces and machining operations would be useful to analyze.

References: 1. *Vasvay, L., Ditroi, F., Takacs, S., Szabo, Z., Szucs, J., Kundrak, J., Mahunka, I.:* Wear Measurement of the Cutting Edge of Superhard Turning Tools using TLA Technique, Nuclear Instruments & Methods in Physics Research, No.85, 1994, pp.255–259. **2.** *Mamalis, A.G., Kundrak, J., Horvath, M.:* On a Novel Tool Life Relation for Precision Cutting Tools, Journal of Manufacturing Science and Engineering – Transactions of the ASME, Vol.127 No.2, 2005, pp.328–332. **3.** *Kundrak, J., Gyani, K., Bana, V.:* Roughness of Ground and Hard-Turned Surfaces on the Basis of 3D Parameters, International Journal of Advanced Manufacturing Technology, Vol.38, No.1-2, 2008, pp.110–119. **4.** *Schmahling, J., Hamprecht, F.A., Hoffmann, D.M.P.:* A Three-Dimensional Measure of Surface Roughness based on Mathematical Morphology, Technical Report from Multidimensional Image Processing, IWR, 2006, University of Heidelberg. **5.** *Legutko, S., Zak, K., Kudlacek, J.:* Characteristic of Geometric Structure of the Surface after Grinding, MATEC Web of Conferences, 2007, 02007. **6.** *Struzikiewicz, G., Sioma, A.:* Evaluation of Surface Roughness and Defect Formation after the Machining of Sintered Aluminum Alloy AlSi10Mg, Materials, No.13, 2020. **7.** *Matras, A., Zębala, W., Machno, M.:* Research and Method of Roughness Prediction of a Curvilinear Surface after Titanium Alloy Turning, Materials, Vol.12, No.3, 502. **8.** *Nadolny, K., Kaplonek, W.:* Analysis of Flatness Deviations for Austenitic Stainless Steel Workpieces after Efficient Surface Machining, Measurement Science Review, Vol.14, No.4, 2014. **9.** *Kundrak, J., Nagy, A., Markopoulos, A.P., Karkalos, N.E.:* Investigation of Surface Roughness on Face Milled Parts with Round Insert in Planes Parallel to the Feed at Various Cutting Speed, Rezanie i Instrumenty v Tekhnologicheskih Sistemah, Vol.91, No.1, 2019, pp.87–96. **10.** *Deltombe, R., Kubiak, K.J., Bigerelle, M.:* How to Select the Most Relevant 3D Roughness Parameters of a Surface? Scanning, Vol.36, No.1, 2014, pp.150–160. **11**. *Grzesik, W., Zak, K., Kiszka, P.:* Comparison of Surface Textures Generated in Hard Turning and Grinding Operations, Procedia CIRP, No.13, 2014, pp.84–89. **12**. *Grzesik, W., Rech, J., Zak, K.:* High-Precision Finishing

Hard Steel Surfaces Using Cutting, Abrasive and Burnishing Operations, Procedia Manufacturing, Vol.1, 2015, pp.619–627. **13.** *Wojciechowski, S., Twardowski, P., Chwalczuk, T.:* Surface Roughness Analysis after Machining of Direct Laser Deposited Tungsten Carbide, Journal of Physics: Conference Series, 483, 2014, 012018. **14.** *Zawada-Tomkiewicz, A.:* Analysis of Surface Roughness Parameters Achieved by Hard Turning with the Use of PCBN Tools, Estonian Journal of Engineering, Vol.17, No.1, 2011, pp.88–99. **15.** *Pytlak, B.:* The Roughness Parameters 2D and 3D and Some Characteristics of the Machined Surface Topography after Hard Turning and Grinding of Hardened 18CrMo4 Steel, Komisja Budowy Maszyn Pan – Oddzial w Poznaniu, Vol.31, No.4, 2011, pp.53–62. **16.** *Abouelatta, O.B.:* 3D Surface Roughness Measurement Using a Light Sectioning Vision System, Proceedings of the World Congress on Engineering 2010 Vol.1, 2010. **17.** Shivanna, D.M., Kiran, M.B., Kavitha, S.D: Evaluation of 3D Surface Roughness Parameters of EDM Components Using Vision System, Procedia Materials Science, No.5, 2014, pp.2132–2141.

Віктор Мольнар, Мішкольц, Угорщина

ПОЗНАЧЕННЯ ОБЛАСТІ ОЦІНКИ ПРИ ТРИВИМІРНОМУ ВИМІРЮВАННІ ШОРСТКОСТІ ПОВЕРХНІ

Анотація. *В деталях для автомобільної промисловості важлива топографія поверхні. Робочі поверхні деталей вимагають високоточної обробки. У цій статті були визначені мінімальні області оцінки 3D шорсткості, щоб зменшити час і вартість вимірювання компонентів та аналізується надійність тривимірних випробувань шорсткості поверхні. Параметри висоти (S_a) і площі (S_{sk}) вимірюються і аналізуються в різних областях оцінки, а мінімальні площі визначалися із застосуванням описових статистичних параметрів. Виміряні поверхні становили 2,3 × 2,3 мм^2. Для фільтрації хвилястості поверхні застосовувався фільтр Гаусса. Граничне значення (підстава для оцінки) було 0,8 для обох поверхонь. В результаті були отримані оціночні площі 1,5×1,5 мм^2. Основна мета дослідження - визначити мінімальну область оцінки в разі двох обраних параметрів шорсткості. На основі даних, отриманих при скануванні вихідної області, були визначені і оцінені подальші менші області (довжина сторін областей становила від 1,5 мм до 0,2 мм). Всього було оцінено 27 ділянок різного розміру. Коли прецизійні компоненти обробляються, топографія поверхні і в межах цієї шорсткості поверхні є визначальними параметрами, вимірювання яких вимагає значного кількість часу, необхідне для проведення вимірювань організаційною одиницею, особливо якщо для оцінки поверхні потрібні 3D-параметри. Розмір вимірюваної області майже лінійно залежить від часу вимірювання. Тому дуже важливо знайти мінімальну площу оцінки. Було виявлено, що в разі поверхні, обробленої гострінням, мінімальна довжина сторони «а» області оцінки становить 1,1 мм і 1,4 мм на основі параметрів шорсткості S_a і S_{sk} відповідно. Мінімальна довжина поверхні при шліфуванні становить 1,2 мм і 1,25 мм відповідно.*

Ключові слова: *області оцінки 3D шорсткості; статистичні параметри; топографія поверхні; мінімальна площа оцінки.*

UDC 621.914.1 **doi: 10.20998/2078-7405.2020.93.08**

A. Nagy, Miskolc, Hungary

INFLUENCE OF MEASUREMENT SETTINGS ON AREAL ROUGHNESS WITH CONFOCAL CHROMATIC SENSOR ON FACE-MILLED SURFACE

Abstract. *Roughness measurement is of highlighted importance in production for describing the quality control of manufacturing processes for the functional, tribological, etc. properties of the surfaces of parts. In the last 15 years or so the areal roughness studied on topographies has also become more common, as it provides a more accurate and detailed characterization of the surfaces. However, with relatively little experience and different technical conditions, topographies are analyzed differently. Sometimes 3D topography is used only as an illustration; however, spatial roughness measurement can provide much more information. The effect of measurement speed and point density during roughness measurement on the areal roughness was investigated using a confocal chromatic sensor.*
Keywords*: surface roughness; areal roughness; confocal chromatic sensor.*

1 INTRODUCTION

Surface roughness is the most commonly used indicator to describe surface quality [1]; therefore, roughness measurement has an emphasized importance in production, which, serves as a tool to describe operational, tribological, and other properties in addition to maintaining quality control of production processes. In the products, the connecting surfaces must perform predictably, due to the functional or application properties prescribed for the components. This is important, for example, regarding sliding friction phenomena and thus wear. A clear definition of the relationships between the technological and application properties of surfaces is complicated, so it is difficult to infer the functional properties of surfaces directly from the profile and spatial roughness parameters of the surfaces [1].

The study of the measurement conditions is also justified by the fact that more and more complex surfaces can be produced, and the increase of productivity and the kinematic solutions applied on machine tools and the technological settings also require more accurate analysis. For example, greater feed rates [2] increase productivity but significantly affect roughness, which increases the difference between roughness values measured in different directions in face milling [3,4].

The roughness of a surface along a profile has been studied for more than 100 years [5], and various methods have been developed to perform the measurements. Based on many years of experience, agreements have been established to unify recording settings in measurement operations, which have been incorporated into various national and international standards.

In the last decade and a half, the areal roughness studied on topographies has also become more widespread, as it provides a more accurate and detailed characterization

of the surfaces than profile examination. However, information obtained from topographies is still not handled in a professional manner [6]. In the following, the overview shows the parameters along which the surfaces can be examined on the measuring device(s).

Klauer et al. [7] examined topographies produced by micro milling on a brass alloy where the tilt angle of the tool axis was changed. The surfaces were analyzed at several locations with a confocal microscope and Gaussian filter was used to evaluate the roughness measurements. Furthermore, based on the distance of a period on the machined topography, two standard L-filters (λ_c=80 and 25 μm) were set and an S-filter (λ_s = 5 μm) was used for the latter to remove the noise of the measurement signal. With the two settings, they examined which filter values have a better correlation with the roughness of the surfaces. The values of S_a and S_q were examined.

Topographies of mono- and polycrystalline ceramics machined by grinding and lapping were studied by Niemczewska-Wójcik et al. [8]. The surfaces were measured with a white light interferometry microscope. Height, spatial, and functional parameters of areal roughness were examined along with R_a average roughness. For the roughness test, an S-filter was used to eliminate the measurement noise and a threshold to eliminate irrelevant valleys and peaks.

In high-speed face milling of magnesium alloy with a PCD tool, the effect of machining parameters (v_c, f_z, a_p) on the surface roughness was investigated [1]. The surfaces were measured with a stylus gauge, the main direction of which was adjusted perpendicular to the edge traces. In the evaluation a Gaussian filter was used, but no information was reported on other steps. In the article, height roughness indices were investigated, and the Abbott-Firestone curve was also analyzed in relation to S_{sk} and S_{ku} parameters.

Wojciechowski et al. [9] studied the effect of change of cutting speed while grooving with a diamond dispersed cemented carbide tool. Here the topography of the surface was not influenced by the feed rate, but mainly by the microprofile of the cutting edge, the vibrations of the machining system and the decohesive mechanisms of the material. The roughness of the machined surfaces was measured with both stylus and optical devices. The profiles were examined with L-filter (2.5 mm) and Gaussian filter, though the method of evaluation of the topography was not reported. Height areal roughness indices were examined in correlation with the cutting speed.

To achieve the required surface quality in Wire EDM, Mouralova et al. analyzed the effect of cutting speed and determined the optimal value [10]. Topographies were measured with a contactless 3D profilometer. The primary and roughness profile parameters and the areal roughness S_a, S_z and S_q of the S-F surfaces were analyzed. Methods of measurement and evaluation were not reported.

Most of the publications dealing with the determination of surface roughness parameter values do not justify the choice of the values set on the roughness measuring instrument. Furthermore, the literature review also shows that topographies are

examined in different ways in terms of size of measured areas, measurement settings and evaluations, so it is not possible to accurately compare machined surfaces.

2 EXPERIMENTAL METHOD AND CONDITIONS

In this paper, the aim of the study is to analyze the effects of the roughness measurement setting options on the values of the areal roughness parameters with the confocal chromatic sensor of the roughness measuring device. In doing so, I vary the measurement speed and the distance between the measured points to examine how and to what extent they affect the roughness values.

2.1 EXPERIMENTAL METHOD

Information on the measurement of areal roughness of the topography is given in the international standard ISO 25178:2012. A part of this, ISO 25178-3:2012 [11] gives a recommendation for measurements, which are briefly the following. The tested topography should be square, the main test direction should be the same as described in the relevant standard for profile measurement. The shape deviation on the measured surface should be removed according to the nominal shape, and the S-filter separating the micro-roughness and the cut-off length of the L-filter separating the roughness from the waviness should be used as Gaussian filtering in both X and Y directions. The value of the L-filter can be selected from the attached table in [11], which may be the same as the corresponding value in ISO 4288:1998. The measuring length should be five times the length of the L-filter in the main direction. I conducted my studies in compliance with these.
The following parameters can be set during roughness measurement:

- Distance between the points in the main measuring direction (X direction)
- Measuring speed in the main measuring direction
- Distance between the points in the perpendicular measuring direction (Y direction)
- Measured area size; start, center and end point
- Type of sensor used for the measurement and the associated configuration data
- Brightness of the emitted light beam.

However, not all of these parameters affect the accuracy of the measurement. The brightness of the light beam has no effect if the sensor can read all the points examined on the surface. Therefore, I set it based on a scan on the entire surface in advance; there was not too little or too much reflected light to the detector. Then I pre-selected the type of sensor used for the measurements; in this respect it does not affect the result. Furthermore, the size of the measured area may determine the accuracy of the roughness, but I selected it in advance based on the above recommendations, and I also defined the measurement positions, so I will not examine their effect now. So, I

determined the measurement setting parameters – the density of the point and the measurement speed – by changing factors that can influence the accuracy.
First, I examine the effect of measurement speed. The measuring program limits this in the main direction by the product of the point distance in the discussed direction and the sampling frequency. On the other hand, if the height value of the points is read equally as often or less frequently than the set frequency of an optical sensor, this theoretically has no effect on the accuracy of the measurement. To prove this, I measured area B (see Figure 1) at different velocities and examine the effect of the speed on roughness. The point distances in X, Y directions were the same. Next, I analyze the effect of the density of the Y-direction points on the roughness in the three measurement areas (see Figure 1). Here, I did not change the other two setting data: the X-direction velocity and the main-direction point density. Finally, I examine the effect of X-direction point density, where I kept the X-direction velocity and the Y-direction point distance constant. The set data is summarized in Table 1. In each case, I compare the values of some frequently used areal roughness parameters defined by ISO 25178-2:2012.

Table 1 – Values set during measurement

Examined parameter		**Fixed values**	
Velocity in direction X	v_x=200,300,400,500,600, 700,800,900,1000 μm/s	X=1 μm,	Y=20 μm
Point distance in Y	Y=1,2,5,10,15,20,25 μm	v_x=1000 μm/s,	X=1 μm
Point distance in X	X=1,2,3,4,5,6,7 μm	v_x=1000 μm/s,	Y=10 μm

2.2 EXPERIMENTAL CONDITIONS

For the topography examination, a specimen was machined on a Perfect Jet MCV-M8 vertical CNC milling machine. A Sandvik R252.44-080027-15M face milling head with a Sandvik R215.44-15T308M-WL type, GC4030 grade coated carbide insert in only one nest was used, with the geometry κ_r=90°, κ_r'=1.5° γ_o=0°; α_o=11°; r_ε=0.8 mm. The workpiece was made of normalized C45 non-alloy steel (1.0503) with a machined surface of 50×58 mm^2. The cutting data were as follows: cutting speed v_c=300 m/min, depth of cut a_p=0.8 mm, width of cut a_e=58 mm, feed rate per tooth f_z=0.1 mm/rev. Due to the tool axis position perpendicular to the working plane, double cutting marks formed on the surface.
An AltiSurf 520 three-dimensional roughness measuring instrument was used for the measurements on the specimen. I measured the surface with a CL2 confocal chromatic sensor with a MG140 magnifier, which has the vertical measurement range 300 μm and its sensitivity 0.012 μm. The sampling frequency of the gauge is 1000Hz. The position of the measured areas is illustrated in Figure 1, their size was chosen to 1.25×1.25 mm^2, based on the recommendation of ISO 25178-3:2012 [11].

I repeated each measurement setting three times, and their arithmetic mean values were used for the examinations.

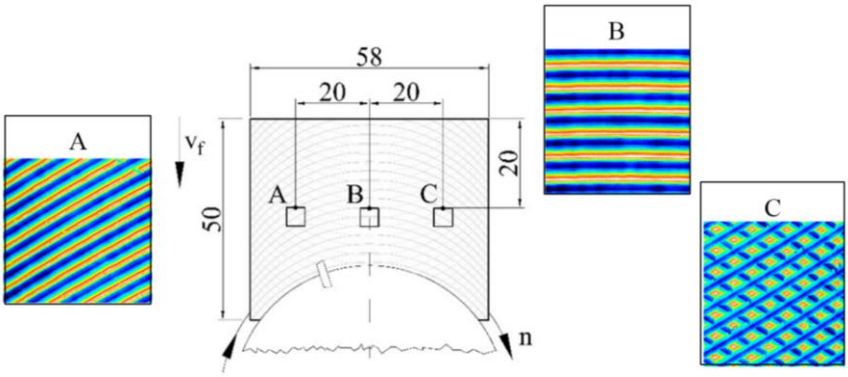

Figure 1 – Positions of the measured areas

There are different tools for measuring surface topography with variable measuring range and vertical accuracy, e.g. coordinate measuring machine, stylus profilometer, interference microscope, confocal microscope, SEM, AFM, STM, etc. Although contact measurement techniques can map topographies with high resolution over a wide measurement range, they are relatively slow and can damage samples. Contactless procedures are used to avoid this. Optical instruments became popular when it was realized that the information obtained from profile measurements was not sufficient for the functional properties of machined parts, but could be satisfied by topographic measurements, and optical instruments could quickly evaluate the surface texture of the area [6]. The measuring range of the confocal chromatic sensor I used is relatively small; however, its vertical resolution is below μm, which is suitable for the examination of surfaces machined with defined edge tools.
The evaluation of the measurements was executed in AltiMap Premium v6.2 software. In each case, I applied different filters on the S-L surfaces, first eliminating the shape defect, which means leveling on a flat surface. Then, with the Threshold function, I cut off the faulty parts on the topographies, and finally I set a Gaussian filter and with it an L-filter (λ_c=0.25 mm) too.

3 RESULTS AND DISCUSSION

First, I analyze the effect of X-direction measurement velocity on roughness. For this, I summarize the results in Table 2 and plot them in Figure 3, in which I bound the range of deviation of each parameter value and indicate its value.

Table 2 – Roughness values according to X-direction measurement speed

Speed [µm/s]	**200**	**300**	**400**	**500**	**600**	**700**	**800**	**900**	**1000**
S_q [µm]	0.490	0.488	0.486	0.488	0.486	0.485	0.485	0.484	0.485
S_a [µm]	0.419	0.417	0.415	0.416	0.414	0.415	0.413	0.413	0.415
S_z [µm]	2.761	2.743	2.702	2.752	2.658	2.669	2.679	2.653	2.640
S_{sk} [-]	0.481	0.479	0.482	0.481	0.479	0.461	0.468	0.466	0.466
S_{ku} [-]	2.129	2.136	2.140	2.131	2.121	2.113	2.123	2.111	2.095

The values of each parameter change slightly, each has a deviation within 0.5–4.5%. Among the parameters S_z total height shows maximum fluctuation. Furthermore, regarding S_q and S_a, the values do not show monotony, they occupy random places in their deviation zone. However, the values of S_z, S_{sk}, and S_{ku} appear to decrease at higher velocities for the most part in the studied range. Considering the values of the parameters together, it can be stated that any value can be used in the speed range between 700 and 1000 µm/s can be used, in which case only minimal error should be expected.

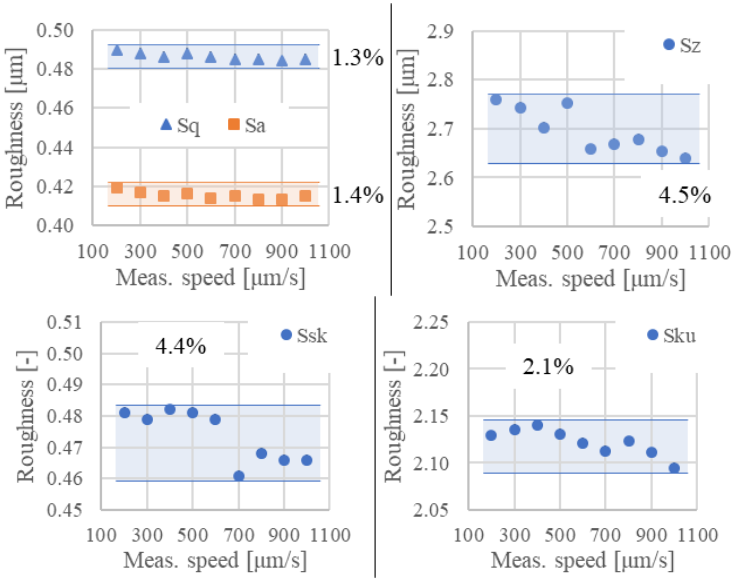

Figure 2 – Roughness values as a function of measurement speed

Table 3 – Roughness values according to Y-direction point density

Distance [μm]	**Area**	**1**	**2**	**5**	**10**	**15**	**20**	**25**
S_q [μm]	A	0.493	0.481	0.471	0.464	0.465	0.419	0.422
	B	0.483	0.484	0.483	0.475	0.477	0.487	0.477
	C	0.518	0.516	0.498	0.469	0.475	0.422	0.430
S_a [μm]	A	0.413	0.403	0.394	0.393	0.394	0.360	0.356
	B	0.415	0.416	0.415	0.409	0.410	0.417	0.410
	C	0.422	0.421	0.407	0.390	0.390	0.352	0.353
S_z [μm]	A	2.764	2.671	2.546	2.376	2.450	2.289	2.393
	B	2.782	2.770	2.562	2.431	2.481	2.646	2.326
	C	2.717	2.712	2.524	2.434	2.524	2.318	2.398
S_{sk} [-]	A	0.563	0.552	0.546	0.500	0.506	0.402	0.450
	B	0.458	0.448	0.443	0.427	0.433	0.465	0.415
	C	0.632	0.622	0.603	0.536	0.555	0.453	0.546
S_{ku} [-]	A	2.223	2.184	2.157	2.079	2.126	2.018	2.208
	B	2.041	2.016	1.988	1.946	1.971	2.096	1.946
	C	2.474	2.434	2.369	2.229	2.318	2.218	2.447

Next, I analyze the effect of the Y-direction point spacing on the roughness in the three measurement areas (see Figure 1), for which I give the results of the roughness parameters in Table 3 and plot them in diagrams (Figure 3).

On the specimen surface, the value pairs of the side areas are always similar, but the value of area B differs to a greater extent in some cases. However, here the smallest derivation of the values is observed. The nature of the change in the values of each area as a function of distance is random, it cannot be determined exactly. By observing the development of the roughness values together in all three planes, I find that by setting the distance between 5 and 15 μm, roughness results can be obtained with the smallest error.

The effect of the setting of X-direction point density is shown in the following. For this, the roughness values in the three measurement areas are gathered in Table 4 and plotted in Figure 4. The changes in the values measured on the surface in all three areas are of the same nature and magnitude as a function of distance. One case is an exception; for the index S_z in area B, the values decrease more significantly as the distance increases. The values of the parameters S_{sk} and S_{ku} change very little, so by setting any spacing value within the examined range, we obtain almost the same roughness parameters, with minimal error. Regarding the values of S_q, S_a and S_z, it was found that for the setting parameter in the range of 1 and 3 μm there is a little difference between the values, so any value in the range can be used with minimal error.

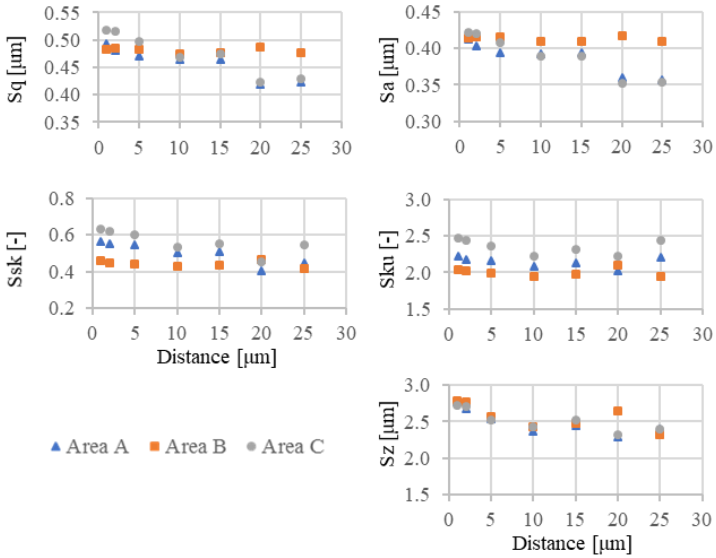

Figure 3 – Roughness values as a function of Y-direction point density

Table 4 – Roughness values according to X-direction point density

Distance [µm]	**Area**	**1**	**2**	**3**	**4**	**5**	**6**	**7**
S_q [µm]	A	0.464	0.458	0.457	0.445	0.443	0.442	0.438
	B	0.475	0.469	0.469	0.461	0.456	0.448	0.447
	C	0.469	0.462	0.460	0.449	0.447	0.438	0.434
S_a [µm]	A	0.393	0.388	0.386	0.377	0.375	0.375	0.373
	B	0.409	0.405	0.405	0.402	0.395	0.391	0.391
	C	0.390	0.384	0.383	0.375	0.375	0.367	0.363
S_z [µm]	A	2.376	2.346	2.363	2.276	2.275	2.242	2.168
	B	2.431	2.404	2.378	2.149	2.159	2.016	1.971
	C	2.434	2.422	2.394	2.368	2.363	2.170	2.132
S_{sk} [-]	A	0.500	0.498	0.494	0.473	0.459	0.460	0.450
	B	0.427	0.418	0.418	0.403	0.380	0.361	0.354
	C	0.536	0.533	0.530	0.511	0.506	0.492	0.484
S_{ku} [-]	A	2.079	2.065	2.063	2.024	2.010	1.992	1.978
	B	1.946	1.908	1.904	1.845	1.880	1.803	1.788
	C	2.229	2.201	2.194	2.150	2.139	2.101	2.086

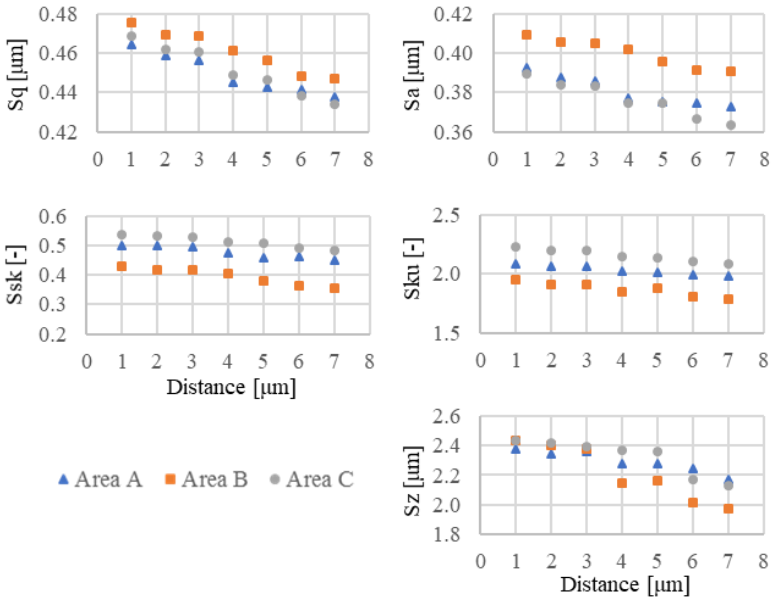

Figure 4 – Roughness values as a function of X-direction point density

4 CONCLUSIONS

The roughness of a topography is a topic increasingly often being studied in industry and in different research areas; however, areal roughness is examined differently in terms of measurement settings and method of evaluation. In the present paper, the effect of three roughness measurement setting parameters on the areal roughness was investigated on a face milled specimen, measured with a confocal chromatic sensor. During the analysis I drew the following conclusions.

Changing the measurement speed in the main direction resulted in small differences in the roughness values in the area aligned to the plane of symmetry, and there was a 4.5% maximum deviance of the values. With the increase of the velocity, there was a random change in S_a, S_q values, and a decrease in S_z, S_{sk}, and S_{ku}. I found the smallest differences within the studied range at higher speed values. The measurement was performed in a speed range where the measurements read from the detector were equal or less than the value of the sensor sampling frequency during the measurements, so the observations are valid only in this range.

The distances of the points taken along the main direction were examined at three different locations on the surface: in the plane of symmetry of the workpiece and at equal distances in two directions from it. There was a slight decrease in roughness values with increasing distance. The skewness and kurtosis values hardly changed, the parameters S_z, S_a, S_q showed the least change at the smaller values of the examined range (1–3 μm).

Analyzing the distance of the points taken perpendicular to the main direction, the variance of the values in each measurement area was small, but it was random/scattered. Overall, minimal deviations were measured per area in the middle part of the studied range (5–15 μm).

Ranking the examined areal roughness parameters in ascending order according to their overall sensitivity to the changed setting parameters, the smallest differences were found in S_{ku} kurtosis and S_{sk} skewness. These are followed by the S_q root-mean-square average, which had a smaller deviation than the S_a average roughness. The greatest variability was given by the values of S_z total height.

ACKNOWLEDGEMENT

The described study was carried out as part of the EFOP-3.6.1-16-00011 "Younger and Renewing University – Innovative Knowledge City – institutional development of the University of Miskolc aiming at intelligent specialization" project implemented in the framework of the program Szechenyi 2020.

References: 1. *I. Zagórski, J. Korpysa:* Surface Quality Assessment after Milling AZ91D Magnesium Alloy Using PCD Tool, Materials vol.13(3) (2020) ArtNo:617. **2.** *B. Karpuschewski, J. Kundrák, T. Emmer, D. Borysenko:* A New Strategy in Face Milling - Inverse Cutting Technology, Solid State Phenomena vol.261 (2017) pp.331-338. **3.** *J. Kundrak, C. Felho:* 3D roughness parameters of surfaces face milled by special tools, Manufacturing technology vol.16(3) (2016) pp.532-538. **4.** *G. Varga, J. Kundrák:* Effects of Technological Parameters on Surface Characteristics in Face Milling, Solid State Phenomena vol.261 (2017) pp.285-292. **5.** *Jiang, X., Scott, P. J., Whitehouse, D. J., Blunt, L.:* Paradigm shifts in surface metrology. Part I. Historical philosophy, Proceedings of the Royal Society A: Mathematical, Physical and Engineering Sciences vol.463(2085), (2007) pp.2049-2070. **6.** *S.K. Fecske, K. Gkagkas, C. Gachot, A. Vernes:* Interdependence of Amplitude Roughness Parameters on Rough Gaussian Surfaces, Tribology Letters vol.68(1) (2020) pp.1-15. **7.** *K. Klauer, M. Eifler, B. Kirsch, J. Seewig, J.C. Aurich:* Ball end micro milling of areal material measures: influence of the tilt angle on the resulting surface topography, Production Engineering vol.14(2) (2020) pp.239-252. **8.** *M. Niemczewska-Wójcik, A. Wójcik:* The multi-scale analysis of ceramic surface topography created in abrasive machining process, Measurement vol.166 (2020) ArtNo:108217. **9.** *S. Wojciechowski, R. Talar, P. Zawadzki, S. Legutko, R. Maruda, C. Prakash:* Study on Technological Effects of a Precise Grooving of $AlSi1_3MgCuNi$ Alloy with a Novel WCCo/PCD (DDCC) Inserts, Materials vol.13(11) (2020) ArtNo:2467. **10.** *K Mouralova, L Benes, T Prokes, J Bednar, R. Zahradnicek, J. Fries:* Machining of pure molybdenum using WEDM, Measurement vol.163 (2020)

ArtNo:108010. **11.** Geometrical product specifications (GPS) — Surface texture: Areal — Part 3: Specification operators. ISO 25178-3:2012. Geneva: International Organization for Standardization.

Антал Надь, Мішкольц, Угорщина

ВПЛИВ НАЛАШТУВАНЬ КОНФОКАЛЬНОГО ХРОМАТИЧНОГО ДАТЧИКА НА РЕЗУЛЬТАТИ ВИМІРЮВАНЬ ШОРСТКОСТІ ФРЕЗЕРОВАНОЇ ПОВЕРХНІ

Анотація. *Вимірювання шорсткості має особливо важливе значення у виробництві для опису контролю якості виробничих процесів щодо функціональних, трибологічних і інших властивостей поверхонь деталей. Поверхнева шорсткість, яка вивчалася на топографії, стала більш поширеною, оскільки вона забезпечує більш точний і докладний опис поверхонь. Для вимірювань зразків використовувався прилад для тривимірного вивчення шорсткості AltiSurf 520. Вимірювалася поверхня конфокальним хроматичним датчиком CL2 з лупою MG140, що має вертикальний діапазон виміру 300 мкм і чутливість 0,012 мкм. Частота дискретизації датчика становила 1000 Гц. Розмір вимірюваних областей був обраний 1,25 × 1,25 мм^2, виходячи з рекомендації ISO 25178-3:2012. Налаштування процесу вимірювання повторювалися тричі, і їх середньоарифметичні значення були використані для досліджень. Оцінка вимірювань виконувалася в програмі AltiMap Premium v6.2. У кожному разі застосовувалися різні фільтри на S-L-поверхнях, спочатку усуваючи дефект форми, що означало вирівнювання на плоскій поверхні, потім за допомогою функції «Поріг» вирізалися дефектні частини на топографії і, нарешті, встановлювався фільтр Гауса, а разом з ним і L-фільтр (λc = 0,25 мм). Зміна швидкості вимірювання в основному напрямку привела до невеликих розбіжностей в значеннях шорсткості в області, суміщеної з площиною симетрії, і максимальне відхилення значень склало 4,5%. Зі збільшенням швидкості відбувалася випадкова зміна значень S_a, S_q і зменшення S_z, S_{sk} і S_{ku}. Найменші відмінності в досліджуваному діапазоні були виявлені при більш високих значеннях швидкості. Вимірювання проводилося в діапазоні швидкостей, в якому вимірювання, зняті з детектора, були рівні або менше значення частоти дискретизації сенсора, тому спостереження дійсні тільки в цьому діапазоні.*

Ключові слова: *шорсткість поверхні; зональна шорсткість; конфокальний хроматичний датчик.*

UDC 621.9.048.4 **doi: 10.20998/2078-7405.2020.93.09**

E. L. Papazoglou, N. E. Karkalos,
A. P. Markopoulos, Athens, Greece,
P. Karmiris-Obratański, Cracow, Poland

ON THE MACHINING OF ALUMINUM ALLOY AL6063 WITH EDM

Abstract. *Electrical Discharge Machining (EDM) is a non-conventional machining process, which allows the machining of any electrical conductive material, regardless its mechanical properties, with high dimensional accuracy, and in complex shapes and geometries. EDM widely utilized by modern industry, taking advantage of its unique inherent capabilities. Aluminum alloys find extensive use in numerous applications, and their machining consist an interesting topic, with tangible industrial interest. The current study presents an experimental investigation of machining Al6063 alloy with EDM. A full scale experiment was conducted, with control parameters the pulse-on current and time. The productivity of the process calculated based on the Material Removal Rate (MRR), while the Surface Roughness of the machined surfaces was estimated in terms of R_a and R_t. For these performance indexes Analysis Of Variance was performed and semi-empirical relations that correlate machining parameters with obtained results were proposed. Finally, the cross sections of the specimens were observed in optical microscopy, in order the formation of the White Layer to be studied.*
Keywords: *Electrical Discharge Machining; Aluminum alloys; Material Removal Rate; Surface Roughness; pulse-on current and time; White Layer; Analysis of Variance*.

INTRODUCTION

Electrical Discharge Machining (EDM) is classified as a non-conventional machining process, which utilizes repetitive rapid sparks to remove material from the workpiece. A pulsed voltage difference is applied between the working electrode and the workpiece, both of which been submerged into a dielectric medium. Under specific conditions of voltage difference and gap distance between electrode and workpiece, the insulating effect of the electric fluid breaks down, resulting a single spark to be discharged. This spark forms a plasma channel between the electrode and the workpiece, with reached temperatures in the range of 6000-12000K. Thermal energy from this plasma channel is absorbed by the electrode and the workpiece, causing material to melt and ablate. At the end of the pulse, the plasma channel collapses, and the electrode - workpiece system returns to its initial state. From every spark, a tiny crater is formed, with the removed material volume been in the range of 10^{-6} - 10^{-4} mm^3; the total material removal is resulted by thousands, even millions of consecutive sparks [1], [2]. Although EDM is a multiparameter process the most significant control parameters are the pulse-on current (I_p) and the pulse-on time (T_{on}) [3]. EDM is widely used in modern industrial environment, since it is a non-contact material removal process,

capable to handle any electrical conductive material, regardless its mechanical properties.

Moreover, by utilizing EDM, high dimensional accuracy can be obtained, in complex shapes and geometries. EDM finds extensive applicability in aerospace, automotive, biomedical and die industry [4]. Finally, the process performance is mainly measured in terms of Material Removal Rate (MRR), Tool Wear Ratio (TWR), and machined Surface Roughness (SR), by often employing the Ra and Rt indexes [5].

Aluminum alloys are widely employed in numerous of industrial applications, hence, in addition to the conventional machining methods, EDM is utilized in their machining, especially where high quality standards are required. In the work of Khan [6] the MRR and the electrode wear were studied during machining aluminum and mild steel with EDM by using copper and brass working electrodes. It was verified the dependence of the machining performances from the electrode and workpiece material, and the pulse-on current. Gatto et al. [7] conducted research concerning the performance optimization in machining aluminum alloys for moulds production with EDM. Namely, the Al2219-T6, Al7050-T6, and Al7075-T6 alloys were studied, in roughing, semifinishing and finishing machining operations, while the machining performances were estimated in terms of dimensional accuracy and surface roughness. According to the relevant literature, the aluminum alloy 6 series gathers research interest. Arooj et al. [8] studied the effect of pulse-on current in machining Al6061-T6 with EDM, focusing mainly on the MRR and the obtained surface roughness and morphology. Al6061 was also studied by Pramarik et al. [9] in its machining with EDM, by employing graphite electrode and two different dielectric mediums, paraffin oil and distilled water. Again their research was mainly focused on the MRR, the electrode wear, and the surface quality. The surface quality was estimated in terms of surface roughness, and Average White Layer Thickness (AWLT). The machining of aluminum alloys with EDM becomes even more interest topic considering that aluminum alloys are utilized as metal matrix in composite materials, and EDM consist a feasible and efficient method in machining these kind of materials [10]–[12]. For example, Radhika et al. [13] presented a study regarding the optimization of EDM parameters in machining aluminum hybrid composites by using the Taguchi method. The experiment control parameters were the pulse-on current, the pulse-on time, and the dielectric fluid flushing pressure, while the machining performances were estimated in terms of MRR, TWR, and R_a .

The current paper presented an experimental investigation of machining aluminum alloy 6063 with EDM. Al6063 is one of the most commonly used aluminum alloys, with a wide range of applications. The experiments were carried out to investigate how the pulse-on current and time affect the MRR and the machined Surface Roughness. The SR was estimated in terms of R_a and R_t, while the surfaces' cross

sections were observed through optical microscopy in order the formation of White Layer to be studied. Finally, for the aforementioned machining performances indexes Analysis of Variance (ANOVA) was performed and semi-empirical relations that correlate machining parameters with results were proposed.

EXPERIMENTAL PROCEDURE

Experiments were carried out on an ANGIETRON EMT 1.10 die sinking EDM machine using plates of aluminum 6063 as workpiece material. Chemical composition and basic thermo-physical properties of Al6063 alloy are presented in table 1. In the experiments a copper electrode with nominal dimensions of 38x23mm was utilized, while the electrode was cleaned between the experiments in order to avoid any depositions accumulation on its surface. Highly purified synthetic hydrocarbon oil was applied as dielectric medium that was properly channeled into the working tank for efficient debris removal. Finally, in order a full surface morphology to be formed a nominal 1mm cut depth was set. A full-scale experiment was carried out for pulse-on current and time from 15 up to 24A and from 100 up to 500μs respectively. In table 2 the machining parameters are listed in details. The machining voltage was kept constant, specifically, 100 and 30V the open and close circuit voltage respectively. The Duty Factor (η) was automatically adjusted by the machine, and could be indirectly estimated based on the mean current. Taking in mind that voltage pulses can approximated by square pulses, the Duty Factor is calculated based on eq. 1:

$$\eta = \frac{\overline{I_p}}{I_p} \tag{1}$$

with $\bar{I}_p$ with the ammeter indication of the mean current intensity in A and I_p the nominal pulse-on current in A.

The MRR is defined as the volume of the removed material per minute, and calculated based on eq. 2:

$$MRR = \frac{W_{st} - W_{fin}}{\rho \cdot t_m} \tag{2}$$

with MRR the material removal ratio in gr/min, $W_{st.}$, W_{fin} the workpiece weight before and after machining, respectively, in gr, ρ the workpiece material density in gr/mm^3 and t_m the machining time in min.

The average (R_a) and the maximum (R_t) surface roughness were calculated as the mean value of five consecutive measurements on each machined surface. Furthermore, the machined surfaces cross sections were grinded, polished and chemically treated with proper etchant, being composed of 92ml distilled water, 6ml nitric acid and 2ml hydrofluoric acid and the etched surfaces were observed in optical microscope. Finally for all the aforementioned measured and/or calculated

indexes, ANOVA was performed and semi-empirical correlations between machining parameters and results were proposed.

Table 1 – Al6063 chemical composition and thermo-physical properties

Component Wt%	Al (max)	Cr (max)	Cu (max)	Fe (max)	Mg	Mn (max)	Si	Ti (max)	Zn (max)
	97.5	0.1	0.1	0.35	0.45-0.9	0.1	0.2-0.6	0.1	0.1
Physical Properties	Density (g/mm^3)		Electrical Resistivity (ohm/m)		Specific Heat Capacity (kJ/kgK)		Thermal Conductivity (W/mk)		Melting Point (K)
	0,0027		3.32e-4		0.9		200		908

Table 2 – Machining parameters

Machining Conditions	**Level 1**	**Level 2**	**Level 3**	**Level 4**
Discharge current I_p (A)	15	18	21	24
Pulse on-Time T_{on} (µs)	100	200	300	500
Dielectric	Synthetic Hydrocarbon Fluid			
Dielectric Flushing	Side Flushing			
Open circuit Voltage (V)	100			
Close circuit Voltage (V)	30			

RESULTS AND DISCUSSION

Table 3 – Experimental results

I_p (A)	**T_{on} (µs)**	**MRR (mm^3/min)**	**Ra (µm)**	**Rt (µm)**
15	100	125,66	8,10	53,40
18	100	189,49	9,30	62,40
21	100	148,15	9,10	64,80
24	100	211,64	10,30	77,60
15	200	139,65	11,20	67,80
18	200	189,30	12,40	88,60
21	200	194,00	11,80	83,40
24	200	233,92	13,40	85,80
15	300	129,63	14,20	89,20
18	300	161,62	14,20	96,40
21	300	189,30	13,80	101,00
24	300	219,91	15,00	94,00
15	500	133,10	13,70	94,80
18	500	177,13	16,00	101,40
21	500	170,37	13,60	85,80
24	500	202,82	16,70	110,20

In table 3 – the experimental results are presented, based on which the following ANOVA was performed.

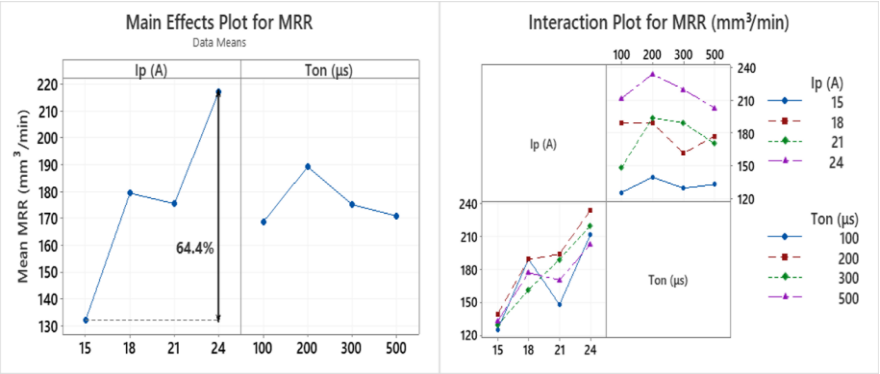

Figure 1 – Main Effects Plot and Interaction Plot for MRR

In figure 1 the Main Effects Plot and the Interaction Plot of MRR are presented. As it is clearly deduced, the pulse-on current has the main and major effect on MRR, while pulse-on time slightly and vaguely affects the MRR. More specifically, as the I_p increased from 15 to 18A the MRR for all pulse-on times increased, while a further increase up to 21A resulted a stabilization, even a slight reduction, in MRR. The increase in pulse-on current to 24A was followed by an increase in MRR, with the mean MRR for 24A be 64.4% higher than for 15A. On the other hand, the pulse-on time seems to have a fuzzy and insignificant influence on MRR. Based on a non-linear regression model, the MRR is correlated with pulse-on current and time according to eq. 3:

$$MRR = 11.373\, I_p^{0.9229} T_{on}^{-0.0002} \quad (3)$$

with MRR in mm^3/min, I_p in A and T_{on} in µs.

The correlation level is considered adequate, with S-value 18.31; moreover, in figure 2 the MRR experimental results and those predicted from the regression model are juxtaposed, confirming the sufficient correlation. Finally, the major effect of I_p on MRR is also confirmed by the eq. 3, where the exponents of pulse-on current and time differ orders of magnitude indicating the significance of I_p.

On the contrary of MRR, for SR the major parameter is the pulse-on time. In figure 3 the Main Effects Plot and the Interaction Plot of R_a are presented. It is clear that increase in T_{on} results an increase in R_a, while the pulse-on current does not affect the R_a in a consistent way. Namely, as the T_{on} increased from 100 to 500µs the mean R_a increased 63%, from around 9µm to 15µm.

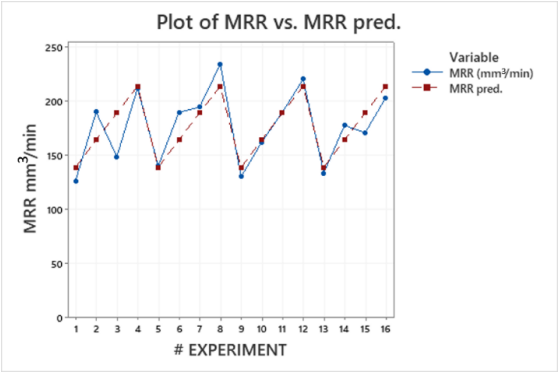

Figure 2 – MRR experimental results vs. predicted ones

On the other hand, increase in I_p resulted both increase and decrease of R_a, depending on the combination of pulse-on current and time. By a more detailed analysis, and based on the Interaction Plot diagram, the constant increase of MRR for higher pulse-on times is confirmed, with only an exception for 15A and 21A and for pulse-on time 500μs, where a slight different behavior is observed. Nevertheless, this does not affect the general rule, namely, that the R_a is mainly affected by the T_{on}, increase of which results an increase in R_a.

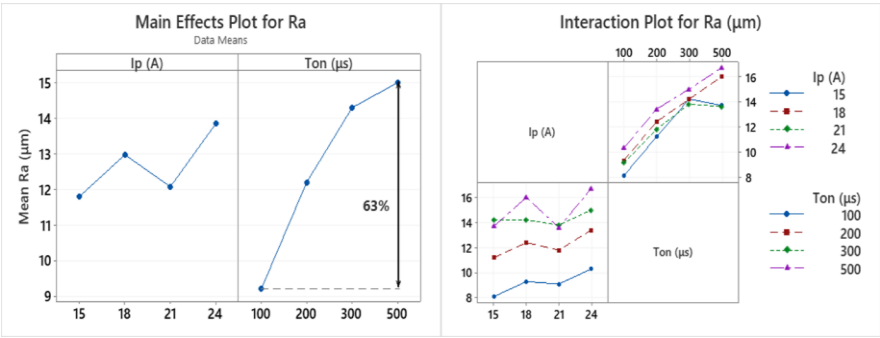

Figure 3 – Main Effects Plot and Interaction Plot for Ra

Again, it is of extreme interest the capability to predict the R_a based on the machining parameters, i.e. the pulse-on current and time. Thus, a semi-empirical relation is proposed, based on the Response Surface Method (RSM). Considering the linear, quadric, and interaction terms, eq. 4 was emerged:

$$Ra = 7.68 - 0.471I_p + 0.0473T_{on} + 0.0167I_p^2 - 0.000054T_{on}^2 - 0.000013I_pT_{on} \quad (4)$$

with R_a in μm, I_p in A and T_{on} in μs. The correlation is adequate, with R-sq 92.05% and S value 0.87. Moreover, the good fit of the model is confirmed by the juxtaposition of experimental and by the model predicted values of R_a in figure 4.

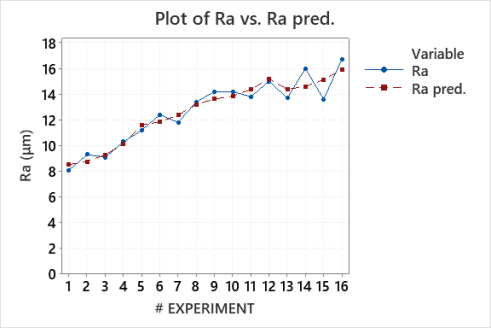

Figure 4 – R_a experimental results vs. predicted ones

Similarly to R_a, the Rt follows the same general rule, namely, it is mostly affected by the pulse-on time, while the pulse-on current seems to have a vague affect on it. In figure 5 the Main Effects Plot along with the Interaction Plot for R_t are presented. An important observation is that plots of R_a and R_t follow almost the same pattern, implying and confirming the existed strong correlation between them. As the pulse-on time increases from 100 to 500μs, the mean R_t increases too, by almost 52%. The Interaction Plot corroborates this trend, with only one exception, and specifically, for 21A and 500μs the R_t was slightly decreased. On the other hand, the increase in I_p results both increase and decrease of R_t, depending on the combination of the machining parameters, thus, any safe and reliable conclusion concerning the affect of pulse-on current on R_t can not be deduced.

The capability to predict the resulted R_t depending on the machining conditions is extremely important and helpful, since R_t is straight related with quality and functionality issues. To correlate the R_t with the pulse-on current and time, for once more, the RSM method was employed. By adopting a model that includes linear, quadric and interaction terms, the semi-empirical correlation of eq. 5 was emerged:

$$Rt = -36.4 + 5.41I_p + 0.3525T_{on} - 0.076I_p^2 - 0.000329T_{on}^2 - 0.00359I_pT_{on} \quad (5)$$

with R_t in μm, I_p in A and T_{on} in μs. The fit of the proposed model is considered adequate, with R-sq 86.05% and S Value 7.25. The good correlation it is further

confirmed by the juxtaposition in figure 5 of the experimentally measured and the predicted values of R_t.

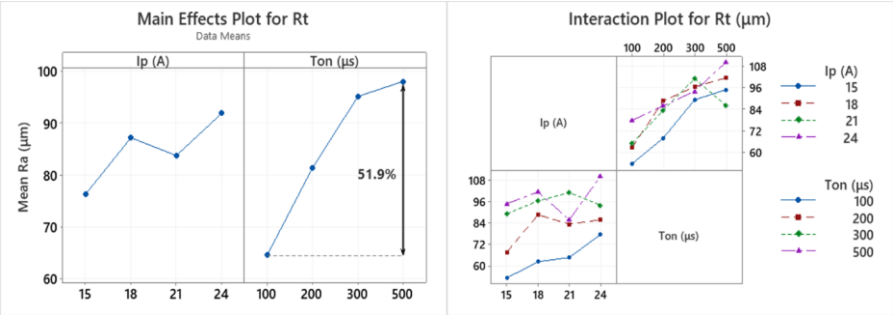

Figure 5 – Main Effects Plot and Interaction Plot for R_t

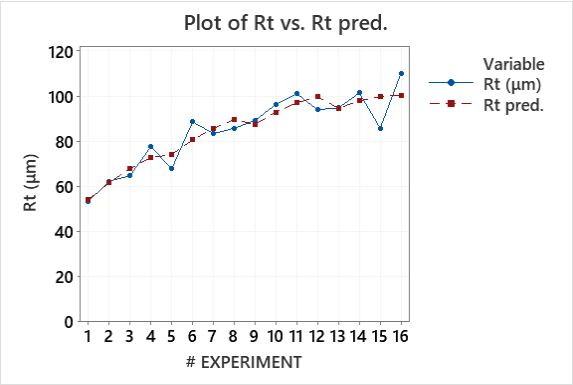

Figure 6 – R_t experimental results vs. predicted ones

During machining with EDM, and as it has already been mentioned, the occurring sparks melt and/or ablate material from the workpiece, forming tiny craters. Nevertheless, only a proportion of the molten material is finally removed by the workpiece, with the rest of it remaining on the workpiece, being re-solidified forming a layer of amorphous material. Additionally, removed and/or ablated material that remained in a close approximation on the surface, it may re-condensed and being deposited on it. This way, a layer of material is formed, well known as White Layer, having different properties from the mother material. WL is differentiated in its thickness and characteristics depending on the machining

parameters, and namely the pulse-on current and time. The machining power, and the per pulse energy significantly affect the WL thickness, with the more intense machining conditions to lead in a thicker WL. Because of the high gradients in temperature and pressure that being developed on the surface, the WL is not always uniform and continuous. In figures 7 and 8 the cross sections of the workpiece for different machining conditions are presented.

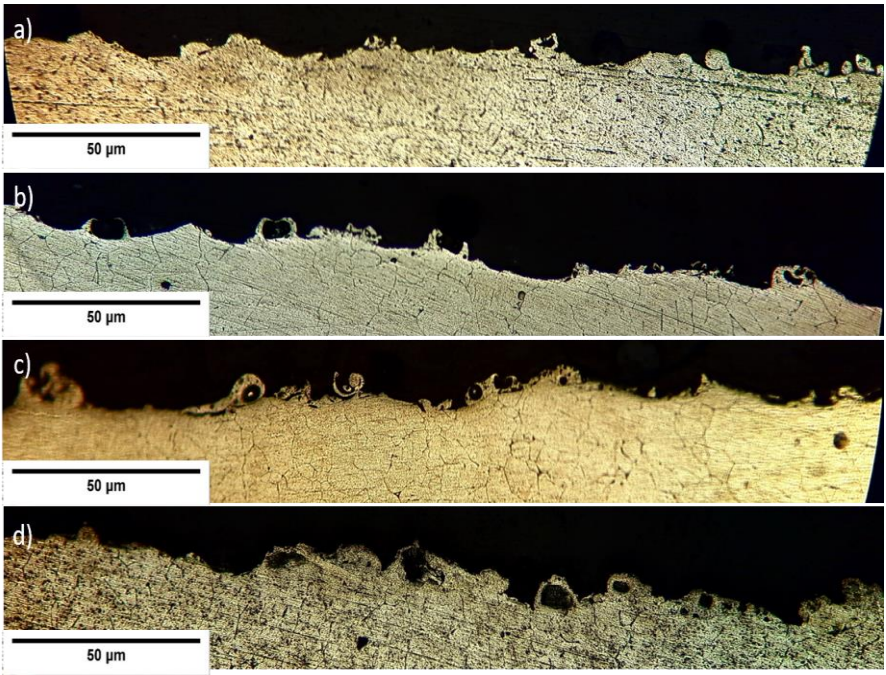

Figure 7 – Machined surface cross sections for 24A and pulse-on time
a) 100µs, b) 200µs, c) 300µs, a) 500µs

The dependence of the WL thickness and its characteristics on the machining conditions is confirmed by the cross section microscopy images that been presented in figure 7. With pulse-on current to remain constant, as the pulse-on time increases the WL becomes thicker, while, some new characteristics are appeared. For T_{on} 100µs the WL is very thin, with some randomly placed formations along its length. For pulse-on time 200µs the WL remains thin, but some hollow formations are emerged. For T_{on} 300µs, a thicker and more uniform WL is formed, while these hollow formations become denser and more bulky.

Finally, for pulse-on time 500μs, a thick continuous WL has been formed, including hollow and bulky formations. These globules of material being shaped because during the rapid material's re-solidification, gases are trapped inside it, resulting these hollow formations. The more intense the machining parameters are, the more bulky and denser these globules become.

In figure 7, the formation of the WL was depicted, as the machining power was kept constant and the per pulse energy being increased (i.e. the pulse-on current was constant and equal to 24A, while the pulse-on time varied from 100 up to 500μs). In figure 8, both, the machining power and the per pulse energy are changing. Similar observations can be made; namely, the WL for the more intense machining conditions become thicker, incorporating more bulky hollow globules For the low pulse-on currents of 15 and 18A, the WL does not have any uniformity, but is appeared more like randomly spread formations. A degree of uniformity is emerged for higher machining powers, where the hollow globules seems to cover major part of the cross section.

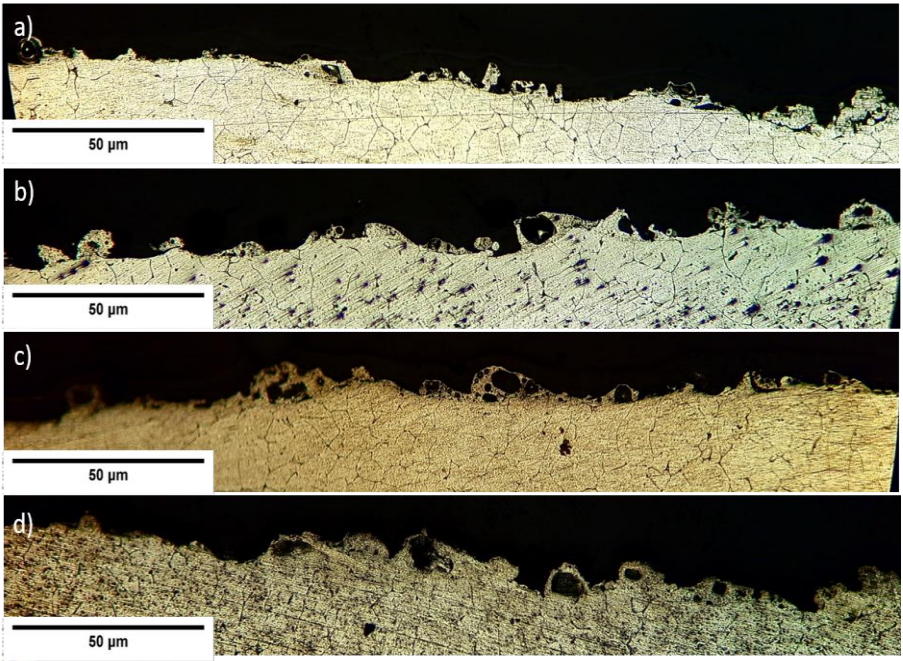

Figure 8 – Machined surface cross sections for 500μs and pulse-on current
a) 15A, b) 18A, c) 21A, a) 24A

CONCLUSIONS

In the current paper an experimental investigation of machining aluminum alloy Al6063 with EDM was presented. A full scale experiment was conducted, with control parameters the pulse-on current and time. The productivity of the machining was calculated based on the MRR, while the surface roughness was estimated in terms of Ra and Rt. For these performance indexes, ANOVA was performed, and semi- empirical relations that correlate machining parameters with its results were proposed. Finally the WL formation was studied through optical microscopy, where the specimens cross sections were observed. The main conclusions of the current study are:

- The MRR is mainly affected by the pulse-on current, as an increase in Ip results an increase in MRR. The pulse-on time has a vague and minor affect on MRR.
- The SR mostly depends on the pulse-on time. Specifically, increase in Ton leads in increase in R_a and R_t. On the other hand, the pulse-on time has a fuzzy influence on SR, hence, no reliable conclusions can be deduced.
- The formation of WL is affected on the machining power, and the per pulse energy. For higher machining power, and pulse energy the WL becomes thicker, while in the more intense machining parameters hollow globules being formed.

References. 1. *M.P. Jahan, Electrical Discharge Machining (EDM):* Types, Technologies and Applications. New York: Nova Science Publishers, 2015. **2**. *E.C. Jameson,* Electrical discharge machining. Michigan: Society of Manufacturing Engineers, 2001. **3.** *J. E. A. Qudeiri, A. I. Mourad, A. Ziout, M. H. Abidi, and A. Elkaseer,* "Electric discharge machining of titanium and its alloys : review," 2018. ***4.*** *N. M. Abbas, D. G. Solomon, and F. Bahari,* "A review on current research trends in electrical discharge machining," vol. 47, pp. 1214–1228, 2007, doi: 10.1016/j.ijmachtools.2006.08.026. **5.** *S. Choudhary and R. Jadoun,* "Current advanced research development of electric discharge machining (EDM): a review," Int. J. Res. Advent Technol., vol. 2, no. 3, pp. 273–297, 2014. **6.** *A. A. Khan,* "Electrode wear and material removal rate during EDM of aluminum and mild steel using copper and brass electrodes," Int. J. Adv. Manuf. Technol., vol. 39, no. 5–6, pp. 482–487, 2008, doi: 10.1007/s00170-007-1241-3. **7.** *A. Gatto, E. Bassoli, and L. Iuliano,* "Performance Optimization in Machining of Aluminium Alloys for Moulds Production: HSM and EDM," in Aluminium Alloys Theory and Applications, T. Kvackaj, Ed. IntechOpen, 2011. **8.** *S. Arooj, M. Shah, S. Sadiq, S. H. I. Jaffery, and S. Khushnood,* "Effect of Current in the EDM Machining of Aluminum 6061 T6 and its Effect on the Surface Morphology," Arab. J. Sci. Eng., vol. 39, no. 5, pp. 4187–4199, 2014, doi: 10.1007/s13369-014-1020-z. **9.** *A. Pramanik, A. K. Basak, M. N. Islam, and G. Littlefair,* "Electrical discharge machining of 6061 aluminium alloy," Trans. Nonferrous Met. Soc. China (English Ed., vol. 25, no. 9, pp. 2866–2874, 2015, doi: 10.1016/S1003-6326(15)63912-7. **10.** *P. Srikanth and C. P. Kumar,* "Electrical discharge machining characteristics of metal matrix composites-A Review," Int. J. Sci. Res., vol. 4, no. 6, pp. 1385–1394, 2015, [Online]. Available: http://www.sciencedirect.com/science/article/pii/S0924013600008232. **11.** *B.C. Kandpal, J. kumar, and H. Singh,* "Machining of Aluminium Metal Matrix Composites with Electrical Discharge Machining - A Review," Mater. Today Proc., vol. 2, no. 4–5, pp. 1665–1671, 2015, doi: 10.1016/j.matpr.2015.07.094. **12.** *L. Selvarajan, J. Rajavel, V. Prabakaran, B. Sivakumar, and G. Jeeva,* "A Review Paper on EDM Parameter of Composite material and Industrial Demand Material Machining," Mater. Today Proc., vol.

5, no. 2, pp. 5506–5513, 2018, doi: 10.1016/j.matpr.2017.12.140. **13.** *N. Radhika, A. R. Sudhamshu, and G. K. Chandran,* "Optimization of Electrical Discharge Machining Parameters of Aluminium Hybrid Composites Using Taguchi Method," J. Eng. Sci. Technol., vol. 9, no. 4, pp. 502–512, 2014.

Емануїл П. Папазоглу, Ніколаос Е. Каркалос,
Ангелос П. Маркопулос, Афіни, Греція,
Панагіотіс Кармініс-Обратанські, Краків, Польща

ПРО ОБРОБКУ АЛЮМІНІЄВОГО СПЛАВУ 6063 ЕЛЕКТРОЕРОЗІЙНИМ СПОСОБОМ.

Анотація. *Електроерозійна обробка (EDM) – це нетрадиційний процес механічної обробки, який дозволяє обробляти будь-який електропровідний матеріал, незалежно від його механічних властивостей, з високою точністю розмірів і складністю форми і геометрії. EDM широко використовується в сучасній промисловості, враховуючи його унікальні можливості. Алюмінієві сплави знаходять широке застосування в багатьох сферах, і їх обробка являє собою цікаву тему, що має відчутний промисловий результат. Ця робота представляє собою експериментальне дослідження обробки металу Al6063 електроерозійним способом. Було проведено повномасштабний експеримент з контрольними параметрами: енергією імпульсів і часом дії імпульсів. Продуктивність процесу розраховувалася на основі швидкості видалення матеріалу (MRR), в той час як шорсткість оброблених поверхонь оцінювалася в одиницях* R_a *і* R_t *. Для показників продуктивності був проведений дисперсійний аналіз і запропоновані напівемпіричні залежності, які корелюють параметри обробки з отриманими результатами. Нарешті, поперечні перерізи зразків вивчали за допомогою оптичної мікроскопії, щоб визначити виникнення «білого шару». Основні висновки цього дослідження такі: На MRR в основному впливає імпульсний струм, так як збільшення сили струму імпульсу Ip призводить до збільшення MRR. Час дії імпульсу* T_{on} *має невизначений і незначний вплив на MRR. Шорсткість поверхні в основному залежить від часу* T_{on} *. Зокрема, збільшення* T_{on} *призводить до збільшення* R_a *і* R_t *. З іншого боку, час* T_{on} *нечітко впливає на SR, тому не можна зробити ніяких надійних висновків. На формування «білого шару» (WL) впливає потужність обробки і енергія в імпульсі. Для більшої потужності обробки та енергії імпульсу WL стає товще, в той час як при більш інтенсивних параметрах обробки утворюються порожні глобули.*

Ключові слова*: електро-ерозійна обробка; сплави алюмінію; швидкість вилучення матеріалу; шорсткість поверхні; енергія імпульсу і час дії; «білий шар»; аналіз дисперсії.*

UDC 621.941.1 **doi: 10.20998/2078-7405.2020.93.10**

I. Sztankovics, Miskolc, Hungary

COMPONENTS OF THE CUTTING FORCE AND THEIR SPECIFIC VALUES AT DIFFERENT FEEDS IN ROTATIONAL TURNING

Abstract. *The alteration of the cutting force is studied by the increase of the feed in rotational turning. The time course of the cutting force components is analysed by experiments done with different edge-geometrical tools, and the specific cutting forces are calculated. One of the findings is the possibility to effectively lower the passive force acting on the cutting tool by the application of rotational turning.*
Keywords: *cutting force; rotational turning; feed; passive force; axial load.*

1. INTRODUCTION

The different applied relative motions and edge geometries of the cutting tools significantly alter the values and ratios of the cutting force and its components. An edge with helical geometry and a tangential circular feed are applied in rotational turning [1], with the geometrical and kinematical relations shown in Figure 1 (n_t: revolutions per minute of the tool; n_w: revolutions per minute of the workpiece; v_a: additional axial feed rate; r_t: radius of the helical cutting edge; λ_s: inclination angle; r_w: radius of the machined surface; R_w: radius of the to be machined surface; a_p: depth of cut; a_w: distance of the symmetry axes).

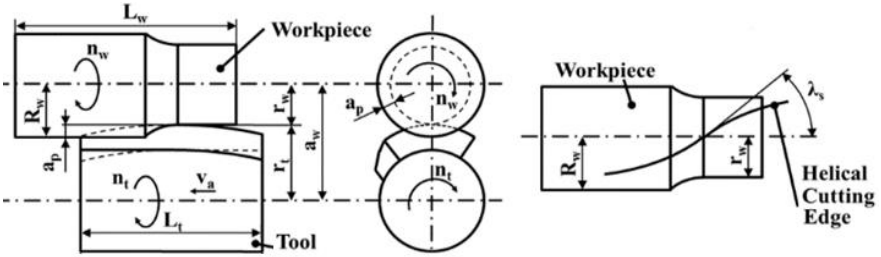

Figure 1 – Geometrical and kinematical relations of rotational turning

In the research of cutting forces the analysis of their specific values is appropriate. Karpuschewski et al. [2] showed that the alteration of the chip ratio by the application of high-feed is a possibility to lower the specific cutting force. Kundrák et al. revealed in their experimental work [3] that the ratio of the force components also varies by the alteration of the feed among the decrease of

the cutting edge specific load. Among the different cutting force components, the tangential component is dominant, according to Denkena et al. [4]. In the work of Tarag et al. [5] we can see that we can achieve stable chip removal by the increase of the feed (among others) due to the decrease of the specific cutting forces and the alteration of the cutting force angle. It can be seen that the value of the feed plays a significant role from the viewpoint of the cutting force. Therefore, the aim of my experiments is to study the specific cutting forces during the increase of the feed in turning with different cutting conditions (rotational and longitudinal turning).

2. EXPERIMENTAL CONDITIONS

The aim of my experiments was the measurement and analysis of the cutting force during chip removal by rotational turning.

The characteristic movement conditions of the procedure are realised on a Perfect-Jet MCV-M8 machining centre during the experiments. The experimental workpiece was clamped in the spindle of the milling machine, whose rotation assured the typical rotational movement of turning. The cutting tool is fixed in the force measurement device (Kistler 9257A) which was clamped on the machine table. The interpolated circular motion of the cutting tool with the machine table realised the relative circular feed around the workpiece. I chose a normalized C45 steel grade with a cylindrical surface of Ø40 mm diameter and 12 mm length. Two rotational turning tools were applied with different inclination angles: R1 – λ_s = 30° (Fraisa P5300682) and R2 – λ_s = 45° (Sandvik Coromant 1P341-1600-XB 1630. For the comparison of the measured values a standard turning tool (S) was also applied (CNMG 120412-PM insert in DCLNL 2525 M 12 holder). I carried out the experiments with 200 m/min cutting speed, 0.1 mm depth of cut and six values of feed for each cutting tool (f = 0.1 mm, 0.2 mm, 0.4 mm, 0.6 mm, 0.8 mm, 1.0 mm).

3. EXPERIMENTAL RESULTS

The X, Y and Z directional forces (linked to the machine table) are measured by the device at a 1000 Hz sampling rate. From the measured values and the momentary position of the workpiece-tool, I calculated for each case the main cutting force (F_c), passive force (F_p) and feed directional force (F_f) in the coordinate system linked to the rotating workpiece. From the completed results of the three cutting tools Figure 2 shows the diagrams of the R1 tool. I also determined the maximal values for the 18 experimental setups (Table 1).

Table 1 – Maximal values of F_c, F_p and F_f

f [mm]		0.1	0.2	0.4	0.6	0.8	1
F_c [N]	R1	51.63	82.50	136.49	180.23	204.30	276.17
	R2	56.06	78.80	130.43	182.38	228.27	268.85
	S	55.56	82.13	130.09	178.06	230.90	280.72
F_p [N]	R1	33.17	49.97	74.83	96.29	102.17	145.16
	R2	36.39	48.84	72.18	90.86	107.26	127.34
	S	73.60	93.60	130.82	171.80	212.16	251.97
F_f [N]	R1	13.52	21.28	38.62	53.15	59.51	83.93
	R2	21.67	30.93	53.53	74.96	96.36	114.84
	S	11.61	8.25	17.84	24.29	25.01	27.69

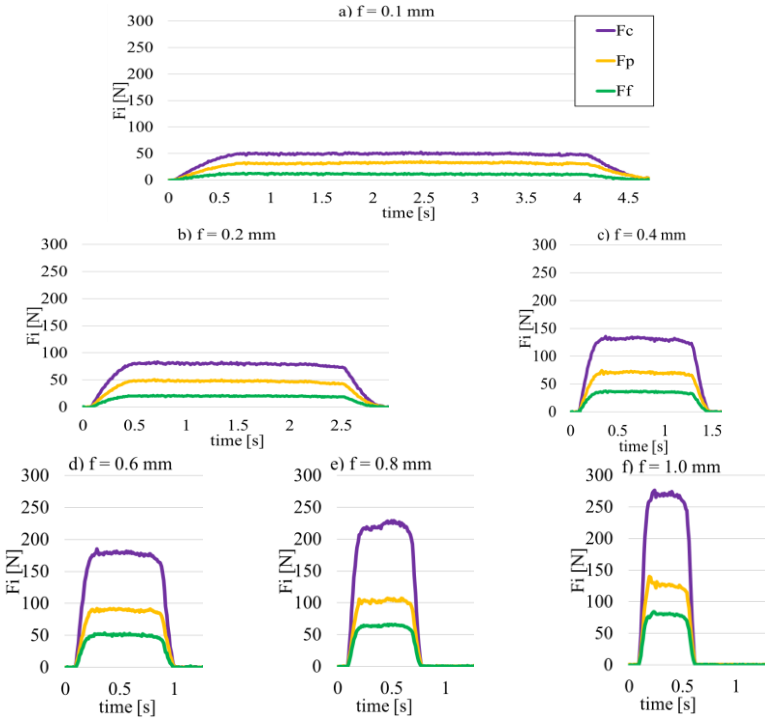

Figure 2 – Cutting force measurements during machining with R1 tool ($\lambda_s = 30°$)

4. DISCUSSION

Several conclusions can be drawn from the force measurement results in Figure 2. In the experiments with different feeds the highest force component was the main cutting force (F_c), which was followed by the passive force (F_p) and feed directional force (F_f). The constant section of the cutting forces shows the removal of constant cross-sectional area of the chip (A_c), where the rotational turning shows traditional turning-like characteristics. The run-in and run-out phases [6] can be seen clearly in the figures, which is specified by the increase and decrease of each cutting force component. These sections have a significantly longer part than in traditional turning due to the high inclination angle of the helical cutting edge. For the cases in Figure 2.a-b the passive force is nearly 60%, the feed directional force is nearly 25% of the main cutting force. For the cases in Figure 2.d-f (where the feed was much higher) the F_p is nearly 50%, the F_f is nearly 30% of F_c. Therefore, I conclude that the ratio of the cutting force components alters with the increase of the feed, and moreover with the direction of the resultant cutting force.
From the values of Table 1 the specific cutting forces (k_i) of F_c, F_p and F_f were also calculated according to Equation 1. The calculation results are shown in Table 2.

$$F_i = k_i \cdot A_c \quad \rightarrow \quad k_i = F_i / A_c \quad (i = c,p,f \quad ; A_c = a \cdot f) \tag{1}$$

Table 2 – Values of the specific cutting forces

f [mm]		0.1	0.2	0.4	0.6	0.8	1
k_c [N/mm^2]	R1	5163.36	4124.76	3412.35	3003.83	2553.77	2761.74
	R2	5605.99	3940.18	3260.72	3039.72	2853.43	2688.51
	S	5556.39	4106.48	3252.35	2967.67	2886.28	2807.17
k_p [N/mm^2]	R1	3316.67	2498.67	1870.78	1604.87	1277.17	1451.63
	R2	3639.15	2442.00	1804.48	1514.27	1340.72	1273.39
	S	7359.85	4680.19	3270.60	2863.32	2651.95	2519.72
k_f [N/mm^2]	R1	1352.19	1063.82	965.56	885.80	743.90	839.28
	R2	2166.64	1546.47	1338.32	1249.27	1204.45	1148.43
	S	1161.45	412.38	445.96	404.75	312.64	276.88

It can be seen in Figure 3 that I obtained nearly the same specific main cutting forces (k_c) with the three cutting tools in different feeds. Also, the load on the specific cross section decreases with the increase of the feed due to the increase in

the chip height. The load reduction is higher in low feeds (0.1 mm-0.4 mm) than in high feeds (0.6 mm – 1.0 mm). Figure 4 shows the specific values of the passive force, which decreases with the feed increasement, similarly to the k_c. The k_p values become nearly constant after reaching 0.4 mm feed. The specific load of the traditional turning tool (S) was nearly twice as that as of the machining with rotational tools (R1, R2). Thus, I can conclude that the shape error can be lowered by the application of rotational turning, due to the decrease in the radial force. The lowest values of the specific feed-directional force were yielded with S, while the highest values were obtained with R2. The k_f can be considered constant after 0.2 feed.

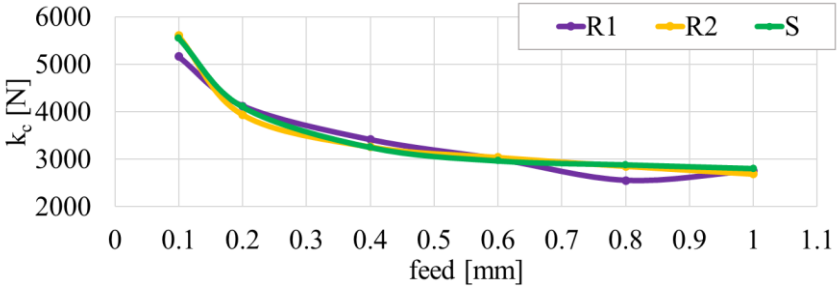

Figure 3 – Alteration of the specific main cutting force

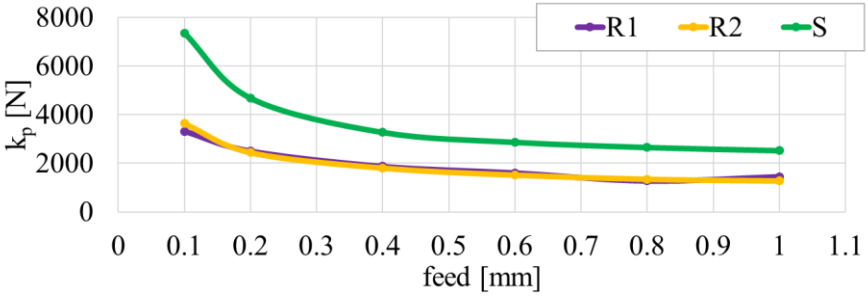

Figure 4 – Alteration of the specific passive force

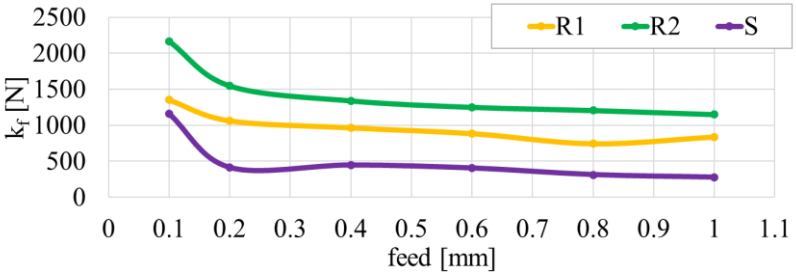

Figure 5 – Alteration of the specific feed-directional force

SUMMARY

The effect of the feed rate on the specific cutting forces was analysed in different turning procedures during experiments. I carried out the experiments at 6 feeds with 2 rotational turning tools with different inclination angles and 1 traditional turning tool. Calculation of the specific cutting forces showed that the specific main cutting force is nearly the same in rotational and traditional turning. However, the specific passive forces are significantly lower in the rotational procedure (nearly half as much as the traditional), while higher values were found during rotational turning (2-4-fold increase) for the specific feed-directional forces than the results of traditional turning. Accordingly, with the same cutting power requirement the force trying to move a workpiece away from a tool will be lower and the axial load on the spindle and tool holder will be higher in rotational turning than in traditional procedure. Hence, we can expect a decrease in workpiece-deflection related errors because the elastic deformation of the dynamical system will be lower. The different axial force must be taken into account during the construction or selection of the tool holder.

ACKNOWLEDGEMENTS

Project no. NKFI-125117 has been implemented with the support provided from the National Research, Development and Innovation Fund of Hungary, financed under the K_17 funding scheme.

The described study was carried out as part of the EFOP-3.6.1-16-00011 “Younger and Renewing University – Innovative Knowledge City – institutional development of the University of Miskolc aiming at intelligent specialisation” project implemented in the framework of the Szechenyi 2020 program. The realization of this project is supported by the European Union, co-financed by the European Social Fund.

References: 1. *J.G. Weisser Söhne GMBH & CO*: Patent Anmeldung, St.Georgen, Germany, 2004; **2.** *Kundrák, J., Markopoulos, A. P., Makkai, T., Deszpoth, I., Nagy, A.:* Analysis of the Effect of Feed on Chip Size Ratio and Cutting Forces in Face Milling for Various Cutting Speeds. Manufacturing Technology Vol 18., pp 431-438, 2018; **3.** *Karpuschewski, B., Kundrák, J., Varga, GY., Deszpoth, I., Borysenko, D.:* Determination of specific cutting force components and exponents when applying high feed rates. Procedia CIRP Volume 77, pp. 30-33, 2018; **4.** *Denkena, B., Vehmeyer, J., Niederwestberg, D., MAAβ, P.:* Identification of the specific cutting force for geometrically defined cutting edges and varying cutting conditions. International Journal of Machine Tools and Manufacture, Volumes 82–83, pp. 42-49, 2014; **5.** *Tarag, Y. S., Hwang, T.S.:* An investigation of the specific cutting force and its direction factors in turning. Computers & Structures, Volume 53, Issue 4, pp. 937-945, 1994; **6.** *Kundrák, J., Gyáni, K., Deszpoth, I., Sztankovics, I.:* Some topics in process planning of rotational turning. Engineering review 34, pp. 23-32, 2014.

Іштван Станкович, Мішкольц, Угорщина

КОМПОНЕНТИ СИЛИ РІЗАННЯ І ЇХ ПИТОМІ ЗНАЧЕННЯ ПРИ РІЗНИХ ПОДАЧАХ В УМОВАХ РОТАЦІЙНОГО ТОЧІННЯ

Анотація. *У статті досліджується зміна сили різання при збільшенні подачі в процесі ротаційного точіння. Динаміка зміни складових сили різання аналізується за допомогою експериментів, проведених різними інструментами з різною геометрією різальних крайок і розраховуються питомі сили різання. Одним з відкриттів є можливість ефективного зниження пасивної сили, що діє на ріжучий інструмент, за допомогою ротаційного точіння. В ході експериментів на обробному центрі Perfect-Jet MCV-M8 були реалізовані характерні для даного процесу руху. Експериментальна заготівля зажималась в шпинделі фрезерного верстата, обертання якого забезпечувало типове обертальний рух токарного оброблення. Ріжучий інструмент був закріплений в пристрої вимірювання сили (Kistler 9257A), яке розміщувалося на столі верстата. Інтерпольований круговий рух ріжучого інструменту зі столом верстата забезпечувало відносну кругову подачу навколо заготовки. В експериментах з різними подачами найвищої складової сили була основна сила різання (Fc), за якою слідували пасивна сила (Fp) і спрямована сила подачі (Ff). Розрахунок питомих сил різання показав, що питомі основні сили різання майже однакові при ротаційному і традиційному точении. Однак питомі пасивні сили значно нижче при ротаційній процедурі (майже вдвічі менше, ніж при традиційній), в той час як при ротаційному точінні були виявлені більш високі значення (збільшення в 2-4 рази) для питомих сил напрямку подачі, ніж при традиційній токарній обробці. Відповідно, при однакових вимогах до потужності різання зусилля, що намагається відсунути заготовку від інструменту, буде нижче, а осьова навантаження на шпиндель і державка інструменту буде вище при обертанні, ніж при традиційній процедурі. Отже, можна очікувати зменшення помилок, пов'язаних з прогином деталі, оскільки пружна деформація динамічної системи буде менше. Різна осьове зусилля необхідно враховувати при виготовленні або виборі держателя інструменту.*

Ключові слова: *сила різання; ротаційне точіння; подача; пасивна складова сили різання; осьове зусилля.*

UDC 621.923 **doi: 10.20998/2078-7405.2020.93.11**

R. Strelchuk, O. Shelkovyi, Kharkiv, Ukraine

EDM GAP MODELING AT ELECTRICAL DISCHARGE GRINDING WITH CHANGE OF ELECTRIC POLARITY

Abstract. *The paper presents an experimental study and modeling in the Simulink graphical environment of the EDM gap at electrical discharge grinding (ED grinding) with change of electric polarit of difficult-to-machine materials. Based on the experimentally obtained oscillograms of currents and voltages in the cutting zone, an EDM gap model has been developed, which implements the nonlinear dependence of the active resistance of the electroerosion gap on its value, which makes it possible to take into account the effect of the interelectrode environment on the parameters of electric discharge pulses. Comparison of the calculated oscillograms obtained in the Simulink model with the experimental ones has shown that during ED grinding, the developed EDM gap model adequately reflects the real electrical processes occurring in the electroerosion gap.*
Keywords: *EDM gap; oscillogram of currents and voltages; equivalent circuit; electrical processes.*

Introduction. The process of interaction of the cutting tool with the surface of the processed material under the conditions of electrical discharge grinding with change of electric polarity has not been studied, and the cutting zone of combined processing has not been investigated [1, 2]. In this regard, the modeling of the process occurring in the cutting zone has been carried out, and the features and patterns of interaction of the cutting tool with the surface of the processed material have been defined in the paper.

Literature Review. The machining zone for ED diamond grinding is a complex electrophysical system [3, 4]. At the same time, it is the place of microcutting and discharge activity in the electroerosion gap. When a voltage is applied, an electric current, which passes through the conductive bridges, the hydraulic fluid, which has a certain electrical conductivity, bridging the electroerosion gap, and through the channel of the resulting discharge during its action, arises in this zone.

The size of the machining zone is determined by the front width of the grinding wheel and the EDM gap value, i.e. the distance between the wheel binder and the surface of the processed material.

In the machining zone, along with chip formation and discharge activity, the complex mechanical and electrophysical processes occur: contact-frictional, thermal, electrical, plasma-chemical, and electrohydraulic ones; high-frequency vibrations and cavitation of the liquid medium take place. The main, dominant effect of electrical energy in the machining zone is manifested in electroerosion processes and phenomena of a combined nature of various duration and intensity.

They occur in the areas of contact and contactless interaction of the wheel with the cut off chips and the processed material, where the surfaces of these electrodes come close to each other and where the contact, the formation of intermittent or tight contacts and their rupture are possible. Thus, the zone of ED diamond grinding is characterized by contact and contactless electric erosion [5].

Research Methodology. The EDM gap model characterizes the electrodynamic processes therein and it is determined by the type and parameters of the equivalent circuit. In order to make a reasonable choice of the type and parameters of the EDM gap model, oscillograms of currents and voltages of technological pulses have been experimentally obtained at various values of this gap (Fig. 1).

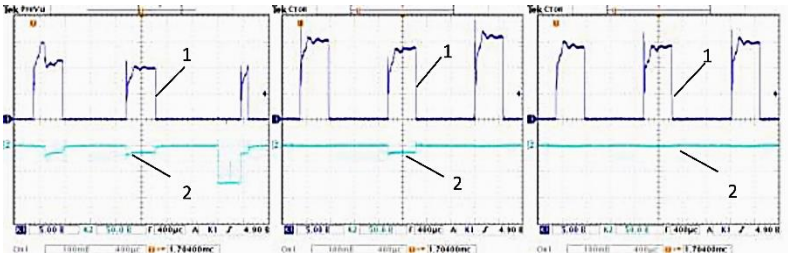

Figure 1 – Oscillograms of currents (1) and voltages (2) in the EDM gap of size: a – 7μm; b – 14μm; c – in case of a short circuit

Experimental studies have been carried out on the basis of a 3Д642Е machine tool. Additional energy was supplied into the cutting zone from a НО 6506 pulse generator, which converts 380V alternating current into a unipolar pulse current. The voltage, discharge current amplitude, frequency and relative pulse duration have been controlled from a pulse generator.

An end-face grinding method has been used, which was carried out with conical cup wheels 12А2-45˚ 150×10×3×32 on a binder М1-01 with diamond grains АС6 with a grain size of 100/80 and a concentration of 4. Before the experiments, the diamond wheels have been pre-straightened and run-in for 5-10 minutes. The processed material was ВК6 carbide plates with dimensions of 14×14×5mm.

Electrical modes of the technological pulse generator: voltage pulse amplitude– 50V, technological pulse frequency–44KHz, relative pulse duration–1.

The oscillograms have been recorded with a GOS-6050 oscilloscope (Good Will Instrument Co), which was connected according to the diagram shown in Fig. 2.

The size of the electroerosion gap has been recorded by a dial indicator with a graduation of 0.001mm. Analysis of the electrical circuit of the NO 6506 pulse

generator and the oscillograms of currents at different EDM gap values makes it possible to go just with the T-shaped equivalent circuit, which takes into account the reactance of the technological pulse generator and the EDM gap.

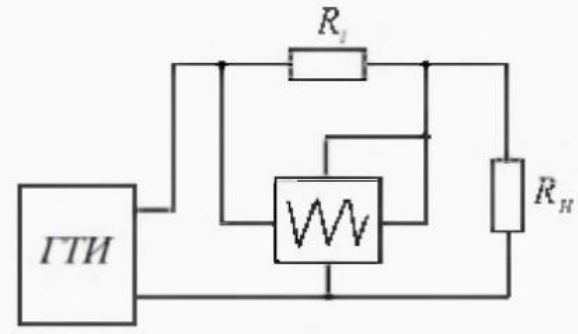

Figure 2 – Oscilloscope connection diagram

Since the current in the EDM gap has a pronounced oscillatory component, the equivalent circuit includes the oscillatory RLC circuit shown in Fig. 3.

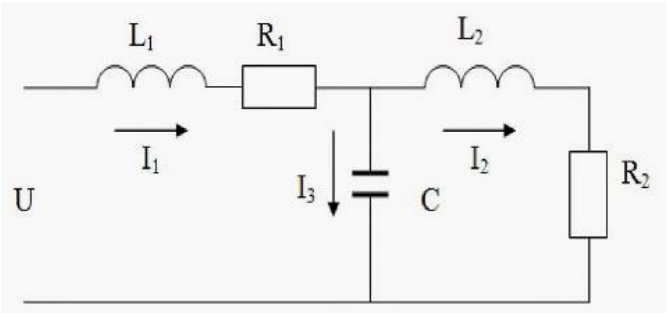

Figure 3 – The equivalent circuit of electroerosion gap

The active resistances of the technological pulse generator R_1 and the load (electroerosion gap) R_2 can be found by the established values of the voltage drop U_2 across the resistance R_2 and the current I_2 at a known value of the amplitude of the no-load pulses of the generator U:

$$R = \frac{U-U_2}{I_1}, \quad (1)$$

$$R_2 = \frac{U_2}{I_2}. \quad (2)$$

As a result of oscillograms processing, the values of active resistances R_1 and R_2 have been obtained for different EDM gap values (Table 1).

Table 1 shows that the resistance of electroerosion gap R_2 nonlinearly depends on the EDM gap value S. Since at a given generator voltage U, there is a limiting value of the electroerosion gap S, at which an electric discharge does not occur, the indicated dependence $R_2=f(S)$ can be approximated by the expression:

$$R_2 = \frac{kS}{t-S}. \quad (3)$$

where k to t approximation coefficients found by the least square method [6], depending on the amplitude of the operating pulse generator and the electrical parameters of the equivalent circuit.

Table 1 – Active resistance values

EDM gap S, μm	R_1, Ohm	R_2, Ohm
14	4.85	2.21
7	4.85	0.35
Short circuit	4.85	0

In order to determine the remaining parameters of the equivalent circuit, namely, L_1, L_2, and C, the coordinates of several characteristic points have been found on the experimentally taken oscillograms of the transient process of a single electric discharge. Parametric identification of the oscillogram (Fig. 4) was digitized in the GetDataDigitizer program.

$$\begin{cases} L_1 \frac{dI_1}{dt} + R_1 I_1 + U_C = U \\ L_2 \frac{dI_2}{dt} + R_2 I_2 = U_C \\ C \frac{dU_C}{dt} = I_1 - I_2 \end{cases}. \quad (4)$$

A measure of the adequacy of the experimental data and the calculated values obtained as a result of solving a system (4) is the square of the distance between the experimental and calculated points [7].

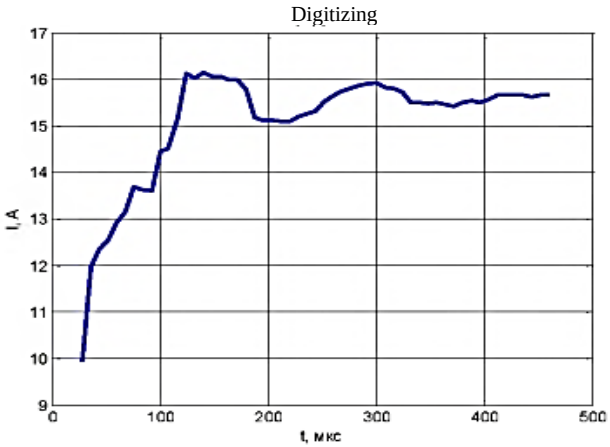

Figure 4 – An example of digitizing a current pulse

$$F(L_1, L_2, C) = \sum_{i=1}^{50}(t_i - t_{pi})^2 + \sum_{i=1}^{50}(I_i - I_{pi})^2 \quad (5)$$

Calculated points are also selected at the extreme values of the resulting solution (4). By minimizing $F(L_1, L_2, C)$ over the variables L_1, L_2, and C, we can determine their value. The minimization has been carried out in the Matlab system using the simplex Nelder-Mead method [8]. As a result, the following values of the sought parameters of the equivalent circuit averaged over the entire series of experiments have been obtained: L_1 = 173μH, L_2 = 173μH, and C = 18μF.

Results. Fig. 5 shows the calculated curve obtained as a result of minimizing the solution (4) by criterion (5) and the experimental curve taken from the graph Fig. 1b, confirming good agreement between the calculated and experimental results.

Based on the accepted type and the found parameters of the EDM gap equivalent circuit, the EDM gap model has been developed for ED diamond grinding in the Simulink graphical simulation environment. The block diagram of the model is shown in Fig. 6.

Simulink model of EDM gap includes two blocks "B1" and "B2". Block 1 ("B1") reproduces the dependence of the EDM gap resistance on its value, block 2 ("B2") simulates the operation of the equivalent circuit (Fig. 7.).

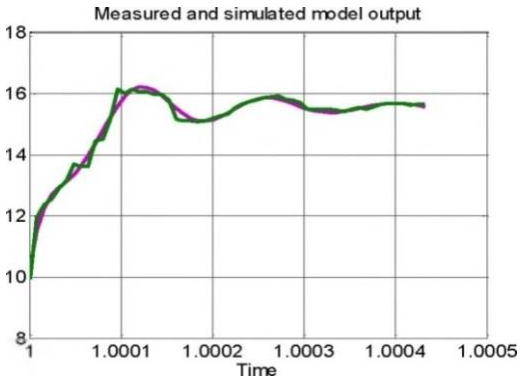

Figure 5 – Calculated and experimental values of current change in EDM gap

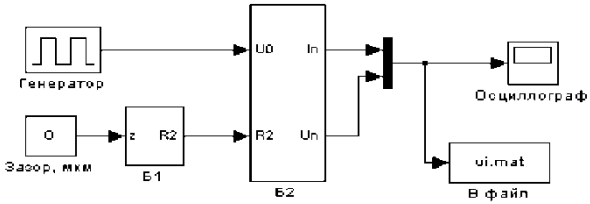

Figure 6 – Block diagram of a Simulink model of EDM gap

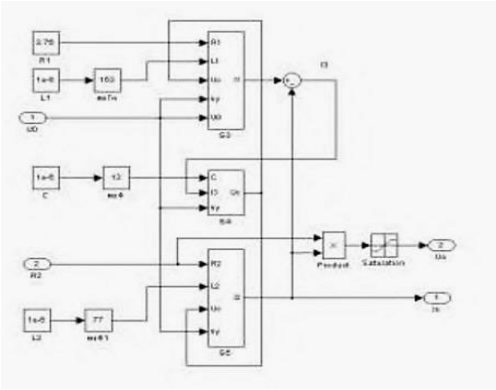

Figure 7 – Blocks of the Simulink model of the EDM gap

Fig. 8 shows oscillograms of currents and voltages obtained in the developed Simulink model of the EDM gap.

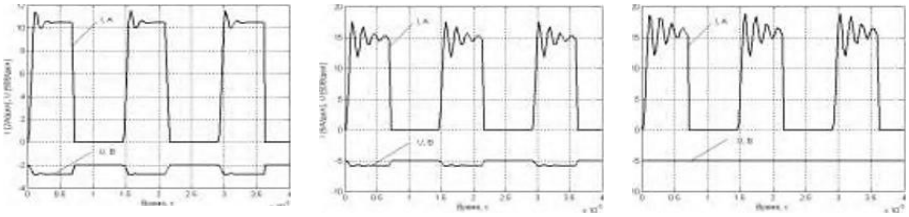

a b c

Figure 8 – Oscillograms of currents and voltages obtained in the Simulink model of the EDM gap at: a – 7μm; b – 14μm; c – in case of a short circuit

Emergence of a current pulse at the initial moment of time on the calculated oscillograms is due to the capacitance of the gap between the diamond wheel and the surface of the processed material before the discharge occurs. The presence of this capacitance in the experiment is not taken into account, since it practically does not affect the ED grinding process.

Conclusions. Thus, as a result of the analysis of the experimental oscillograms of the operating pulse currents, it was found that the electrical processes occurring in the EDM gap during ED grinding are of an oscillatory nature. The environment in which these processes take place can be represented with sufficient accuracy in the form of a T-shaped equivalent circuit, which includes active resistances, inductances, and capacitance. It was found that the active resistance of the EDM gap nonlinearly depends on its value. The root-mean-square deviation between the calculated and experimental pulses of current and voltage, referred to its established value, does not exceed 12-15%.

The found values of equivalent circuit parameters made it possible to obtain the Simulink model of the EDM gap for ED grinding.

The good agreement of the calculated oscillograms obtained in the Simulink model with the experimental ones has shown that the developed EDM gap model for ED grinding adequately reflects the real electrical processes occurring in the EDM gap.

References: 1. *Strelchuk R.M., Uzunian M.D.* Sposib elektroeroziinoho almaznoho shlifuvannia zi zminnoiu poliarnistiu elektrodiv, Patent UA, no. 131894, 2019. **2**. *Arun, I., Yuvaraj, C., Jyothibabu, P.* Influence of Silica on Microstructural Modification of Electrical Discharge Composite Coating and its Wear Performance // Silicon 12, p. 2375–2386 (2020). **3.** *Montes, J., Cuevas, F., Reina, F.* Modelling and Simulation of the Electrical Resistance Sintering Process of Iron Powders // Met. Mater. Int. 26, p.

1045–1059 (2020). **4.** *D'Urso, G., Maccarini, G., Ravasio, C.* Influence of electrode material in micro-EDM drilling of stainless steel and tungsten carbide // Int J. Adv. Manuf. Technol. 85, p. 2013–2025 (2016). **5.** *Giridharan, A., Samuel, G.* Investigation into erosion rate of AISI 4340 steel during wire electrical discharge turning process // Machining Science and Technology, p. 287-298, (2018). **6**. *Sukhov A .N.* Matematicheskaya obrabotka rezultatov izmerenij. – Moscow: MISI, 1982. – 89 p**. 7.** *Tarasik V. P.* Matematicheskoe modelirovanie tekhnicheskikh sistem. – Minsk: DizajnPRO, 2004 – 640 p. **8.** R.Andreani, G.Haeser, J.M.Martínez // On sequential optimality conditions for smooth constrained optimization , Optimization 60 (2011), pp. 627–641.

Роман Стрельчук, Олександр Шелковий, Харків, Україна

МОДЕЛЮВАННЯ МІЖЕЛЕКТРОДНОГО ЗАЗОРУ ПРИ ЕЛЕКТРОЕРОЗІЙНОМУ ШЛІФУВАННІ ЗІ ЗМІНОЮ ПОЛЯРНІСТЮ ЕЛЕКТРОДІВ

Анотація. *У статті проведено експериментальне дослідження та моделювання в графічному середовищі Simulink межелектродного зазору при електроерозійному шліфуванні зі змінною полярністю електродів важкооброблюваних матеріалів. Проведено моделювання процесу, що відбувається в зоні різання, і встановлено особливості та закономірності взаємодії різального інструменту з поверхнею оброблюваного матеріалу деталі. Розроблена модель межелектродного зазору дозволяє характеризувати електроерозійні процеси, що протікають в зоні шліфування, і вона визначалася типом і параметрами схеми заміщення. За експериментально отриманими осцилограмами струмів і напруг в зоні різання розроблена модель межелектродного зазору, що реалізує нелінійну залежність активного опору міжелектродного проміжку від його величини, яка дозволяє враховувати вплив міжелектродного середовища на параметри електророзрядних імпульсів. Порівняння розрахункових осцилограм, отриманих в Simulink-моделі, з експериментальними, показало що розроблена модель межелектродного зазору при електроерозійному шліфуванні досить адекватно відображає реальні електричні процеси, що протікають в міжелектродному проміжку. В результаті аналізу експериментальних осцилограм струмів робочих імпульсів було встановлено, що електричні процеси, що протікають в міжелектродному зазорі при електроерозійному шліфуванні носять коливальний характер. Середовище, в якому протікають ці процеси може бути з достатньою точністю представлено у вигляді Т-подібної схеми заміщення, що включає в себе активний опір, індуктивності та ємність. Середньоквадратичне відхилення між розрахунковими і експериментальними імпульсами струму і напруги, віднесене до його сталого значення, не перевищує 12-15%.*

Ключові слова: *міжелектродний зазор; осцілограмма струму і напруги; схема заміщення; електричні процеси; зона різання.*

UDC 621.923.4 **doi: 10.20998/2078-7405.2020.93.12**

R. Turmanidze, G. Popkhadze, Tbilisi,
K. Inasharidze , Batumi, Georgia

IMPROVING THE PERFORMANCE CHARACTERISTICS OF HUMAN HIP-JOINT IMPLANTS BY INCREASING THE QUALITY OF PROCESSING AND GEOMETRIC ACCURACY OF THEIR SPHERICAL SURFACES

Abstract. *In view of the fact that the endo-prosthesis heads of human hip-joint are operated in extreme conditions, in respect of load, the selection of corresponding material and also increase of precision and quality of machining of spherical surfaces is rather topical task.*
In the submitted work are reviewed the problems connected with definition of the influence degree of orientation of the sapphire crystal on its workability during diamond grinding with a butt of the ring and elaboration of the perspective, original scheme of formation of the incomplete spherical surface, particularly, of the sapphire head of endo-prosthesis of the human hip-joint.
Keywords: *single crystal sapphire, anisotropy, grind ability, endo-prosthesis, precision grinding, forming and spherical surface.*

In the last thirty years, one of the current trends in the field of material processing by cutting is the production of implants from different materials for hip-joints with high performance properties, which will ensure their use for more than 30-40 years. This is due to the fact that the heads of the said endoprosthesis, in terms of the nature and magnitude of the load, are operated under extreme conditions. Therefore, in each specific case, the selection of the necessary material with the appropriate physical and mechanical characteristics, as well as improving the accuracy and quality of processing of the most significant part of the endoprosthesis - spherical surfaces, is a very important task, the severity of which has been rapidly increasing in recent years. This is due to the fact that if earlier the need for such operations was mainly caused by the age factor of a person or traumatic fractures, then in the last twenty years the number of patients at a young age has sharply increased, even at 30-40 years old, both men and women, without any injuries or fractures. According to doctors, the main reasons for this disaster are the inactive lifestyle of young people, the composition of modern artificial foods and metabolic disorders, as well as the intensive growth of various fractures as a result of transport and other accidents. All of the above reasons determine the number of endoprostheses used - several tens of millions of pieces per year and statistics show that, unfortunately, this number is increasing annually.

Medical practice proves that the repeated prosthetics of the human hip joint is associated with great problems. In many cases, the implementation of such

transactions becomes almost impossible. Therefore, the service life of a hip joint endoprosthesis until the end of life for a patient, especially after operations at a young age, is extremely important.

This circumstance explains the fact that in such leading countries of the world as the USA, Germany, England, Japan, France, etc., large-scale research work is being carried out to develop optimal shaping schemes, characteristics of abrasive tools for finishing operations and the technological process as a whole, for the manufacture of spherical endoprosthesis heads from different materials with a minimum form error and with high surface quality indicators.

Today, in world practice, these heads are made from various alloys, composite materials and ceramics, which are mainly isotropic materials. Therefore, the data of the above-mentioned works do not provide the necessary information on the processing of anisotropic materials, in particular, an artificial sapphire crystal.

In addition, the wear resistance of the aforementioned materials in most cases does not meet the requirements for them. And our comparative experiments prove that the most biocompatible with the human body, wear-resistant and durable material for the production of the above-mentioned product is an artificial monocrystal of sapphire.

In this regard, an international project was carried out by the Ukrainian Science and Technology Center, the executors of which were the Georgian Technical University (Tbilisi), the Institute of Super hard Materials of the National Academy of Sciences of Ukraine (Kiev) and the Institute of monocrystal of the National Academy of Sciences of Ukraine (Kharkov).

The project participants solved certain scientific problems, in particular: the Georgian Technical University investigated the effect of sapphire crystal anisotropy on the machinability and quality of the material surface during grinding; promising, theoretical schemes for the shaping of an incomplete spherical surface have been developed in order to improve the geometric accuracy of the spherical part of the endoprosthesis, which is of fundamental importance for increasing the service life of their operation by increasing the contact area between pairs of endoprostheses and, accordingly, reducing the load per unit area their contact surfaces. The Institute for Super hard Materials investigated the relationship between the friction coefficient and the crystallographic features of sapphire and annealing modes; machinability of materials with anisotropy of properties, in particular sapphire, according to traditional technology to assess the effect of anisotropy on the accuracy of shaping a spherical surface; Recommendations have been developed for the process of diamond finishing of the heads of endoprostheses of the hip joint made of artificial sapphire monocrystal. The Kharkov Institute of monocrystals investigated the optimal growth regimes that ensure the maximum purification of the sapphire material, as a result of which a

sapphire with a crystallographic direction having a minimum anisotropy was obtained.

The aim of the presented work is: to determine the degree of influence of the orientation of the sapphire crystal on its processing by grinding by the NSP method created at the Department of Mechanical Engineering Technology of the Georgian Technical University and the development of a promising, original scheme the shaping of an incomplete spherical surface, in particular, a sapphire head of a human hip joint endoprosthesis. A detailed description of the low-temperature grinding process (LGP) method, the kinematic diagram of the laboratory setup and the experimental technique can be found in previous publications [1,2,3,4].

Studies of the influence of the orientation of the sapphire crystal on the workability of the material were carried out on sapphire samples with the orientation (0001), (1010) and (1012). Sample sizes: 10x10x6 mm and Φ 10x6 mm.

Experimental studies were carried out on a laboratory setup equipped with a special precision head. We used diamond wheels with grain size 14/10 and 28/20 on ceramic, metal and organic bonds, form 6A2.

The output parameters of the process were: processing productivity, linear minute material removal - q, μm / min; height of surface roughness irregularities - Rz, μm; relative reference profile length at level 03 - t_{P03}, %; under-relief damaged layer - H, μm.

Process factors cutting speed - V, m / s; pressure in the cutting zone P, kPa and characteristics of the diamond tool: grain size - d_3, μm; concentration bundle - K, %.

The experiments were carried out under the following conditions: cutting speed range - V = 1 ... 12 m / s; pressure in the cutting zone - P = 100 ... 1500 kPa. Cooling liquid - filtered running water.

Based on the analysis of the data of our complex, comprehensive experimental studies, we can draw the following conclusion:

The nature of the influence of process factors on the output parameters for the selected orientations of the sapphire crystal ((0001), (1010), (1012)) is constant.

All other things being equal, the most difficult to machine is the orientation (0001). For all tested diamond wheels, the ratio of linear material removal - q is within the range

$$q_{0001} / q_{1010} = 0{,}25 \ldots 0{,}5,$$

while,

$$q_{1012} / q_{1010} = 0{,}75 \ldots 1.$$

In the studied ranges of cutting modes V and P, the processing productivity increases at V = ... 6 m / s, and at V> 6 m / s - it remains constant, also at P = 100 ... 1500 kPa - it grows, at P> 1500 kPa - remains almost constant.

Of the characteristics of a diamond tool, the grit size and bond of the diamond tool predominantly affect productivity. The effect of concentration is negligible. With an increase in the grain size within d_3 = 14/10 ... 28/20, the productivity increases by 1.5 ... 2.5 times.

The maximum value of productivity is achieved by a tool on a ceramic bond - SK6 - 130 ... 300 μm / min, for all selected orientations of the sapphire crystal. This increases the ratio

$q_{0001} / q_{1010} =$ 0,4 … 0,5.

The tool on this bond works in self-sharpening mode.

All other things being equal, processing on the (0001) orientation achieves a higher surface quality than on the other two. The difference is in 1 ... 1.5 grades of roughness.

The surface quality is predominantly influenced by the grit size and the material of the tool bond. With an increase in the grain, in the investigated range, the height of the irregularities Rz grows within 1 ... 1.5 class, and the depth of the disturbed layer H - 1.5 ... 2 times.

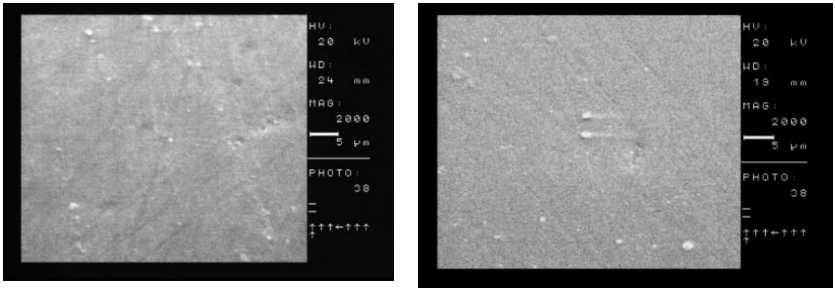

а в

Figure 1 –Micrographs of surfaces of experimental sapphire samples processed by the NSP method:
a- Orientation 1010, b- 1012. Diamond wheel - ACM 14/10, special organic bond, 50%. Cutting conditions: V = 1m / s, P = 750 kPa

In terms of the quality of the treated surface, the best results are obtained by diamond wheels on organic bonds VS-11 and organic special ones, which have been developed by us and are in the process of patenting. Compared to diamond wheels on metal and ceramic bonds, the Rz parameter is an order of magnitude lower ~ 0.25 μm, the t_{P03} parameter is 1.5 higher than ~ 35 ... 45% and the H parameter in 3 ... 5 is less than ~ 2...5 μm.

The study of the morphology of the treated surface proved the possibility of cutting sapphire material by plastic deformation of the removed layer at low

cutting speeds V = 1 ... 3 m / s, with the smallest depth of the damaged under-relief layer (Fig. 1).

This result is worthy of special attention, since the processing of glassy materials, in particular, a sapphire crystal, by plastic deformation of the removed layer is a guarantee of obtaining a treated surface with practically no hereditary defects - without a disturbed under-relief layer. The value of H turned out to be the smallest in these sapphire samples.

The development of a new, or improvement of the existing technological process of mechanical processing of a sapphire head poses an urgent task of creating new, highly efficient shaping schemes. Optimization criteria for technological operations, such as productivity, surface quality indicators and processing accuracy, determine the place of new shaping schemes in the technological process, taking into account their advantages.

The methods of abrasive processing of an incomplete spherical surface of general-purpose products used today, as separate operations of the technological process of machining an incomplete sphere, can be divided into two groups: grinding with abrasive diamond wheels, finishing with a free abrasive.

Our method belongs to the first group, however, as a method for diamond abrasive processing of flat surfaces, in contrast to existing methods, it combines the positive aspects of the methods of the above two groups, namely: with high processing accuracy and surface quality.

To develop a theoretical scheme for diamond processing of sapphire spheres, taking into account the kinematic and other positive features of the NSP, the known schemes for the formation of an incomplete spherical surface were considered and analyzed.

The closest in kinematics to the NSP method is the method of grinding an incomplete sphere with the end of a grinding wheel with double rotation of the part with angular velocities ω_2 and ω_3 (Fig. 2), which is taken as the basis for the development of an original version of the theoretical scheme of diamond processing of sapphire spheres, taking into account the kinematic and other positive features of the NSP method.

We have developed several versions [5, 6] of theoretical schemes for the formation of an incomplete spherical surface. One version of the original kinematic scheme for shaping an incomplete spherical surface of a sapphire head (Fig. 3) by an end grinding wheel is shown in (Fig. 4). The cutting tool is a special, combined face grinding wheel with two concentric diamond-bearing layers, with cutting surfaces in the form of internal, at point A, and external, at point B, cut off cones.

The grinding wheel rotates with an angular velocity ω_1. The workpiece being machined - the ball - performs a double rotary motion with angular velocities ω_2 around its own axis 4 and ω_3 around axis 3, which is the axis of the part's spindle. The direction of the angular velocities ω_1, ω_2 and ω_3 is the same. The workpiece 2

to be machined is pressed against the cutting surface of the grinding wheel at two points A and B by a spring-loaded force P. In this case, the cutting surfaces of the grinding wheel in the axial section form an angle β.

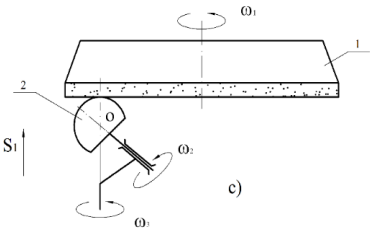

Figure 2 – Scheme of forming an incomplete spherical surface with an end diamond wheel with double rotation of the part:
1 - diamond grinding wheel;
2 - work piece - incomplete sphere

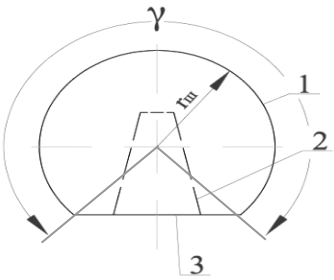

Figure 3 – Sapphire Ball Head:
rш is the radius of the sphere;
γ is the angle of the spherical surface segment

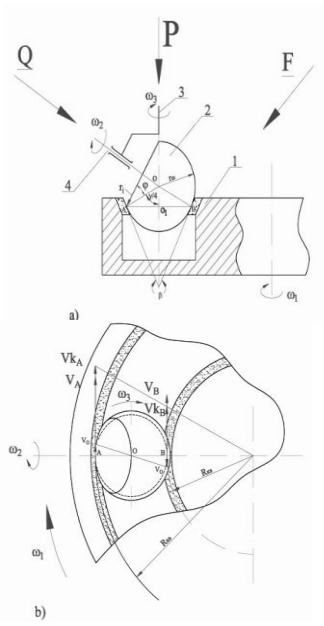

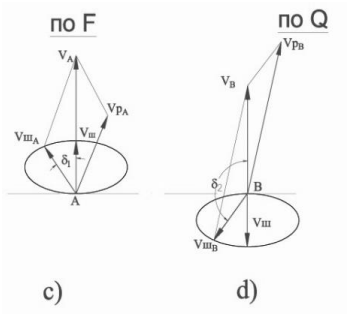

Figure 4 – Kinematic diagram of shaping incomplete spherical end face grinding based on the NPS method:
1 - face grinding wheel;
2 - work piece - incomplete sphere;
3 - axis of rotation of the part spindle;
4 - the axis of rotation of the part

Distinctive features of the theoretical scheme from the NSP such as the shape of the working surface of the tool, additional movement of the workpiece - rotation of the ball around its own axis at a speed ω_2, the form of contact of the workpiece surface with the cutting surface of the grinding wheel.

To create equal processing conditions at two points A and B, it is necessary to observe the equality of both the speeds and the cutting forces.

Cutting speed. Equality of processing conditions in terms of cutting speed means equality of the maximum values of cutting speeds and the identity of their laws of change in the cycle in two cutting zones.

Cutting speeds when grinding an incomplete sphere according to the proposed scheme at points A and B are given in Fig. 4 c, c, and d.

Resulting cutting speed v_{PA}- at point A

$$\vec{v}_{PA} = \vec{v}_B - \vec{v}_{IIIB} \quad (1)$$

$$v_{P_A} = \sqrt{v_A^2 + v^2{}_{ш_A} - 2 v_A \cdot v_{ш_A} \cdot \cos\delta_1} \quad , \quad (2)$$

where

$$v_A = v_{KA} - v_0 = R_{KA} \cdot \omega_1 - r_ш \sin\frac{\gamma}{4} \cdot \omega_3 \quad (3)$$

and $$v_{IIIA} = r_{iA} \cdot \omega_2 \quad . \quad (4)$$

Similar to point A, at point B the resulting cutting speed is

$$\vec{v}_{PB} = \vec{v}_B - \vec{v}_{IIIB} \quad , \quad (5)$$

$$v_{P_B} = \sqrt{v_B^2 + v^2{}_{ш_B} - 2 v_B \cdot v_{ш_B} \cdot \cos\delta_2} \quad , \quad (6)$$

where

$$v_B = v_{KB} - v_o = (R_{KA} - 2r_ш \cdot \sin\frac{\gamma}{4}) \cdot \omega_1 + r_ш \cdot \sin\frac{\gamma}{4} \cdot \omega_3 \quad (7)$$

and $$v_{IIIB} = r_{iB} \cdot \omega_2 \quad . \quad (8)$$

Linear speed of the part from rotary motion with angular speed ω_2

$$v_{IIIi} = r_i \cdot \omega_2 = \omega_2 r_{III} \cdot \cos\varphi =$$

$$\omega_2 \cdot r_ш \sqrt{\sin^2\frac{\gamma}{4} \cdot \cos^2\alpha + \frac{1}{4} \cdot \sin^2\frac{\gamma}{2}(1+\sin\alpha)^2} \quad , \quad (9)$$

Where is φ the angle of inclination of the axis 4 relative to the generatrix of the working surface of the circle in the axial section, α is the angle of rotation of the axis 4 relative to the axis 3 with an angular velocity ω_3.

The current radius of the point of the surface of the part, when you rotate axis 4 around axis 3 by 180^0, changes within $0 \le r_i \le r_ш$. Thus, for a complete description of a spherical surface during one cycle, one revolution of the part around axis 4 is sufficient, when axis 4 is rotated about axis 3 by half a revolution, i.e. by 180^0. Consequently, under these conditions, the processed spherical surface of the part is described twice during one cycle. Once in each treatment area.

Based on the foregoing, between the angular velocities ω_2 and ω_3 we have the dependence

$$\omega_2 = 2\,\omega_3 . \tag{10}$$

v_{P_A} reaches a maximum at $\alpha = \pi 3/2$, and therefore, $\delta_1 = \frac{\pi}{2}$.

$$v_{P_{Amax}} = v_A = R_{KA} \cdot \omega_1 - r_ш \cdot \sin\frac{\gamma}{4}\omega_3 \tag{11}$$

v_{P_B} reaches a maximum at $\alpha = \pi/2$, and therefore, $\delta_2=\pi$.

$$v_{P_{Bmax}} = R_{KA} \cdot \omega_1 - 2r_ш \sin\frac{\gamma}{4}\omega_1 + r_ш \cdot \sin\frac{\gamma}{4}\cdot\omega_3 + r_ш \sin\frac{\gamma}{2}\omega_2 \tag{12}$$

On condition $v_{P_{Amax}} = v_{P_{Bmax}}$, by expressions (10), (11) and (12) the ratio of angular velocities and ω_3 и ω_1

$$\frac{\omega_3}{\omega_1} = \frac{1}{1+2\cos\frac{\gamma}{4}} . \tag{13}$$

Thus, according to the proposed scheme for shaping an incomplete spherical surface, in order to achieve equality of processing conditions in terms of cutting speed, it is necessary to observe the ratios of angular speeds ω_1, ω_2 and ω_3, according to expressions (10) and (13).

Clamping force. The equality of conditions at two points in terms of the clamping force is achieved by the location of the workpiece in relation to the grinding wheel. The spring-loaded force P passes through the center O of the sphere and coincides with the bisector of angle β and thus passes at equal distances from two A and B processing zones. In each zone, equal efforts on P / 2 are created, which in turn are composed of two components, normal PN and tangential Pτ (not shown in the figure). Wherein:

$$P_N = \frac{P}{2} \cdot \cos\frac{\gamma}{4}, \quad P_\tau = \frac{P}{2} \cdot \sin\frac{\gamma}{4}.$$

The kinematic similarity of the new shaping scheme with the LPS method, taking into account the preservation of the physics of the cutting process with the LPS, which determined its name "Low temperature" (low compared to conventional grinding, the cutting speed is -1.6 m / s and, as a consequence, the low temperature in contact is -100^{0}C), also "Precision" (high accuracy of the shape of the working surface of the tool is achieved during straightening and is maintained in operation by the kinematics of the process, which ensures high processing accuracy - plane-parallelism on a 10x10 mm <1μm plate), allows the proposed shaping scheme. The name, as coming from the first, is called Low-temperature precision grinding of an incomplete sphere, in abbreviated form - NPSHNS, which is in the process of patenting.

It is assumed that the NPSHNS method, in comparison with the traditional methods of diamond grinding, which are used today in the technological process of mechanical processing of a sapphire head, all other things being equal, will allow: to significantly (at least twice) increase the processing productivity without deteriorating performance surface quality and shape accuracy; to significantly improve the quality of the processed surface and the accuracy of the shape of the product, without increasing the productivity of processing, thereby also significantly reducing the operating allowance, as a result, the time and cost of processing in finishing operations (transitions).

Thus, in our opinion, the NPSHNS method can be quite competitive in preliminary operations, up to finishing, in the technological process of machining a sapphire head.

The long-term program provides for the organization of a European project with the creation of the necessary equipment, tools, technological equipment and the entire technological process for manufacturing high-precision spherical surfaces from various brittle materials of increased strength, including sapphire.

Conclusion

As a result of the study of the effect of the crystallographic orientation of a sapphire monocrystal on the rate of removal of the processed material, as well as the state of the subsurface layer during surface finishing by the method of low-temperature flat grinding, it was found that:

1. The processing capacity of a sapphire monocrystal significantly depends on the crystallographic orientation. The relative values of material removal for samples with different crystallographic orientations (1010) are in the range $q_{0001} / q_{1010} = 0.25\ldots 0.5$, and $q_{1012} / q_{1010} = 0.75\ldots 1$. Under other equal conditions of the LPS process, the highest quality of the polished surface is achieved for the crystalographic orientation (1010). The difference with the other two orientations of the crystallographic plane is in the range of 1 ... 1.5 roughness class.
2. The study of the morphology of the processed surface proved the possibility of cutting sapphire material by plastic deformation of the removed layer without cracking at a low cutting speed. Under such machining conditions, the smallest depth of the damaged subsurface layer was found.
3. New kinematic schemes for the processing of incomplete spherical surfaces have been proposed, which provide a higher geometric accuracy of parts, in particular, the spherical heads of the human hip joint endoprosthesis.

Acknowledgment

This work was supported by Shota Rustaveli National Science Foundation (SRNSF) [PHDF-19-2224, Improving the efficiency of mechatronic systems in order to ensure the reform of "Industry-4.0"]

References: 1. *Batiashvili B.I., Butskhrikidze D.S., Mamulashvili G.L., Mgaloblishvili O. B., Turmanidze R.S., Kromp K., Mills B., Steinkellner W., Schafler E., Rösel F. G., Peterlik H.* Evaluation of surface preparation techniques, SFG: Swing Frame Grinding and LPG: Low Temperature Precision Grinding, by comparison of results on alumni and siliconcarbide model materials. FRACTOGRAPHY OF ADVANCED CERAMICS. International Conference Stará Lesná, High Tatras, May 2001. **2.** *Batiashvili B.I., Butskhrikidze D.S., Mamulashvili G.A, Turmanidze R.S., Kromp K., Mills B., Mgaloblishvili O.* Technological Possibilities of Low Temperature Precision Grinding Process when Machining Hard and Brittle Materials. FRACTOGRAPHY OF ADVANCED CERAMICS, International Conference, Stará Lesná, High Tatras, May 2001. **3.** *Turmanidze R.S, Burtskhrikidze D.S, Kromp K., Mills B.*, "Low temperature precision grinding of hard and brittle materials". Problems of mechanics and physiko-chemistry of the process of abrasive machining, Kiev 2002, 490-499 pp. **4.** *Turmanidze R.S., Butskhrikidze D.S., Mamulashvili G.L., Kromp K., Mills B., Morgan M., Mgaloblishvili O.* Low-temperature precision grinding of hard and brittle materials and Outlook of its development and application. Proceedings of 19th NCMR Conference. Glasgow, September 2003. **5.** *R. Turmanidze, D. Butskhrikidze, E. Kutelia, M. Beridze,* Influence of the Sapphire Crystal Anisotropy of Medical Purpose on Workability of the Endoprosthesis Material at a Low Temperature Precision Grinding. "MicroCAD 2008" International Scintific Conference. 20-21 March, 2008. Section

N: Production Engine¬ering and Manufactu¬ring Systems. University of Mishkolc, Hungary. ISBN 978-963-661-812-4 Ö ISBN 978-963-661-823-0. **6.** *R. Turmanidze, G. Popkhadze,* Selection criteria of optimal characteristic material and technologies for precision processing of basic working surface of human hip-joint implant. 9TH INTERNATIONAL CONGRESS ON PRECISION MACHINING. ATHENS, GREECE-2017, ISSN 0377-6883.*Kundrak J., Varga G., Deszpoth I., Molnar V.* Some aspects of the hard machining of bore holes // Applied Mechanics and Materials, 309, pp. 126–132 (2013).

Рауль Турманідзе, Георгі Попхадзе, Тбілісі,
Кетеван Інашарідзе, Батумі, Грузія

ПОЛІПШЕННЯ ЕКСПЛУАТАЦІЙНИХ ХАРАКТЕРИСТИК ІМПЛАНТІВ КУЛЬШОВИХ СУГЛОБІВ ЛЮДИНИ ШЛЯХОМ ПІДВИЩЕННЯ ЯКОСТІ ОБРОБКИ І ГЕОМЕТРИЧНОЇ ТОЧНОСТІ ЇХ СФЕРИЧНИХ ПОВЕРХОНЬ

Анотація. *У зв'язку з тим, що головки ендопротезів тазостегнового суглоба людини експлуатуються в екстремальних умовах по навантаженню, вибір відповідного матеріалу, а також підвищення точності і якості обробки сферичних поверхонь є досить актуальним завданням. У поданій роботі розглянуто питання, пов'язані з визначенням ступеня впливу орієнтації кристала сапфіра на його оброблюваність при алмазному шліфуванні торцем кола і розробкою перспективної, оригінальної схеми формування неповної сферичної поверхні, зокрема, сапфіровою головки ендопротеза кульшового суглоба людини. В результаті дослідження впливу кристалографічної орієнтації монокристала сапфіра на інтенсивність знімання оброблюваного матеріалу, а також стану подповерхностного шару при доведенні поверхонь методом низькотемпературного плоского шліфування (НПШ) встановлено, що обрабативаемость монокристалла сапфіра значно залежить від кристалографічної орієнтації. Відносні величини знімання матеріалу при зразках з різними кристалографічними орієнтаціями (1010) знаходяться в межах* $q_{0001} / q_{1010} = 0.25 ... 0.5$, *і* $q_{1012} / q_{1010} = 0.75 ... 1$. *При інших рівних умовах процесу НПШ вища якість шліфованої поверхні досягається для кристалографічної орієнтації (1010). Різниця з двома іншими орієнтаціями кристаллографической площині знаходиться в межах 1...1.5 класу шорсткості. Вивченням морфології обробленої поверхні доведена можливість різання матеріалу сапфіра пластичним деформуванням шару, що знімається без утворення тріщин при низькій швидкості різання. При таких умовах механічної обробки була виявлена найменша глибина пошкодженого подповерхностного шару. Запропоновано нові кінематичні схеми обробки неповних сферичних поверхонь забезпечують більш високу геометричну точність деталей з різних матеріалів, зокрема сферичних головок ендопротеза кульшового суглоба людини.*

Ключові слова: *монокристалічний сапфір; анізотропія; подрібнення; ендопротезування; точне шліфування; формування; сферична поверхня.*

UDC 621.923.7 **doi: 10.20998/2078-7405.2020.93.13**

G. Varga, V. Ferencsik, Miskolc, Hungary

EXPERIMENTAL EXAMINATION OF SURFACE MICRO-HARDNESS IMPROVEMENT RATIO IN BURNISHING OF EXTERNAL CYLINDRICAL WORKPIECES

Abstract. *This paper deals with the experimental examination of surface micro-hardness improvement ratio in burnishing of external cylindrical workpieces. The material of the examined workpiece was AISI 304 austenitic stainless steel. In our experiments, we investigated the sliding frictional burnishing of an outer cylindrical surface when the burnishing tool had a diamond material-grade spherical tip. Using the full factorial experimental design technique, we aimed to determine how the changes in burnishing parameters, i.e., burnishing speed, burnishing feed, and burnishing force effect on the changes of surface micro-hardness and surface micro-hardness improvement ratio. Based on examinations, the best burnishing parameter combination could be selected.*
Keywords: *AISI 316Ti austenitic stainless steel; slide diamond burnishing; micro hardness; improvement ratio of micro hardness.*

1. INTRODUCTION

Due to their increased corrosion resistance, stainless steels are widely used in various fields of engineering practice, such as food industry, chemical industry, and automotive industry. The most common requirements for the surfaces of parts made of such steels are low roughness, high micro-hardness and wear resistance. These requirements can largely be satisfied by the use of cold-plastic burnishing technologies.

Sliding friction burnishing is kinematically similar to turning, but instead of the insert of the cutting tool, the deforming element is a large radius sphere tip that is moved by applying a certain amount of pressure to the surface to be machined. This creates a plastic deformation on the surface of the workpiece and in the layers close to the surface (Fig. 1) [1].

Burnishing improves the surface roughness, creates compressive residual stress and increases the hardness. The implementation possibilities of surface plastic deformation based on the work of Maximov et al. [2] are illustrated in Fig. 2.

Dynamic methods can almost always be used indefinitely to treat complex surfaces. Static methods are more suitable for improving the surface integrity of rotationally symmetric parts. Sliding friction burnishing was classified in detail by Maximov et al. [3] and analysed from different perspectives. Examples of classification criteria were: a) the object studied (surface integrity, functional characteristics of burnished surfaces, physical nature of the process), b) the material and shape of the deforming element, c) the method of testing, d) the machined material qualities

(steel, non-ferrous metal alloys), e) type of machined surface (outer cylindrical surfaces, inner cylindrical surfaces, flat surfaces, complex surfaces, discontinuous cylindrical surface), f) examination of process parameters (ironing force, ironing depth, feed, ironing speed, the number of passes, the lubricant, the radius of the spherical tool, the diameter of the cylindrical tool).

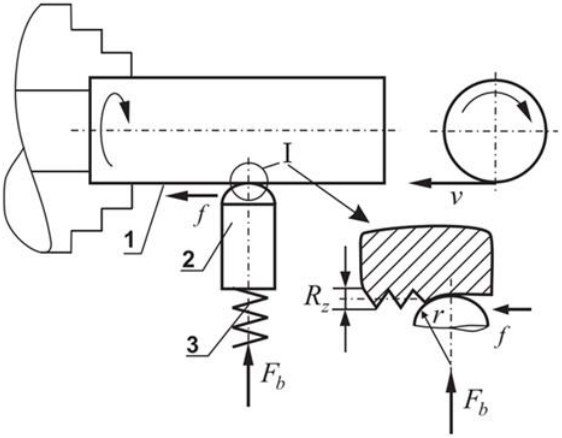

Figure 1 – Schematic of sliding friction burnishing [1]
1 - workpiece, 2 - forming element, 3 - spring

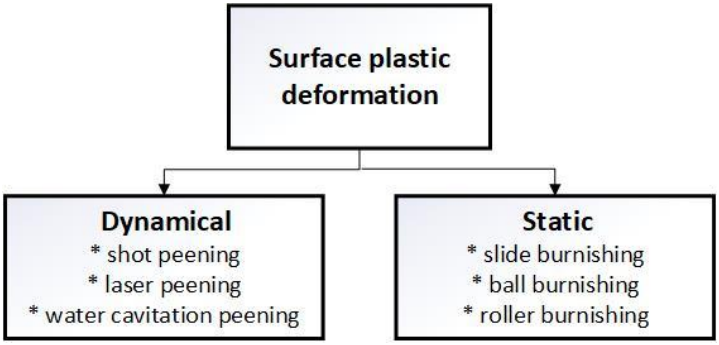

Figure 2 – Implementation possibilities of surface plastic deformation [2]

In the analysis of surface integrity, it was found that 33% of the more than 100 dissertations examined dealt with roughness while 21% dealt with micro-hardness. 79% of the studies implemented sliding friction ironing with a diamond deforming

part. Another interesting fact is that three-quarters of the studies used an experimental test method. 75% of the studies analysed focused on the examination of the external cylindrical surface. The three most commonly studied parameters were ironing force, feed, and ironing speed. 65% of the reinforced workpieces were made of steel, of which 28% dealt with the cold-plastic burnishing of stainless steels. In the following, we deal with the research of the burnishing of stainless steels.

2. COLD FORMING MACHINING OF STAINLESS STEELS

The research by Shiou et al. [4] aims to develop a new burnishing tool embedded in a measuring cell integrated with a CNC lathe that improves the hardness of smoothly turned AISI420 stainless steel. Based on the experimental results, the appropriate combination of process parameters is as follows: sphere material WC, burnishing force 650 N, feed rate 0.05 mm/rev, speed 25 m/min, coolant-lubricant (oil/water concentration 1/20) and the number of passes is 3. The surface hardness of the smoothly turned specimen could be increased from HRc 51 to HRc 52.5 on average by using the appropriate process parameters. Sachin et al [5] performed diamond burnishing in a minimal quantity lubrication (MQL) environment on 17-4PH stainless steel. Their aim was to investigate the effect of process parameters on surface integrity characteristics, including surface hardness, when using a new, modified tool. With their burnishing, they achieved that the improved maximum surface hardness of 405HV using diamond spheres with radii of 3 mm and 4 mm. The paper of Varga and Ferencsik [6-7] deals with the analysis of hardness of diamond burnished workpiece surfaces of low alloyed aluminium. Within the studied parameter range, the rate of improvement in terms of surface micro-hardness was maximized at 13.67%, which could be increased by increasing the force and by decreasing the feed rate.

3. EXPERIMENTAL CONDITIONS

3.1. Material, specimen

Austenitic chromium-nickel stainless steel 1.4301/AISI 304, often used for equipment in the chemical, oil and food industries, was the subject of the experiment. It is characterized by high corrosion resistance and easy formability. Its chemical composition is given in [7], its mechanical properties in Table 1.

Table 1 – Chemical composition of AISI 304 stainless steel (wt. %) [8]

C %	Si %	Mn %	P %	S %	Cr %	Ni %	N %
≤ 0.07	≤ 1.00	≤ 2.00	≤ 0.045	≤ 0.015	17.5 -19.5	8.0 - 10.5	≤ 0.11

Table 2 – Mechanical properties of AISI 304 stainless steel at 20°C [8]

Hardness HB 30	0.2% Yield strength, Rp	Tensile strength, Rm	Elongation A5	Modulus of elasticity
≤ HB	≥ N/mm²	N/mm²	≥ %	kN/mm²
215	190	500-700	45/35	200

The physical properties of AISI 304 stainless steel at 20°C were [8]: Density 7.9 g/cm³, Specific heat capacity 500 J/kg K, Thermal conductivity 15 W/m K, and Electrical resistivity 0.73 Ω mm²/m.
Geometrical dimensions of the specimens used for the reinforcement experiments: 5 adjacent cylindrical surfaces with a diameter of Φ49.48 mm and a length of 26 mm. The machining parameters for the fine turning of the test piece before ironing were: cutting speed v_c = 90 m/min, feed f = 0.05 mm/rev and the depth of cut a_c = 0.05 mm. Micro-hardness data can be found in Table 4.

Figure 3 – The technological realization of sliding burnishing process

Burnishing of outer cylindrical surfaces can be executed on conventional universal lathe or up-to-date CNC lath. The previous one was applied because of it rigidity as can be seen in Fig. 3.

3.2. Research methodology, measuring techniques

For the present series of experiments, we examined the effect of three factors, each at 2–2 levels according to the method of factorial experiment design [9-10].

The advantage of this method is that an empirical function relations can be written between the input (independent) parameters and the output (dependent) variable. Independent variables are called factors. The different set values of the factors are called levels.
The burnishing experiments were performed on a renovated, sufficiently rigid EU-400/01 type SZIM lathe at the Institute of Manufacturing Sciences of the University of Miskolc. The material of the burnishing tool was PCD and its radius was R = 3.5mm. Manual application of lubricant, type SAE 15W-40, was small.
The experimental design matrix of the reinforcement parameter variants is shown in Table 3.

Table 3 – Burnishing parameter variants

No.	Adjusted parameters			Transformed parameters		
	v [m/min]	f [mm/rev]	F [N]	X_1	X_2	X_3
1	41.17	0.0125	30	-1	-1	-1
2	58.26	0.0125	30	+1	-1	-1
3	41.17	0.0500	30	-1	+1	-1
4	58.26	0.0500	30	+1	+1	-1
5	41.17	0.0125	40	-1	-1	+1
6	58.26	0.0125	40	+1	-1	+1
7	41.17	0.0500	40	-1	+1	+1
8	58.26	0.0500	40	+1	+1	+1

The following burnishing parameters were examined: burnishing speed, feed rate and burnishing force, as it can be seen on Table 3. Table 3 contains the burnishing parameters in natural dimensions and in transformed (dimensionless) way.

3.3. Measuring of micro-hardness of the surface

The surface hardness of the test pieces was measured (before and after ironing) on an (Wilson Instruments Tukon 2100B) hardness tester at the Institute of Metallurgy, Plastic Formation and Nanotechnology of the Faculty of Metallurgical Engineering. The device measures Vickers hardness too. The principle of it, as is usually the case with all hardness measurements, is to examine how the test material withstands plastic deformation using a standard resource. During the measurement, a 136 ° diamond pyramid was pressed with 1 N force for 10 seconds on the surface to be measured at 3 points along a generatrix.
Figure 4 illustrates a state of the measurement process. In our investigation we have created a dimensionless ratio (1) to make the changing of surface micro-hardness more visible.

$$IRHV = \frac{HVa - HVb}{HVa} \cdot 100,\% \quad (1)$$

where

IRHv is the ratio of surface micro-hardness improvement (%).

HVb is the surface micro-hardness before burnishing process.

HVa is the surface micro-hardness after burnishing process.

The highest the value of IRHV, the greater is the improvement. The measured data and the calculated improvement ratios are summarized in Table 4.

Table 4 – Measured values and calculated improvement ratios

No.	*HV* 1		IRHV, %
	After Turning	After Burnishing	
1	316,00	370,33	17,19
2	341,00	360,00	5,57
3	324,00	379,67	17,18
4	319,33	381,67	19,52
5	310,67	383,67	23,50
6	308,67	365,00	18,25
7	318,67	381,67	19,77
8	313,67	384,33	22,53

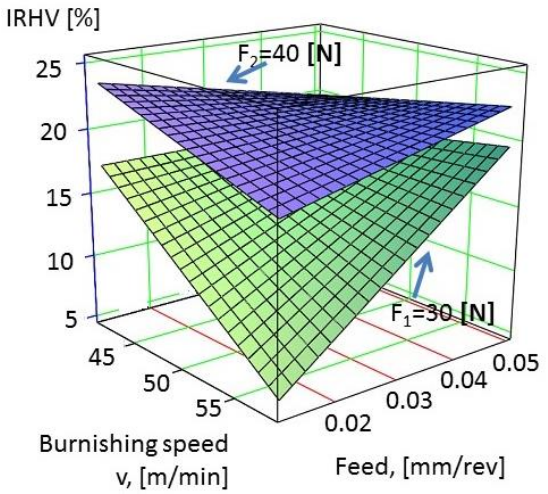

Figure 4 – Changing of surface micro-hardness improvement ratios

Application of Full Factorial Experiment Design method empirical formula (2) could be created from the calculated values. Calculations and axonometric figure (Fig. 4) was prepared using „MathCAD 15.0" software.

$$IRHV = 94.119 - 2.419 \cdot v - 1.746 \cdot 10^3 \cdot f - 1.257 \cdot F + 49.634 \cdot v \cdot f + 0.049 \cdot v \cdot F + 28.304 \cdot f \cdot F - 0.928 \cdot v \cdot f \cdot F \quad (2)$$

4. SUMMARY AND DISCUSSIONS

The paper deals with the experimental analysis of sliding burnishing when the material of the workpiece is austenitic chromium-nickel stainless steel. Experimental parameters were the burnishing speed, feed rate and burnishing force. The aim of the experiments was to determine the effect of the change of these parameters to the surface micro-hardness.

On the base of the present research work it can be stated:

- Among the examined parameters the effect of burnishing force is the most dominant and it is followed by the feed, and the less dominant parameter is the burnishing speed.
- The best improvement ratio of surface micro-hardness resulted when the burnishing parameters were as follows: F=40 N, f=0.0125 mm/rev and v=41.17 m/min.

ACKNOWLEDGEMENTS

"Project no. NKFI-125117 has been implemented with the support provided from the National Research, Development and Innovation Fund of Hungary, financed under the K_17 funding scheme."

References 1. *J.T. Maximov, A.P. Anchev, V.P. Dunchev, N. Ganev, G.V. Duncheva, K.F. Selimov*: Effect of slide burnishing basic parameters on fatigue performance of 2024-T3 high-strength aluminium alloy, Wiley Publishing Ltd. Fatigue Fract Engng Mater Struct 00 (2017) 1–12. https://doi.org/10.1111/ffe.12608. **2.** *J.T. Maximov, G.V. Duncheva, A.P. Anchev, N. Ganev, I.M. Amudjev, V.P. Dunchev:* Effect of slide burnishing method on the surface integrity of AISI 316Ti chromium-nickel steel, J Braz Soc Mech Sci Eng (2018) 40(194). https://doi.org/10.1007/s40430-018-1135-3. **3.** *J.T. Maximov, G.V. Duncheva, A.P. Anchev, M.D. Ichkova:* Slide burnishing review and prospects. The Int. Journ.l of Adv. Manuf. Technology (2019) 104: 785–801, https://doi.org/10.1007/s00170-019-03881-1. **4.** *F.J. Shiou, S.J. Huang, A.J. Shin, J. Zhu, M. Yoshino:* Fine surface finish of a hardened stainless steel using a new burnishing tool. Procedia Manuf. (2017) 10: 208–217. **5.** *B. Sachin, S. Narendranath, D. Chakradhar:* Sustainable diamond burnishing of 17-4 PH stainless steel for enhanced surface integrity and product performance by using a novel modified tool. Mater Res Express (2019) 6: 046501. **6.** *G. Varga, V. Ferencsik:* Analysis of hardness and residual stress of diamond burnished workpiece surfaces, GÉP, LXVIII. Vol., 4: (2017) 89-92 (In Hungarian). **7**. *G. Varga, V. Ferencsik:* Analysis of Surface Micro-hardness on Diamond Burnished Cylindrical Components, REZANIE I INSTRUMENTY V TEKHNOLOGICHESKIH SISTEMAH 90: 1, (2019) pp. 146-152. **8.** http://www.metalcor.de/en/datenblatt/5/ (2020.05.17). **9.** *G. Taguchi:* System of Experiment Design, (1984) p. 143. UNIPUB, Kraus International Publications, White Plains.

10. *L. Fridrik*, Chosen chapters from the topics of experimental design of production engineering. Műszaki Könyvkiadó, Budapest (1987) (In Hungarian). **11.** *C. Montgomery*: Design and Analysis of Experiments, 7th edn., (2009) International Student Version, Arizona State University.

Дьюла Варга, Вікторія Ференчик, Мішкольц, Угорщина

ЕКСПЕРИМЕНТАЛЬНЕ ДОСЛІДЖЕННЯ СТУПЕНЯ ПІДВИЩЕННЯ МІКРОТВЕРДОСТІ ПОВЕРХНІ ПРИ ВИГЛАДЖУВАННІ ЗОВНІШНІХ ПОВЕРХНОСТЕЙ ЦИЛІНДРИЧНИХ ДЕТАЛЕЙ

Анотація. *Робота присвячена експериментальному дослідженню ступеня підвищення мікротвердості поверхні при вигладжуванні зовнішніх поверхонь циліндричних деталей. Вигладжування тертям ковзання по кінематиці аналогічно токарній обробці, але замість вставки різального інструменту, деформуючий елемент являє собою сферичний наконечник з великим радіусом, який переміщається шляхом застосування притиску з певною силою до оброблюваної поверхні. Це створює пластичну деформацію на поверхні заготовки і в шарах, близьких до поверхні. Такий процес обробки покращує шорсткість поверхні, створює залишкову напругу стиснення і збільшує твердість. Матеріалом досліджуваної заготовки була аустенитна нержавіюча сталь AISI 304. У даних експериментах було досліджено фрикційне вигладжування ковзання зовнішньої циліндричної поверхні, коли вигладжувальний інструмент мав сферичний наконечник зі штучного алмазу. Використовуючи методику повного факторного експерименту, переслідувалася мета визначити, як зміни параметрів вигладжування, такі як: швидкість вигладжування, подача і сила притиску вигладжувача впливають на зміни мікротвердості поверхні і коефіцієнту поліпшення мікротвердості поверхні. На підставі досліджень можна вибрати кращу комбінацію параметрів цього процесу. Для даної серії експериментів було досліджено вплив трьох чинників, кожен на 2-2 рівнях відповідно до методу факторного планування експериментів. Перевага цього методу полягає в тому, що між вхідними (незалежними) параметрами і вихідною (залежною) змінною може бути записана емпірична функція. На підставі проведеного дослідження можна констатувати, що серед розглянутих параметрів вплив сили притиску вигладжувача є найбільш домінуючим, за ним слідує подача, а менш домінуючим параметром є швидкість вигладжування. Найкращий коефіцієнт поліпшення мікротвердості поверхні був досягнутий, коли параметри процесу вигладжування були наступними: F = 40 Н, f = 0,0125 мм / об і v = 41,17 м / хв.*

Ключові слова: *аустенітна нержавіюча сталь AISI 316Ti; алмазне вигладжування; мікротвердість; коефіцієнт поліпшення мікротвердості.*

UDC 621.922 **doi: 10.20998/2078-7405.2020.93.14**

V. Naddachyn, Odessa, Ukraine

RELATIONSHIP BETWEEN PROCESSING TEMPERATURE AND INTERRUPTION IN THE GRINDING PROCESS

Annotation. *This article discusses issues related to the processing of grinding wheels with an intermittent working surface and their influence on the grinding process. To solve this problem, it was necessary to first identify the relationship between the discontinuity of the process and the shock load. Next, determine the trajectory of movement of the forming point of the circle. A diagram of the movement of the center of mass of the circle and the forces acting on it is constructed. Equations are derived that determine these displacements. A system of equations describing the movement of the spindle axis under the action of cutting forces and power imbalance of the wheel is presented. The relationship between the frequency, amplitude of forced vibrations and displacements of the axis under the action of a harmonic disturbing force has been established. Theoretical calculations are confirmed by practical results. Based on the movement of the forming point of the circle, the parameters of the profile of the machined surface are set. The influence of the discontinuity of the process on the grinding temperature is considered.*

Keywords. *intermittent grinding; vibrations during grinding; trajectory of movement; hit; surface profile; grinding temperatures.*

One of the ways to improve the technical level and quality of products is to improve existing technological processes, incl. and grinding.

It is known that the operational properties of machine parts depend not only on the accuracy of their manufacture, but also on the high quality of surfaces achieved in the final machining operations - grinding operations.

At the same time, one of the most common defects in these operations can be burned surfaces and, as a result, a violation of the structure and physical and mechanical properties of the surface layer. The solution to this problem is possible:

1) By reducing the grinding modes, and, consequently, the processing efficiency.

2) The use of new technological methods of processing, in particular, an abrasive tool with an intermittent working surface.

Discontinuous circles can be directly attributed to this type of tool design (a description of the design and technological capabilities are given in numerous works of Prof. A.V. Yakimov and his students, composite wheels, segment grinding wheels.

However, the use of this type of abrasive tool is constrained by the presence of tool vibrations (caused by the impact of the protrusion at the moment of contact with the workpiece), the possibility of waviness and unsatisfactory roughness on the work surface.

For purposeful control of these parameters during intermittent grinding, it was necessary to identify how waviness is formed on the treated surface, as well as to determine the relationship of the formed waviness with the design of the intermittent circle, its oscillations, processing modes and temperature dependences.

It is known that during grinding there are certain possibilities to control the quality parameters of the processed surface. But for an effective solution to this process, you need to know the reasons affecting these parameters.

The process of forming geometric parameters, in particular, roughness and waviness on the processing surface.

Basically, the works deal with the formation of roughness [1, etc.]. Conditions conducive to the appearance of waviness are rarely considered [2, 3].

The choice of the optimal parameters of waviness and roughness is proposed to be made based on the service purpose of the part and the corresponding operating conditions of the friction pairs.

The relationship between the parameters of the shock load and the amplitude of forced vibrations with the design of the grinding wheel.

As noted above, the oscillation parameters of the grinding wheel-spindle system, its amplitude and frequency, are a consequence of the impact of the shock load arising from grinding with intermittent wheels. The carried out experiments also found that the repetition rate of shock pulses depends on the number of protrusions and the speed of rotation of the circle. For example, for a circle with a diameter of Ø250 mm and with a constant rotation speed n ≈ 3000 rev/m, the frequency of additional forced oscillations will be: f = 182 ... 546 Hz; (for circles with 4 ... 12 lugs)).

This is clearly confirmed by the oscillograms of the shock load (Fig. 1). With a change in the number of protrusions, the repetition time of shock pulses also changes, and with a change in the design of the circle (intermittent or compositional), the amplitude of the shock load changes.

The action of the shock load accordingly causes the grinding wheel to vibrate with a certain amplitude and frequency. The magnitude of the vibration amplitude is also influenced by the processing modes.

With an increase in the table speed, the relative speed of collision of the cutting edge of the tool with the workpiece surface [4] increases, the impulse of the force and the kinetic energy of the colliding bodies, depending on the speed (f. 1).

$$E_0 = \frac{M \cdot V_0^2}{2}. \quad (1)$$

At the same time, due to the closed nature of the "cutting process - EES" system, the change in the kinetic energy of impact (E_0), according to dependence (2)

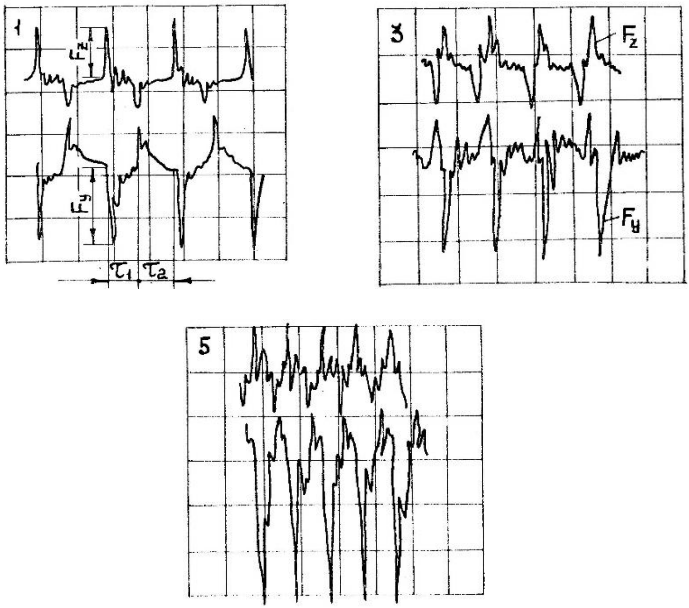

Figure 1 – Changes in the repetition rate of the shock load and its amplitude from the structure of the circle.
(1 - broken circle with 2 protrusions (at V_d = 0.17 m/s, t = 10 10^{-6} m, gain F_z = 1 V/div, F_y = 2 V/div); 3 - circle with n = 8 pcs.; 5 - circle with n = 12 pcs. (at V_d = 0.3 m/s, t = 50 10^{-6} m, gain F_z (F_y) = 5 V/div))

$$A^2 = \frac{2 \cdot E_0}{m\omega^2}, \qquad (2)$$

causes a change in the amplitude of oscillations (A) [4].

Therefore, it is necessary to determine the magnitude of the vibration amplitude caused by the shock load, as well as the trajectory of the displacement of the center of the circle and the "forming point".

It is known that the trajectory of the grinding wheel is a complex closed cycloidal or quasi-cycloidal curve.

First, consider the trajectory of the axis of the grinding wheel in the presence of imbalance. Then, the imbalance of the spindle assembly can be represented in

the form of: structural imbalance ($\overline{q_k}$) (for example, a violation of the symmetry of the location of the projections and depressions of the circle); technological ($\overline{q_т}$) (associated with a certain tolerance in the manufacture of elements of the spindle assembly, assembly inaccuracy, etc.); operational ($\overline{q_э}$) (associated with a change in the size of the grinding wheel during processing and a shift in its center of mass due to the uneven density of its material). That is, representing as the main vector of unbalanced forces ($\overline{Q}$) (3).

$$\overline{Q} = \overline{q_т} + \overline{q_k} + \overline{q_э} \tag{3}$$

These imbalances will cause low-frequency oscillations (let's call them the carrier (fundamental) frequency) of the "grinding wheel - spindle" system, the amplitude of which depends on the value of the displacement of the center of mass of the grinding wheel $A_0 = f(E)$, (that is, its imbalance), and vibration frequency - from the angular speed of rotation of the spindle $\omega = f(n_{rev})$. When additional counterbalancing forces are introduced into the system, opposite in sign, the main vector of unbalanced forces can be reduced to the minimum permissible, in terms of technological capabilities. That is, by balancing the grinding wheel or the spindle unit as a whole.

$$\overline{Q} = -\overline{Q}_д \rightarrow \min$$

Taking into account additional forced vibrations, associated with the specific features of grinding with these wheels, we will compose a differential equation of motion of the center of mass of the wheel and the relative rotations of the spindle axis about the center of mass.

Let's make a number of assumptions:

1). When recording an oscillogram during grinding, oscillations are clearly visible associated with the presence of cutting forces and imbalance of the wheel, the frequency of which corresponds to the spindle rotation speed, with the superposition of a higher order harmonic on the fundamental component, caused by the action of impact forces F_v, the frequency of which corresponds to the frequency of change of these forces (the number of protrusions on the circle) (Fig. 2, 3).

That is, system vibrations will occur due to imbalance of the grinding wheel and impact forces caused by the intermittent cutting process.

2). There is no damping in an elastic technological system.

3). Studies carried out on a surface grinding machine (type 3G71) showed that the rigidity of the magnetic table, and, consequently, of the part installed on it,

is approximately 2 orders of magnitude higher than the rigidity of the spindle supports. That is, it is assumed that the part has absolute rigidity and table vibrations can be ignored.

4). The spindle of the machine, together with the grinding wheel, is considered rigid, mounted on flexible supports, since the bending stiffness of the spindle significantly exceeds the stiffness of the supports.

5). The spindle axis is aligned with the geometric center of the circle.

Let's find the equation of motion of the circle, taking into account its imbalance.

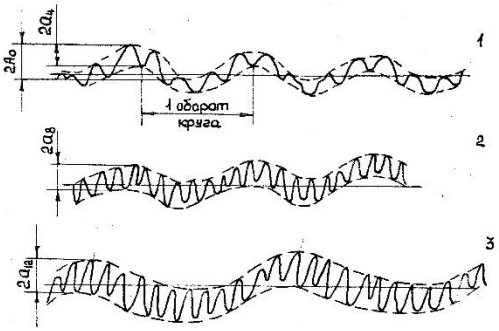

Figure 2 – Sample vibration displacement recording

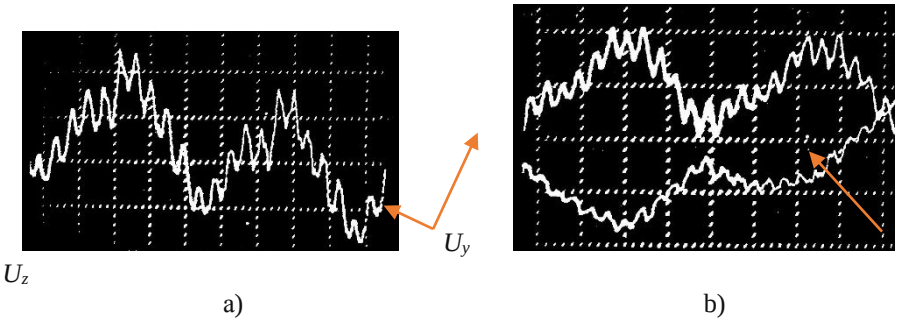

Figure 3 – Oscillograms of vibration displacements (a) sweep (circle with 4 protrusions); (b) with 12 projections

Let y_1, y_2, z_1, z_2 represent small displacements of the spindle axis in the supports during vibrations in the radial and tangential directions (on the 1st and 2nd supports, respectively) (Fig. 4).

We find the displacement of the center C of the grinding wheel mass through the movement of the spindle in the supports (Fig. 5) (in the vertical and horizontal planes).

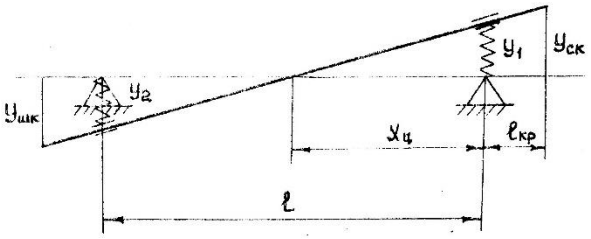

Figure 4 – Diagram of the radial movement $y_{ск}$ of the center of mass of the grinding wheel depending on the movement of the spindle axis in the supports

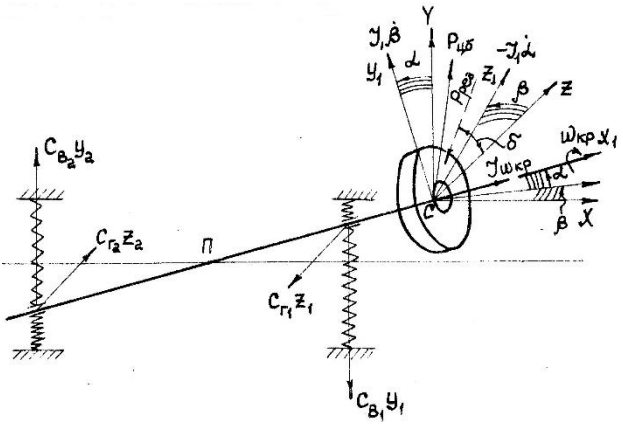

Figure 5 – Scheme of the acting forces of an unbalanced cantilever spindle with a grinding wheel

$$y_{ск1} = y_1 \cdot \frac{l_{кр} + x_ц}{x_ц}, \qquad z_{ск1} = z_1 \cdot \frac{l_{кр} + x_ц}{x_ц},$$

where $x_ц$ – is the point of intersection of the beam axis with the horizontal line under equilibrium conditions.

Let's designate $C_{в1}$, $C_{в2}$, $C_{г1}$, $C_{г2}$ stiffness of supports. Bearing reactions in the Y and Z directions caused by small displacements y_1, y_2, z_1, z_2, will be $C_{в1} \cdot y_1$,

$C_{в2} \cdot y_2$, $C_{г1} \cdot z_1$, $C_{г2} \cdot z_2$. The disturbing factors for an ordinary circle, taking into account its imbalance, will be the cutting force $P_{рез}$ and the unbalanced centrifugal force $P_{ц.б.}$ (fig. 5).

The equation that determines the displacement of the center of mass in projections on the Y and Z axes has the form (4)

$$\left.\begin{aligned} \frac{P}{g} \cdot \ddot{y}_{ск} + C_{в1} \cdot y_1 - C_{в2} \cdot y_2 + P_{рез} \cdot \sin\delta + P = P_{ц.б.} \cdot \sin\omega_{кр} t; \\ \frac{P}{g} \cdot \ddot{z}_{ск} + C_{г1} \cdot z_1 - C_{г2} \cdot z_2 + P_{рез} \cdot \cos\delta = P_{ц.б.} \cdot \cos\omega_{кр} t, \end{aligned}\right\} \quad (4)$$

where P – is the force of gravity.

To fully determine the movement of the spindle axis, it is necessary to compose differential equations describing the rotations of the spindle axis x_1 relative to the fixed axes X and Z. According to the law of change in the angular momentum, the time derivative of the total angular momentum of a moving system about a fixed axis is equal to the moment of forces about the same axis. As a result of elastic deformations, the axis of rotation x_1 makes small angles α and β with the fixed coordinate planes XY and XZ. The angles of rotation of the spindle axis in the vertical and horizontal planes through the movement of the spindle in the supports will be

$$\propto = \frac{y_2 - y_1}{l}; \qquad \beta = \frac{z_2 - z_1}{l}. \quad (5)$$

The components of the angular momentum about the axes x_1, y_1, z_1 are determined

$$L_{x1} = -I \cdot \omega_{кр}; \quad L_{y1} = -I_1 \cdot \dot{\beta}; \quad L_{z1} = I_1 \cdot \dot{\propto},$$

where I – is the moment of inertia of the grinding wheel relative to the x_1 axis;

I_1 – moment of inertia of the grinding wheel relative to the axes oy_1 and oz_1.

We find the angular momentum relative to the fixed axes X and Z by designing the moments $L_{x1}; L_{y1}; L_{z1}$ on these axes.

$$L_Y = L_{y1} + L_{x1} \cdot \propto = -I_1 \cdot \dot{\beta} - I \cdot \omega_{кр} \cdot \propto;$$
$$L_Z = L_{z1} + L_{x1} \cdot \beta = -I_1 \cdot \dot{\propto} - I \cdot \omega_{кр} \cdot \beta.$$

Based on the law of changing the amount of motion, the moments of external forces are defined as (6)

$$M_Y = \frac{d}{dt} L_Y; \qquad M_Z = \frac{d}{dt} L_Z. \tag{6}$$

Taking into account (5) and (6) the differential equations describing the rotations of the spindle axis can be written

$$\left.\begin{aligned} M_Z + C_{в1} \cdot y_1 \cdot l_{кр} - C_{в2} \cdot y_2 \cdot \left(l + l_{кр}\right) = 0; \\ M_Y - C_{г1} \cdot z_1 \cdot l_{кр} + C_{г2} \cdot z_2 \cdot \left(l + l_{кр}\right) = 0 \end{aligned}\right|. \tag{7}$$

The system of differential equations describing the movement of the spindle axis of the grinding wheel in space under the action of cutting forces and imbalance of the wheel has the form (8):

$$\left.\begin{aligned} \frac{P}{g} \cdot \left(\ddot{y}_1 \cdot \frac{l_{кр} + x_ц}{x_ц}\right) + C_{в1} \cdot y_1 - C_{в2} \cdot y_2 + P_{рез} \cdot \sin\delta + P = P_{ц.б.} \cdot \sin\omega_{кр} t; \\ \frac{P}{g} \cdot \left(\ddot{z}_1 \cdot \frac{l_{кр} + x_ц}{x_ц}\right) + C_{г1} \cdot z_1 - C_{г2} \cdot z_2 + P_{рез} \cdot \cos\delta = P_{ц.б.} \cdot \cos\omega_{кр} t; \\ I_1 \cdot \frac{\ddot{y}_2 - \ddot{y}_1}{l} + I \cdot \omega_{кр} \cdot \frac{\dot{z}_1 - \dot{z}_2}{l} + C_{в1} \cdot y_1 \cdot l_{кр} - C_{в2} \cdot y_2 \cdot \left(l + l_{кр}\right) = 0; \\ I_1 \cdot \frac{\ddot{z}_1 - \ddot{z}_2}{l} + I \cdot \omega_{кр} \cdot \frac{\dot{y}_1 - \dot{y}_2}{l} - C_{г1} \cdot z_1 \cdot l_{кр} + C_{г2} \cdot z_2 \cdot \left(l + l_{кр}\right) = 0. \end{aligned}\right\} \tag{8}$$

The system of equations (8) is compiled for the power imbalance of the circle, at which the vibration amplitude is 2 ... 3 times greater than the vibration amplitude caused by momentary imbalance.

In the presence of gyroscopic moments, vibrations in the YOX and ZOX planes are interconnected, that is, plane vibrations of the shaft are impossible and represent "direct" precession with an angular velocity equal to the spindle rotation speed.

A particular solution of the system of differential equations (8), which are oscillations of a spindle with a circle under the action of cutting forces and the presence of an imbalance, has the form (9)

$$\left.\begin{aligned} y_1 = y_{10} + B_1 \cdot \sin\omega_{кр} t; \qquad y_2 = y_{20} + B_2 \cdot \sin\omega_{кр} t; \\ z_1 = z_{10} + A_1 \cdot \cos\omega_{кр} t; \qquad z_2 = z_{20} + A_2 \cdot \cos\omega_{кр} t, \end{aligned}\right| \tag{9}$$

where $y_{10}, y_{20}, z_{10}, z_{20}$ – are the displacements of the points of the spindle axis lying in the plane of the supports caused by the action of the cutting forces $P_{рез}$ and the gravity force of the circle *P* (Fig. 6).

A_1, A_2, B_1, B_2 – vibration amplitudes of the grinding headstock supports (horizontal and vertical).

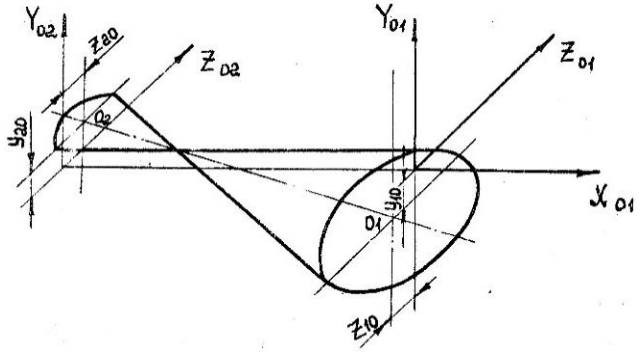

Figure 6 – Surface described by the spindle axis in space under the influence of imbalances of the grinding wheel

After transforming equations (9) and substituting in (8), taking into account the representation of the cutting force $P_{рез}$ in the form of a permanently acting force changing according to a sinusoidal law, and the force of gravity *P* as a uniformly distributed mass over the entire volume of the circle, we find the determinants of the Δ system, and on the first support ΔA_1, and ΔB_1. And after excluding the parameter *t* from equation (9), we obtain the canonical equations of ellipses (10) with the origin at the points O_1 (y_{10}, z_{10}) and O_2 (y_{20}, z_{20}), respectively.

$$\frac{(y_1 - y_{10})^2}{B_1^2} + \frac{(z_1 - z_{10})^2}{A_1^2} = 1;$$
$$\frac{(y_2 - y_{20})^2}{B_2^2} + \frac{(z_2 - z_{20})^2}{A_2^2} = 1. \quad (10)$$

Consequently, under the action of unbalanced forces, as a result of the addition of gyroscopic vibrations in the vertical and horizontal directions, the end of the spindle axis describes an elliptical trajectory.

As studies have shown, on the main component of wheel vibrations (Fig.3a) associated with its imbalance, another harmonic of a higher order is superimposed, arising under the action of a disturbing force $F_в$ (i.e. shock load), associated with the specific conditions of processing these circles (Fig. 7).

Representing the disturbing force $F_в$ in the form of two components $F_{вy}$ and $F_{вz}$, expanding them in a Fourier series and considering certain harmonics, then

$$F_{вy} = B \cdot \sin \omega_1 t;$$
$$F_{вz} = A \cdot \sin \omega_1 t,$$

where A and B are the amplitude values of the forces $F_{вz}$ and $F_{вy}$

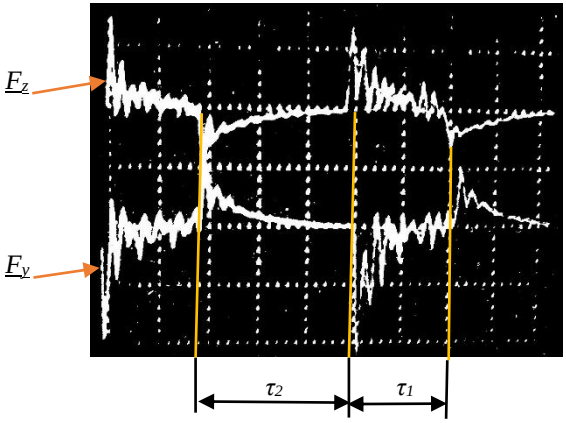

Figure 7 – Oscillograms of the shock load arising in the process of grinding (τ_1 – is the time of passage of the protrusion, τ_2 – is the time of passage of the groove)

Equations of motion of the center of a circle under the action of a shock load in the *YOZ* plane

$$\ddot{y} + \omega^2 y = B \cdot \sin \omega_1 t; \qquad (11)$$
$$\ddot{z} + \omega^2 z = A \cdot \sin \omega_1 t.$$

Making the appropriate transformations, we find the displacement of the axis under the action of a harmonic disturbing force $F_в$

$$\left.\begin{aligned} y^* &= \frac{B}{\omega^2 - \omega_1^2} \cdot \sin \omega_1 t; \\ z^* &= \frac{A}{\omega^2 - \omega_1^2} \cdot \sin \omega_1 t. \end{aligned}\right| \qquad (12)$$

That is, under the action of a harmonic disturbing force, the spindle axis relative to the ellipsoidal curve will also perform harmonic sinusoidal oscillations.

Thus, based on the principle of superposition when grinding with intermittent wheels, the center of mass of the wheel will describe in the section plane *YOZ*, perpendicular to the spindle axis, a complex closed curve described by expression (13) which determines the position of the center of mass of the wheel at a given time t_c relative to the fixed coordinates *O'Y* and *O'Z*.

$$\left.\begin{aligned} Y &= B_{\text{св}} \cdot \sin \omega_0 t_c + U_y \cdot \sin \omega_{\text{в}} t_c \cdot \sin \omega_0 t_c ; \\ Z &= A_{\text{сг}} \cdot \cos \omega_0 t_c + U_z \cdot \sin \omega_{\text{в}} t_c \cdot \cos \omega_0 t_c , \end{aligned}\right\} \qquad (13)$$

where $A_{\text{сг}}$ and $B_{\text{св}}$ – are the amplitudes of horizontal and vertical (respectively) oscillations associated with the imbalance of the circle;

U_y and U_z – are the amplitudes of forced radial and tangential oscillations associated with the action of the forced disturbing force;

ω_0 and $\omega_{\text{в}}$ – are the frequencies of the fundamental and high-frequency components of forced oscillations (respectively).

That is, a system of equations (13) was obtained, which determines the coordinates of the movement of the grinding wheel axis, taking into account the amplitude and frequency of its oscillations under the action of the emerging forces in the section plane perpendicular to the spindle axis, along which the trajectory of the wheel center movement was calculated (Fig. 8).

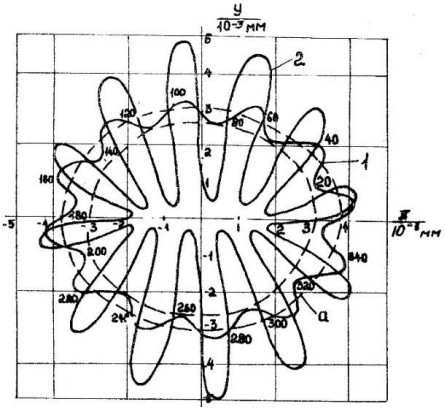

Figure 8 – Estimated trajectory of movement of the center of the circle in the plane *(YOZ)*, for one revolution, with different processing modes (the circle is intermittent with 12 projections) 1) at V_{∂} = 0.05 m/s, t = 10 10^{-6} m; 2) at V_{∂} = 0.03 m/s, t = 50 10^{-6} m

The figure shows that under the influence of the above factors, the center of the circle describes a rather complex trajectory. Moving along the ellipsoidal curve (a), it also performs sinusoidal displacements relative to this curve. With an increase in processing modes, the amplitude of sinusoidal displacements increases. The theoretically calculated trajectory is similar to the trajectory of displacement obtained experimentally (Fig. 9, 10).

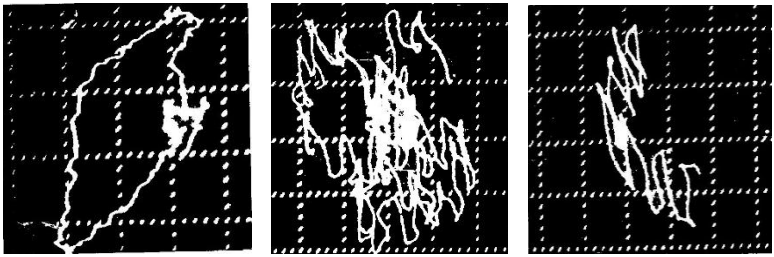

a) *b*) *c*)

Figure 9 – Oscillograms of vibration displacements of the circle center.
a) displacement during idle rotation as a result of imbalance;
b) vibration displacement when working in a circle with 10 projections;
c) part of a circle with 10 projections

During idle rotation (Fig. 9a), as a result of imbalance, the center of the circle makes ellipse-like movements. In the process of grinding, under the action of the protrusions of the circle, its center moving along a closed trajectory, simultaneously makes additional sinus-like movements relative to this trajectory (Fig. 9b, c).

Therefore, knowing the movement of the center of mass of the circle, we can proceed to the consideration of the formation of the profile of the treated surface.

Formation of a profile on the treated surface when grinding with intermittent wheels.

The shaping point of the circle, copying the movement of the center along the path *1'*, would also sequentially occupy positions *1'*, *2'*, *3'*, *4'*, etc., moving along the path *2'*. But since the grinding wheel is a volumetric body with a radius R, then the profile formed on the surface of the part will be the envelope of a family of arcs formed by the forming point of the periphery of the circle (with radius R_{kp}) and having the form (Fig. 11)

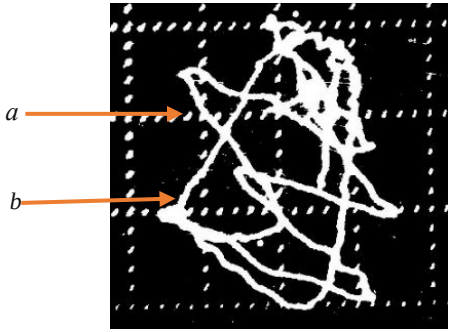

Figure 10 – The trajectory described by the center of the circle at idle rotation (*a*), while grinding (*b*) by a wheel with 4 protrusions

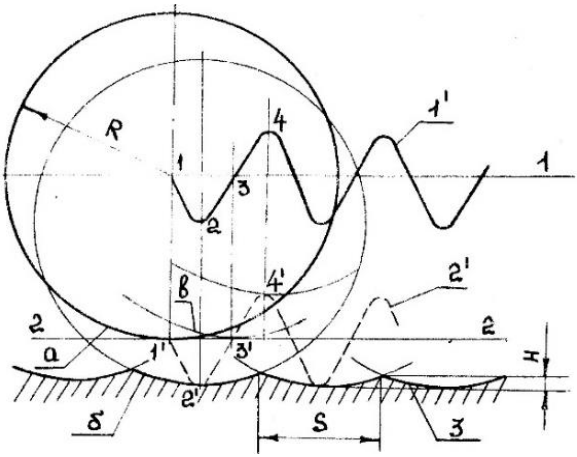

Figure 11 – Scheme of surface profile (waviness) formation

The relationship between the profile formed on the processed surface with the dynamic and kinematic parameters of the working tool can be represented as [3]

$$Y_в = Y_{огиб.дин.} + Y_{огиб.кин.}, \quad (14)$$

where $Y_{огиб.дин.} = f_1(X_{дин})$ – curve parameters associated with the dynamics of the process;

$Y_{огиб.кин.} = f_2(X_{кин})$ – the parameters of the curve associated with the kinematics of the formation of irregularities, depending on the geometric parameters of the circle (the number and length of protrusions and depressions).

The coordinates of the profile of the wavy surface during flat grinding with the periphery of the circle are determined by (f. 15),

$$\left.\begin{aligned} X_{дин} &= X \pm \frac{R \cdot \dot{y}}{\sqrt{(\dot{x})^2 + (\dot{y})^2}}; \\ Y_{дин} &= Y \pm \frac{R \cdot \dot{x}}{\sqrt{(\dot{x})^2 + (\dot{y})^2}}, \end{aligned}\right\} \quad (15)$$

where R – is the radius of the circle;

X and Y – are the coordinates of the center of the circle.

Substituting equations (13), taking into account the longitudinal displacement ($V_д \cdot t$) of the part relative to the circle in (15) and making some simplifications, we obtain the parameters of the dynamic component of the profile of the wavy surface for the *i-th* harmonic formed during intermittent grinding (where Y → y, Z → x):

$$\left.\begin{aligned} X_{дин} &= \left(A_{сг_i} + U_{z_i} \sin \omega_{в_i} t_c\right) \cos \omega_{0_i} t_c + V_д t_c + \\ &+ \frac{R\left[\left(B_{св_i} + U_{y_i} \sin \omega_{в_i} t_c\right)\omega_{в_i} \cdot \cos\omega_{0_i} t_c + U_{y_i} \cdot \omega_{в_i} \cos\omega_{в_i} t_c \cdot \sin \omega_{0_i} t_c\right]}{V}; \\ Y_{дин} &= \left(B_{св_i} + U_{y_i} \sin \omega_{в_i} t_c\right) sin\, \omega_{0_i} t_c + \\ &+ \frac{R\left[U_{z_i} \cdot \omega_{в_i} \cos\omega_{в_i} t_c \cos \omega_{0_i} t_c + V_д - \left(A_{сг_i} + U_{z_i} \sin \omega_{в_i} t_c\right)\omega_{0_i} \sin\omega_{0_i} t_c\right]}{V}, \end{aligned}\right\} \quad (16)$$

where

$$V = \sqrt{(\dot{x})^2 + (\dot{y})^2} = \sqrt{\begin{aligned}&\left[U_{z_i} \cdot \omega_{в_i} \cos\omega_{в_i} t_c \cos \omega_{0_i} t_c + V_д - \left(A_{сг_i} + U_{z_i} \sin \omega_{в_i} t_c\right)\omega_{0_i} \sin\omega_{0_i} t_c\right]^2 \\ &+\left[\left(B_{св_i} + U_{y_i} \sin \omega_{в_i} t_c\right)\omega_{в_i} \cdot \cos\omega_{0_i} t_c + U_{y_i} \cdot \omega_{в_i} \cos\omega_{в_i} t_c \cdot \sin \omega_{0_i} t_c\right]^2\end{aligned}}.$$

The solution of the system of equations (16) makes it possible to obtain the parameters of the wavy surface ($X_в$, $Y_в$) taking into account the dynamics of the cutting process.

Macroroughnesses obtained from the second ($Y_{огиб.кин.} = f_2(X_{кин})$) component in (f. 14), in fact, are quantities of the second order of smallness, in comparison with the waviness formed due to the dynamics of the process and they can be neglected.

Based on the data calculated from dependencies (16), the trajectory of movement of the shaping point of the circle and the profile of the generated wave is constructed (Fig. 12).

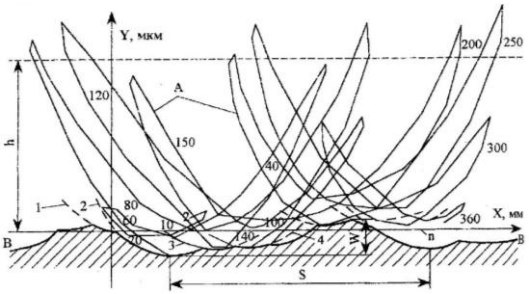

Figure 12 – The formation of waviness when machining with a broken circle (with 12 ridges). A - trajectory of the shaping point (for one revolution of the circle); 1, 2, 3, 4 ... n - the position of the forming arcs of the circle; B-B - envelope of the arc system (wave profile); h – is the depth of grinding

The shape-forming point of the circle, making loop-like oscillating movements, moves along the trajectory (A) repeatedly passes through the same zone of space, gradually cutting off the entire layer of metal. Arcs 1, 2, 3, 4 ... n of a circle of a circle of radius R leave a corresponding trace on the surface of the part. The envelope curve B-B for these arcs is the profile of the waviness formed on the surface of the part.

Depending on the presence of oscillations, their amplitude and frequency (the design of the circle), the trajectory described by the shaping point of the circle and the profile of the formed waviness change somewhat (Fig. 13).

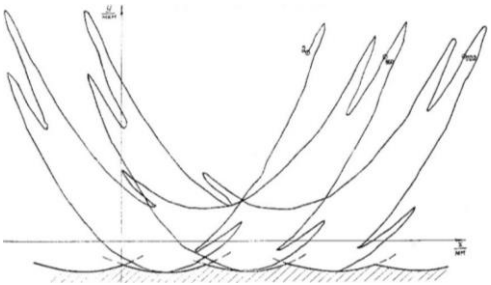

Figure 13 – The formation of waviness and the trajectory of the shaping point of the discontinuous circle (with 4 projections)

From the analysis of the above schemes (Fig. 12, 13), one more rather significant conclusion can be drawn. As a result of the presence of such oscillating displacements, performed by an intermittent circle, at certain points in time, the forming point separates from the treated surface, and the allowance is removed in separate thin layers (portions), which will serve as one of the reasons for reducing the cutting forces, and as a result, the heat intensity of the process.

References: **1.** *Novoselov YU.K.* Dinamika formoobrazovaniya poverkhnostey pri abrazivnoy obrabotke: Monografiya / YU. K. Novoselov. - Sevastopol': SevNTU, 2012. - 304 p **2.** *Suslov A.G.* Nauchnyye osnovy tekhnologii mashinostroyeniya [Tekst] / A. G. Suslov, A. M. Dal'skiy. – Moscow : Mashinostroyeniye, 2002. – 684 p. **3.** *Naddachin V.B.* Ispol'zovaniye vibratsiy pri preryvistom protsesse rezaniya [Tekst] / V. B. Naddachin, A. V. Babyuk // Sb.NT Obrabotka dispersnykh materialov i sred. Teoriya, issledovaniya, tekhnologii, oborudovaniye. – Odessa: NPO «Votum», 2002. – Vyp. №12. – pp. 126-130. **4.** *Biderman V.L.* Teoriya mekhanicheskikh kolebaniy [Tekst] / V. L. Biderman. – Moscow : Vysshaya shkola, 1980. – 408 p. **5.** *Naddachin V.B.* Vliyaniye vibratsiy na parametry kolebaniy abrazivnogo instrumenta [Tekst] / V. B. Naddachin, A. V. Balanyuk //Novyye i netraditsionnyye tekhnologii v resurso- i energosberezhenii. Sb. MNTK 19-22.09.2011 g. Odessa. – Kyiv, 2011 – pp. 145-147. **6.** *Prilutskiy V.A.* Tekhnologicheskoye obespecheniye tochnosti i kachestva poverkhnostnogo sloya detaley mashin putem upravleniya periodicheskimi pogreshnostyami obrabotki [Tekst] : avtoref. dis. … d.t.n. : 05.02.08 / V. A. Prilutskiy ; [Bryanskiy gos. tekhn. un-t] . – Bryansk, 2004. – 36 p.

Валерій Наддачин, Одеса, Україна

ВЗАЄМОЗВ'ЯЗОК МІЖ ТЕМПЕРАТУРОЮ ОБРОБКИ ТА ПЕРЕРИВЧАСТІСТЮ ПРОЦЕСУ ШЛІФУВАННЯ

Анотація. *У наведеній статті розглядаються питання, пов'язані з обробкою шліфувальними кругами з переривчастою робочою поверхнею і їх вплив на процес шліфування. Розглянуто теоретично можливі варіанти формування поверхні. Для вирішення цього завдання необхідно було на початку виявити взаємозв'язок уривчастості процесу і ударного навантаження. Встановлено, що зі зміною кількості виступів на крузі, буде змінюватися частота удару і амплітуда додаткових вимушених коливань системи. Розглянуто вплив режимів шліфування на коливальний процес. Побудована схема переміщення центру мас круга і діючих на нього сил. Наведено систему рівнянь, що описують рух осі шпинделя під дією сил різання і силову неврівноваженість круга. Встановлено взаємозв'язок між частотою, амплітудою змушених коливань і переміщень осі під дією гармонійно вимушених коливань. Наведено експериментально записані осцилограми удару і траєкторії переміщення центру. На підставі переміщення формотворної точки круга встановлені параметри профілю оброблюваної поверхні. Розглянуто вплив уривчастості процесу на температуру шліфування. Експериментально доведено, що в процесі обробки шліфувальними кругами з переривчастою робочою поверхнею, відбувається періодичний відрив «формотворної точки» круга від оброблюваної поверхні. В результаті такого процесу, зняття припуску відбувається більш тонкими шарами, ніж набрана (встановлена) глибина різання. І як наслідок, зниження сил різання і температури шліфування. Тобто основним параметром (більшою мірою), що впливає на зниження температури буде вібраційний процес, а не уривчастість процесу різання, за період проходження западини круга.*

Ключові слова: *переривчасте шліфування; вібрації при шліфуванні; траєкторія руху; удар; профіль поверхні; температури при шліфуванні.*

UDC 621.9 **doi: 10.20998/2078-7405.2020.93.15**

G. Klymenko, Y. Vasylchenko,
V. Kvashnin, Kramatorsk, Ukraine

MODELING OF CUTTING TOOLS WEAR FOR LATHES

Abstract. *A mathematical model to estimate the average number of parts, processing which is possible to achieve the criterion of maximum allowable wear on the back of the cutter heavy lathe, and the maximum allowable amount of tool material, removed from the front surface of the tool. Experimental equipment for measuring tool wear has been developed. Insert wear curves derived from industrial test results. Confirmation of the adequacy of the models of the instrument gives a possibility of their adjustment to the basic criteria of their dullness.*
Keywords: *wear; contact stress; cutting edge; cutting temperature;, adhesive wear; the adequacy of the models.*

The tool wear of cutting tools has a very strong impact on the product quality as well as on the efficiency of the machining processes. Despite the current high automation level in the machining industry, a few key issues prevent complete automation of the entire turning process. One of these issues is tool wear, which is usually measured off the machine tool. A well-known model for the tool wear rate was developed by Usui et al (Usui& Shirakashi, 1984), and it is based on the idea of contact mechanics and wear. The most famous tool life model is Taylor's model in which the tool life depends mainly on the cutting speed and a constant determined by materials of the tool and the workpiece, feed rate, etc. (Taylor, 1906). In the past over thirty years, much work has been contributed to the tool wear modeling [1-6].

While working on the details of heavy lathes main types of fault-alloy cutters are wearing them on the front and back surfaces, as well as fatigue damage cutting plates. Determination of maximum permissible values of wear on the back surface were carried out based on economic criteria.

For practical use have a value of mathematical models to estimate the average number of parts, which was processed to reaching the criterion of wear.

Evaluation of resistance of cutting tool criterion for maximum allowable wear on the rear surface.

Developing a model to assess the average number of parts, processing, which is possible to achieve the criterion of maximum allowable wear on the rear surface is made to the following basic assumptions:

– criterion of maximum allowable adhesion wear on the back of the formation of a high wear areas $[h_{zp}] = 1,2$ mm;

– basic mechanism of cutting tool wear on the back of the adhesion mechanism is;

– average temperature of the material the instrument is fixed for the whole region back surface contact with the processed material;

– stress of the cutting tool is a flat;

– tool material in contact with the workpiece the tool is characterized by a constant value for the whole region stresses fluidity $R_{см}$;

– number of parts, processing which is possible to achieve the maximum allowable height of platform wear $[h_{zp}]$ is:

$$N_{0.1} = \frac{[\mathrm{h}_{zp}]}{h_{zp}}, \tag{1}$$

where h_{zp} – increased wear platform for processing one part.

Based on studies of normal contact pressure distribution on the back of the instrument $q(\mathrm{x})$ can be represented by dependence:

$$q(\mathrm{x}) = \mathrm{q}_{\max.z}\left(1-\sqrt{\frac{x}{h_{zp}}}\right), \tag{2}$$

where h_{zp} – width areas of physical contact in this case – wear areas; x – distance from the cutting edge cutter; $\mathrm{q}_{\max.z}$ – maximum contact pressure at the back of the:

$$q_{\max.\mathrm{z}} = 2\tau_{\phi}\left(1,3\pm\gamma\right)\pm\tau_{\phi}\sin 2\gamma, \tag{3}$$

(plus sign corresponds to negative front angles);

where τ_{ϕ} – tension changes in a layer that trimmed, with the average temperature at the site contact the back of the instrument with the processed material. To Determine the value used τ_{ϕ} dependence:

$$\tau_{\phi} = 0,72R_{\theta}\cdot 6^{0.6\delta_5}, \tag{4}$$

where R_{θ} – ultimate strength of the material processed at an average temperature at the site of contact; δ_5 – elongation of the material processed at an average temperature at the site of contact. To evaluate the quantities R_{θ}, δ_5 used depends obtained on the basis of statistical data processing:

$$R_{\theta}\left(\Theta\right) = R_{\theta_0}\exp\left(a_1\left(\Theta_0-\Theta\right)\right),\ \delta_5\left(\Theta\right) = \delta_{5_0}\exp\left(b_1\left(\Theta-\Theta_0\right)\right), \tag{5}$$

where Θ – average temperature cutting; R_{θ_0}, δ_{5_0} – tensile strength and elongation of the material processed at a temperature test $\Theta_0 = 700^\circ C$; a_1, b_1 – coefficients determined by the method of least squares.

The average contact pressure at the back of the instrument can measure the expression q:

$$q = \frac{1}{h_{zp}} \int_0^{h_m} q_{\max.z} \left(1 - \sqrt{\frac{x}{h_{zp}}} \right) dx . \quad (6)$$

To determine the average temperature dependence of cutting used by the author, obtained by statistical progressing of experimental data:

$$\Theta = a_1 v^{a_2} s^{a_3} t^{a_4} , \quad (7)$$

where a_1, a_2, a_3, a_4 – calculated ratios determined by the method of least squares.

To determine the number of the parts to achieve the criterion of maximum allowable adhesion wear on the back of the take that amount of material d, removed from the back of the instrument for the elementary time interval $d\tau$ physical contact with the workpiece material back of the cutter, can be estimated from geometrical considerations:

$$dQ = b \left(h \cdot dh \cdot \tan\alpha + \frac{1}{2} dh^2 \cdot \tan^2 \alpha \cdot \tan\gamma \right); \; b = \frac{t}{\sin\varphi} , \quad (8)$$

where h – altitude areas of wear, which corresponds to the moment of time τ; dh – increase in areas of wear during $d\tau$; γ, α, φ – under the front corner and rear corner of the main corner in terms of the instrument; t – depth of cut.

On the other hand, the volume of material removed from the rear surface during $d\tau$, measured the expression:

$$dQ = P_u v \eta \delta b \cdot d\tau , \; \eta = \frac{q}{q^*} \quad (9)$$

where P_u – the likelihood that the zone of adhesion failure of communication is not in the treated material, and material of the instrument; v – speed cutting; δ – thickness of which is the destruction of products bearing adhesive ties: $\delta \cong 3 \cdot 10^{-5} .. 5 \cdot 10^{-9}$ m; η – the relative share areas of plastic surface microirregularity crumple in contact with the back of the instrument of processed material; q^* – maximum pressure required to crumple the full surface microirregularity processed material at the site of contact, estimated the expression:

$$q^* = 2,5R_e\left(1-\mu\right), \tag{10}$$

where R_e – meaning limits yield of processed materials in accordance with the average temperature in the cutting zone; μ – constant friction.

If the average pressure at the site of contact, the workpiece material with the rear surface instruments such that the value $\eta > 1$, we adopted $\eta = 1$. Size P_u can be estimated from the ratio of the critical crack lengths Hryffitsa that triggered the destruction of adhesion due:

$$P_u = \frac{l_u}{l_u + l_m},\ \frac{l_u}{l_m} = \frac{R_m^2}{R_u^2}, \tag{11}$$

where l_u, l_m – under the critical length of cracks in the surface layers of tool and workpiece material; R_u, R_m – tensile strength of the material and tool material processed at an average temperature at the site of contact. Taking the tool material and workpiece material hard plastic, the expression $\frac{R_m^2}{R_u^2}$ can be replaced by $\frac{R_e^2}{R_{eu}^2}$, where R_e, R_{eu} – border fluidity workpiece material and tool material at an average temperature at the site of contact, respectively. To determine the value of R_e used the dependence obtained by statistical processing of experimental data:

$$R_e\left(\Theta\right) = R_{e_0} \cdot \exp\left(b\left(\Theta_0 - \Theta\right)\right), \tag{12}$$

where Θ – the average temperature at the site of contact; R_{e_0} – the boundary strength of the material processed at a temperature test $\Theta_0 = 700^\circ C$; b – estimated coefficient determined by the method of least squares.

To determine the value of R_{eu} used dependence obtained by statistical processing of experimental data:

$$R_{eu} = 1,1R_T\left(\frac{\Theta_p}{\Theta}\right)^S arsh\left(\frac{\dot{e}\cdot e}{\dot{e}_0 \cdot e_0}\right),\ \Theta \geq \Theta_p, \tag{13}$$

where $\dot{e}_0$, e_0 – intensity of deformation speed and intensity of accumulated strain during mechanical testing instrument; R_T – boundary strength of the material instrument at ambient temperature; S – constant characteristic of the tool material. If the temperature does not exceed Θ cutting temperature early intensive removed Θ_p, instrumental material, it shall $R_{eu} = R_T$.

Comparing expressions (8) and (9) and respect for value dh^2, as the second largest order little, after the integration date was changing altitude areas of wear from time to time contact:

$$h_{zp} = \sqrt{\frac{2\nu\delta\eta P_u}{\tan\alpha}},\ \tau = \frac{l}{nS}, \tag{14}$$

where τ – time of processing one part, n – speed spindle.

After substituting the values of η and P_u obtained:

$$h_{zp} = \begin{cases} \sqrt{\dfrac{2\cdot q_{\max}\cdot\nu\cdot\tau\cdot\delta}{4,5\cdot tg\alpha\cdot(1-\mu)}\cdot\dfrac{R_e}{R_e^2+R_{eu}^2}} & if\ \dfrac{q_{\max}}{7,5\cdot R_e(1-\mu)}<1 \\ \sqrt{\dfrac{2\cdot\nu\cdot\tau\cdot\delta\cdot R_e^2}{tg\alpha\cdot(R_e^2+R_{eu}^2)}} & if\ \dfrac{q_{\max}}{7,5\cdot R_e(1-\mu)}\geq 1 \end{cases} \tag{15}$$

Then the number of parts, processing of which is available until a maximum allowable height of areas on the back of the depreciation is:

$$N_{0.1} = \begin{cases} [\mathrm{h}_{zp}]\cdot\sqrt{\dfrac{3,75\cdot\tan\alpha(1-\mu)\left(R_e^2+R_{eu}^2\right)}{q_{\max}\cdot\nu\cdot\tau\cdot\delta\cdot R_e}} & if\ \dfrac{q_{\max}}{4,5\cdot R_e(1-\mu)}<1 \\ [\mathrm{h}_{zp}]\cdot\sqrt{\dfrac{\tan\alpha\left(R_e^2+R_{eu}^2\right)}{2\cdot\nu\cdot\tau\cdot\delta\cdot R_e}} & if\ \dfrac{q_{\max}}{4,5\cdot R_e(1-\mu)}\geq 1 \end{cases} \tag{16}$$

The main mechanism of wear of cutting tools on the front surface are adhesion mechanism.

As a criterion of maximum allowable wear of the front surface is proposed to adopt the appearance of the front surface of the hole cutter wear depth $[h_{nn}]$.

Average number of blocks and treatment are possible until a maximum allowable depth of the hole wear, can be evaluated dependence:

$$N_{0.2} = \frac{[Q]}{Q}, \tag{17}$$

where $[Q]$ – the maximum allowable amount of tool material, removed from the front surface of the tool that meets $[h_{nn}]$; Q – volume of tool material, removed from the front surface of the tool during the processing of one part.

Value $[Q]$ is determined from geometric considerations the following expression:

$$[Q] = fb,\ f = \frac{R^2\alpha - \left(R - [h_{nn}]\right)l}{2},\ R = \frac{[h_{nn}]}{2} + \frac{l^2}{8[h_{nn}]}, \tag{18}$$

where l – length of the hole, b – width of the contact front surface of cutting tools with workpiece:

$$b = \frac{t}{\sin\varphi}. \tag{19}$$

The volume of material ∂Q, which is removed by an elementary interval of time of physical contact with the chip front surface of the tool is determined by the equation $d\tau$:

$$\partial Q = P_u \nu_c \eta \delta b \cdot dt,\ \nu_c = \frac{\nu}{\xi}, \tag{20}$$

where P_u – the likelihood that the zone of adhesion failure of communication is not in the treated material, and material tools, assessments expression (13); ν_c – speed chips on the front surface of the tool; ν – speed cutting; ξ – coefficient of shrinkage of the chip; δ – thickness of the layer from which the products bearing the destruction of adhesive contacts: for most metals and alloys $\delta \cong 3\cdot10^{-10}..5\cdot10^{-9}$ m; η – the relative share of regions full of plastic crumple microroughness chip surface in contact with the chip front surface:

$$\eta = \frac{q}{q^*}, \tag{21}$$

where q – the average pressure at the site of contact; q^* – average pressure required to crumple the full surface microroughness processed material on this site, estimated expression (10).

Based on studies of normal contact pressure distribution on the back of the instrument $q(x)$ can be represented by dependence:

$$q(x) = q_{\max.n}\left(1-\sqrt{\frac{x}{l_k}}\right), \tag{22}$$

where l_k – chip contact length on the front surface:

$$l_k = a\left(\xi\left(1-\tan\gamma\right)+\sec\gamma\right),\ a = s\cdot\sin\varphi; \tag{23}$$

$q_{\max.n}$ – maximum normal pressure on the front surface:

$$q_{\max.n} = 2\tau_\varphi\left(1{,}3-\gamma\right). \tag{24}$$

The average value of normal pressure on the site of contact is:

$$q = \frac{1}{l_k}\int_0^{l_k} 2\tau_\varphi\left(1{,}3-\gamma\right)\left(1-\sqrt{\frac{x}{l_k}}\right)dx. \tag{25}$$

The volume of material instrument removed from the front surface of the tool during the processing of one part τ, is recognized by dependence:

$$Q = \int_0^{\tau} P_u \nu_c \eta \delta b \cdot dt . \tag{26}$$

Then, taking into account (23), (24):

$$Q = \frac{R_e^2}{R_e^2 + R_{eu}^2} \frac{\nu}{\xi} \frac{1}{q^*} \delta \frac{t}{\sin\varphi} \frac{1}{l_k} \int_0^{l_k} \int_0^{\tau} q_{\max} \left(1 - \sqrt{\frac{x}{l_k}}\right) dx dt . \tag{27}$$

On the assumption that the value of P_u, ν_c, δ, b insignificant change in contact time, according to a theorem on the average integral obtained:

$$Q = \begin{cases} \dfrac{R_e}{R_e^2 + R_{eu}^2} \dfrac{\nu}{\xi} \delta \dfrac{q_{\max} t \tau}{4,5 \sin\varphi (1-\mu)} & if \ \dfrac{q_{\max}}{4,5 \cdot R_e (1-\mu)} < 1 \\ \dfrac{R_e^2}{R_e^2 + R_{eu}^2} \dfrac{\nu}{\xi} \delta \dfrac{t\tau}{\sin\varphi} & if \ \dfrac{q_{\max}}{4,5 \cdot R_e (1-\mu)} \geq 1 \end{cases} \tag{28}$$

Then the number of parts, processing which is possible to achieve the criterion of maximum permissible adhesion wear on the front surface is:

$$N_{0.2} = \begin{cases} \dfrac{[Q](R_e^2 + R_{eu}^2)\xi \cdot 4,5 \sin\varphi (1-\mu)}{R_e \nu \delta q_{\max} t \tau} & if \ \dfrac{q_{\max}}{4,5 \cdot R_e (1-\mu)} < 1 \\ \dfrac{[Q](R_e^2 + R_{eu}^2)\xi \cdot \sin\varphi}{R_e^2 \nu \delta t \tau} & if \ \dfrac{q_{\max}}{4,5 \cdot R_e (1-\mu)} \geq 1 \end{cases} \tag{29}$$

Evaluation of resistance of cutting tool criterion for maximum allowable wear size.

For the finishing details stochastic equation has the form of wear:

$$\frac{dx}{dt} + dx = N(t), \tag{30}$$

Failure occurs when the details of its size to achieve maximum permissible value $x_{\max}$, which happens after a random interval of tool $t = T_n$. Maximum permissible value of the parameter $x_{\max}$ determined from the condition of normal operation of the instrument. Operating time to failure T_n is a function of random arguments tool wear rate of change of C, i.e. $T_n = f(\mathrm{C})$. Failure occurs tool for achieving detail maximum permissible value $x_{\max}$, what happens after a random period of time to process it.

Processed on a machine part has size, which tolerance is within the boundaries $x_{\min}$ – $x_{\max}$. With increasing wear on the back of the instrument the size of parts changed. In average (Fig. 1) size of the parts is beyond the tolerance only after an interval time T_4. But during work tool in the initial period of operation from T_1 to T_2 there is a danger for details, treated on the upper field tolerance, then the reliability of their increases. Excess of the tolerance field components finished to the lower limit of tolerance is possible at time $t = T_3$, with $T_2 < T_3$, $T_3 < T_4$, as

$$(a,b) = \left(\frac{C}{\lambda}; \frac{C}{\lambda} + \Delta_{\max} \right) = \left(x_{\min}, x_{\max} \right). \quad (31)$$

Expected value and variance of dimensional stability of the instrument from the initial values gap Δ_0, constant velocity component wear C and the coefficient of proportionality λ: $W(\Delta_0) = \delta(\Delta_0 - \Delta_{03})$:

$$W(C) = \delta(C - C_3),\ W(\lambda) = \delta(\lambda - \lambda_3). \quad (32)$$

in this case, the probability density of the coordinates x in equation (30) at the initial time $t = 0$ is a delta-like function, i.e.

$$W_0(x) = \delta(x - x_0) = \delta\left(x - \frac{C_3}{\lambda} - \Delta_{03} \right). \quad (33)$$

The probability that a random x coordinate at the time t reaches the limits of the interval ($x_{\min}$, $x_{\max}$) through $Px_{\min}, x_{\max}(t, x)$. For continuous Markov process that can take wear and tear, the specific probability satisfies the equation:

$$\frac{\partial Px_{\min,\max}}{dt} = K_1(x_0) \frac{\partial Px_{\min,\max}}{dx_0} + \frac{1}{2} K_2(x_0) \frac{\partial^2 Px_{\min,\max}}{dx_0^2}, \quad (34)$$

with initial conditions $Px_{\min,\max}(0, x_0) = 0$ and boundary conditions $Px_{\min}, x_{\max}(t, x_{\min}) = Px_{\min}, x_{\max}(t, x_{\max}) = 1$.

$$\lim_{t \to \infty} Px_{\min}, x_{\max}(\mathrm{t}, \mathrm{x}) = 1. \quad (35)$$

Coefficients $K_1(x_0)$, $K_2(x_0)$ in equation (34) as determined in accordance with expectation rate depreciation in the initial time and a spectral density of the process $N(t)$ by the formula :

$$K_1(x_0) = C + \lambda\Delta_0;\ K_2(x_0) = \frac{1}{2}\sigma_N^2. \tag{36}$$

Marked the one-dimensional moments in time limits to achieve a

$$T_n = T_n(x_{\min}, x_0, x_{\max}) = \int_0^{\infty} t^n \frac{\partial P x_{\min}, x_{\max}}{\partial t} dt, \tag{37}$$

Equation (34) differentiating both parts by t, multiplying result by $\exp(j\nu t)$ and then integrating in t from 0 to ∞, returned the following equation for the characteristic function:

$$-j\nu\Theta x_{\min}, x_{\max} = K_1(x_0) = \frac{\partial\Theta x_{\min}, x_{\max}}{dx_0} + \frac{1}{2}K_2(x_0)\frac{d^2\Theta x_{\min}, x_{\max}}{dx_0^2}, \tag{38}$$

$$\Theta x_{\min}, x_{\max}(j\nu, x_0) = -\int_0^{\infty} \frac{\partial}{\partial t} P x_{\min}, x_{\max}(t, x)\, e^{j\nu t}\, dt. \tag{39}$$

Equation (35) to find the first moments of time reaching the limits of tolerance parts and used to determine stability of the instrument (Fig. 1).

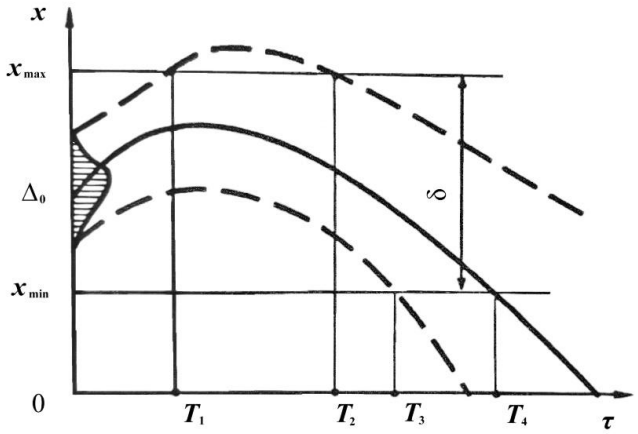

Figure 1 – Moments of time reaching the limits of tolerance parts

To check the adequacy of the models developed experimental unit for measuring tool wear. Based on performance testing tools in industrial conditions obtain wear curves cutting plates, their example shown in Fig. 2. The probability of adequacy of mathematical models is 0.71.

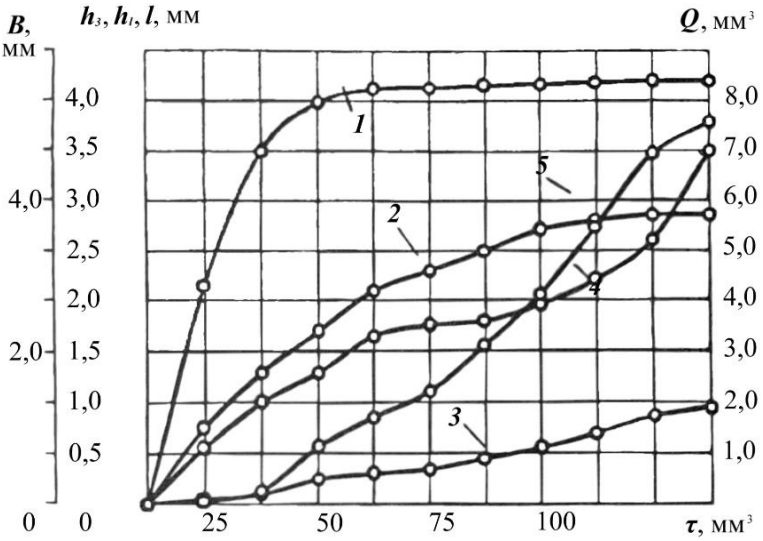

Figure 2 – Crooked wear plate cutting SNMG 380932
(1 – width, 2 – length, 3 – deep hole, 4 – width chamfer wear on the rear surface, 5 – the amount of material the tool is withdrawn from the front surface)

On the basis of students have developed analytical calculation based cutting tool wear on the front and back surfaces of the parameters of the operation, which averages to estimate the period of stability instrument, proposed method of determining the dimensional stability of the instrument with a given probability (for finding the size of workpieces in a given field admission), which depends on tool wear during the finishing details.

References: 1. *Palanisamy, Ponnusamy & Shanmugasundaram, S.* (2008). Modelling of tool wear and surface roughness in hard turning using regression and artificial neural network. International Journal of Machining and Machinability of Materials. 4. 10.1504/IJMMM.2008.020912. **2.** *Čerče, L., Pušavec, F., & Kopač, J.* (2015). A New Approach to Spatial Tool Wear Analysis and Monitoring. *Strojniški vestnik - Journal of Mechanical Engineering, 61*(9), 489-497. doi: http://dx.doi.org/10.5545/sv-jme.2015.2512. **3.** *P. Huang and W. B. Lee*, "Cutting Force Prediction for Ultra-Precision Diamond Turning by Considering the Effect of Tool Edge Radius," International Journal of Machine Tools and Manufacture 109 (October 2016): 1–7, https://doi.org/10.1016/j.ijmachtools.2016.06.005. **4.** *Zhang X, Zheng G, Cheng X, Xu R, Zhao G, Tian Y.* Fractal Characteristics of Chip Morphology and Tool Wear in High-Speed Turning of Iron-Based Super Alloy. *Materials (Basel)*. 2020;13(4):1020. Published 2020 Feb 24. doi:10.3390/ma13041020. **5.** *Maruda R.W., Krolczyk G.M., Nieslony P., Wojciechowski S., Michalski M., Legutko S.* The influence of the cooling conditions on the cutting tool wear and the chip formation mechanism. J. Manuf. Process. 2016;24:107–115. doi: 10.1016/j.jmapro.2016.08.006.

[CrossRef] [Google Scholar]. **6.** *Hao Z.P., Fan Y.H., Lin J.Q., Yu Z.X.* Wear characteristics and wear control method of PVD-coated carbide tool in turning Inconel 718. Int. J. Adv. Manuf. Technol. 2015;78:1329–1336. doi: 10.1007/s00170-014-6752-0. [CrossRef] [Google Scholar].

Галина Клименко, Яна Васильченко,
Владислав Квашнін, Краматорськ, Україна

МОДЕЛЮВАННЯ ЗНОШУВАННЯ РІЗАЛЬНИХ ІНСТРУМЕНТІВ ДЛЯ ТОКАРНИХ ВЕРСТАТІВ

Анотація. *Для визначення періоду стійкості інструменту, а також базових показників процесу його експлуатації, які характеризують зношування інструменту, розроблено математичні залежності зношування різального інструменту по передній та задній поверхням від параметрів його експлуатації на важких верстатах. Для перевірки адекватності моделей зношування проведені експериментальні дослідження зміни геометричної форми різального клину методом неруйнівного контролю за допомогою спеціально розробленого приводу. Вимірювались геометричні розміри лунки зношування по передній поверхні. В результаті досліджень проаналізовані види відмов інструменту та побудовано криві зношування різальних пластин в умовах виробництва. Запропоновано методику розрахунку величин зношування контактних передньої та задньої поверхонь на основі енергетичної теорії зношування, що дозволяє визначити такі характеристики зношування різця, як величина й форма фаски зношування на його задній поверхні, величина радіального зношування, геометричні розміри й форма лунки зношування на його передній поверхні. Розроблено математичну модель для оцінки середньої кількості деталей, при обробці яких, можливе досягнення критерію максимально допустимого зносу на задній поверхні різця важкого токарного верстату та максимально допустимої кількості інструментального матеріалу, що знімається передньою поверхнею інструменту. Величина розбіжності розрахованої форми зношеного різального клину від певної, здобутої експериментальним шляхом, не перевищує 10%. Підтвердження адекватності моделей зношування інструменту дає змогу використовувати їх для розрахунку базових показників критеріїв його затуплення. Запропонована методика визначення розмірної стійкості різального інструменту з заданною імовірністю.*

Ключові слова: *зношування; контактне напруження; ріжуча кромка; температура різання; адгезійне зношування; адекватність моделі.*

ЗМІСТ (CONTENT)

Наукове видання

РІЗАННЯ ТА ІНСТРУМЕНТИ
в технологічних системах

Міжнародний науково-технічний збірник

Випуск № 93

Укладач *д.т.н., проф. О.М. Шелковий*
Оригинал-макет *А.М. Борзенко*
Відп. за випуск *к.т.н., проф. Є.В. Островерх*

В авторській редакції

Матеріали відтворено з авторських оригіналів

Підп. до друку 12.02.2019.Формат 60х84 1/16. ПапірСоруРарег.
Друк - ризографія. Гарнитура Таймс. Умов.друк.арк. 10,93. Облік.вид.арк. 11,0. Наклад 300 прим.
1-й завод 1-100. Зам. № 1149. Ціна договірна.

Видавничий центр НТУ «ХПІ»
Свідоцтво про державну реєстрацію ДК № 116 від 10.07.2000 р.
61002, Харків, вул. Кирпичова, 2